University of Alberta

New Roles for B-Cell Lymphoma 10 in the Nucleus

by

Ashley Dronyk

A thesis submitted to the Faculty of Graduate Studies and Research
in partial fulfillment of the requirements for the degree of

Master of Science
in
Experimental Oncology

Department of Oncology

Spring 2011
Edmonton, Alberta

Examining Committee

Andrew Shaw, Oncology

Michael Hendzel, Oncology

Michael Weinfeld, Oncology

Shelagh Campbell, Biological Sciences, University of Alberta

This thesis is dedicated….

To a very special little boy who taught me that you can do anything you put your mind to. Jayden you were the strongest and most courageous little boy I ever met, we miss you and love you dearly. You will always be our little angel.

To my Grandma who graciously battled breast cancer during the course of this thesis project.

To my loving family who has always supported me in my many endeavors.

Abstract

Radiation therapy targets cancer cell death by overwhelming cells with harmful DNA damage. Understanding how cells repair radiation damage and in particular how they become resistant to radiation therapy is important for effective cancer treatment. Our lab made the novel discovery that Bcl10, a cytoplasmic protein important for NF-κB activation, localizes to endogenous γH2AX foci in the nucleus of breast cancer cells. We determined that following radiation treatment Bcl10 is recruited to ionizing radiation-induced foci in a dose-dependent matter and that it is important for the repair of radiation-induced DNA damage. We also observed that breast cancer cells are extremely sensitive to Bcl10 knockdown, causing cellular senescence, while normal breast epithelial cells are insensitive. Our findings identify Bcl10 as potent anti-cancer target.

Acknowledgements

I would like to thank Xiuying Hu for doing all the groundwork on this project and for being my sounding board, your help and support is greatly appreciated. To my supervisory committee members, Dr. Michael Hendzel and Dr. Michael Weinfeld, thank you so much for all your input and enthusiasm, I would not have been as successful without you. Enormous thanks to Dr. Xuejun Sun, Gerry Baron, and the rest of the imaging facility, your help has been outstanding and I literally would have not been able to complete this project without you. Finally I would like to thank my supervisor Dr. Andrew Shaw, you have been an amazing mentor. You have fostered my scientific creativity and shaped my analytical thinking but your passion and enthusiasm is what I have appreciated the most. It has gotten me through those tough days and has fired my own scientific passion. Special thanks to all of you!

Table of Contents

List of Tables

List of Figures

Abbreviations

ATM	Ataxia telangiectasia mutated
ATR	Ataxia telangiectasia and Rad3-related protein
Bcl10	B cell lymphoma 10
BCR	B cell receptor
BRCA1	Breast cancer 1
BRCA2	Breast cancer 2
BSA	Bovine serum albumin
CARD	Caspase recruitment domain
CBM	Carma/Bcl10/MALT1
Chk2	Checkpoint homolog 2
Con	Control
CSK	Cytoskeletal buffer
DAPI	4’,6-diamidino-2-phenylindole
DDR	DNA damage response
DMSO	Dimethyl sulfoxide
DNA	Deoxyribonucleic acid
DNA-PK	DNA-dependent protein kinase
DNA-PKcs	DNA-dependent protein kinase catalytic subunit
DSB	Double strand breaks
DTT	Dithiothreitol
EDTA	Ethylenediaminetetraacetic acid
EGF	Epidermal growth factor

FANCD2	Fanconi anemia complementation group D2
FBS	Fetal bovine serum
FcγR	Fc-γ receptor
FHA	Forkhead-associated domain
FISH	Fluorescent in situ hybridization
Gy	Gray
HDM2	Human homologue of murine mdm2
HR	Homologous recombination
h	Hour
IgG	Immunoglobulin G
IKK	IκB kinase
IKKα	IκB kinase α
IKKβ	IκB kinase β
IKKγ	IκB kinase γ
IR	Ionizing radiation
IRIF	Ionizing radiation-induced foci
IκB	Nuclear factor of κ light polypeptide gene enhancer in B-cells inhibitor
IκBα	Nuclear factor of κ light polypeptide gene enhancer in B-cells inhibitor α
LPA	Lysophosphatidic acid
LPS	Lipopolysaccharides
MAGUK	Membrane-associated guanylate kinases
MALT1	Mucosa-associated lymphoid tissue lymphoma translocation protein 1

MDC1	Mediator of DNA damage checkpoint protein 1
mins	Minutes
mL	Millilitre
mM	Millimolar
MRN	Mre11-Rad50-Nbs1
NA	Numerical aperture
NES	Nuclear export signal
NF-κB	Nuclear factor-κB
NIK	NF-κB-inducing kinase
NHEJ	Non-homologous end joining
nM	Nanomolar
Non-T	Non-transfected
P	Phosphorylated
P-ATM	Phosphorylated ataxia telangiectasia mutated
PBS	Phosphate buffered saline
PI3-K	Phosphatidylinositol 3-kinase
PMSF	Phenylmethanesulfonylfluoride
PP2A	Protein phosphatase 2A
PS	Penicillin-Streptomycin
Rpm	Revolutions per minutes
RT	Room temperature
SA-β-gal	Senescence-associated β galactosidase
SDS	Sodium dodecyl sulfate

SEM	Standard error of mean
siRNA	Small interfering RNA
SSB	Single strand break
ssDNA	Single strand DNA
TBST	Tris-buffered saline tween-20
TCR	T cell receptor
TE	Tris EDTA buffer
TFIIB	Transcription factor II B
Ub	Ubiquitin
XRCC4	X-ray cross complementing group 4
γH2AX	H2AX phosphorylated on serine-139
µM	Micromolar

Chapter 1.Introduction

The rationale behind effective cancer therapy is to specifically target cancer cells without harming normal cells. In order to achieve this it is essential to identify key molecules that differentiate cancer cells from normal cells that can be targeted for therapy. A large proportion of current cancer therapies, including radiation and chemotherapeutics, aim to overwhelm cancer cells with genotoxic lesions leading to programmed cell death and senescence. The problem with these types of therapies is two-fold: 1) these therapies do not selectively target cancer cells 2) cancer cells have evolved mechanisms to resist lethality. If we could improve these therapies by selectively targeting cancer cells and overcoming resistance to lethality we would significantly improve their efficiency.

In my thesis I describe how, a protein, B-cell lymphoma 10 (Bcl10) plays a central and novel role in the repair of radiation-induced DNA damage and cellular senescence. Interestingly, we have found that breast cancer cells are extremely sensitive to reduction in Bcl10 protein levels resulting in senescence. In contrast normal breast epithelial cells are relatively unaffected. Together these identify Bcl10 as a promising new therapeutic target in breast cancer.

1.1 Structural features and historical roles of Bcl10

Bcl10 is a 33 kDa protein with an N-terminal caspase recruitment domain (CARD) and a serine/threonine rich C-terminus [1, 2]. The CARD domain belongs to the death domain superfamily and consists of 6 antiparallel helices that

align in a parallel fashion and mediate strong homotypic interactions [3, 4]. The CARD domain mediates CARD-CARD interactions and plays an important role in Bcl10 function by allowing Bcl10 to homo-oligomerize as well as hetero-oligomerize with other CARD-containing proteins leading to their activation [1]. Bcl10 also contains multiple sites for post-translational modifications by phosphorylation and ubiquitylation suggesting that it is highly regulated. The majority of these modifications are targeted to the C-terminus and act to both positively and negatively modulate Bcl10 function [2]. Bcl10 may therefore play an important role in the assembly and function of complexes involving its interaction partners. However, the only well-characterized function for Bcl10 to date is in activation of the nuclear factor-κB (NF-κB) signaling pathway. NF-κB is a family of transcription factors that regulates genes involved in the cognate immune response, cell proliferation and survival [5]. In lymphoid cells Bcl10 plays an important role in activating NF-κB downstream of antigen receptor binding (TCR and BCR), and lipopolysaccharide (LPS) binding while in non-lymphoid cells it mediates the response to lysophosphatidic acid (LPA), G-coupled protein receptor binding, and angiotensin-II [6-13]. Importantly, there is evidence that constitutive NF-κB activation can result in neoplastic and autoimmune disorders while NF-κB deficiency results in immune impairment [10].

NF-κB consists of 5 DNA-binding subunits, RelA/p65, RelB, and c-Rel, that bind in heterodimers with p50 and p52, which are produced from the larger p105 and

p100 precursors, respectively [10]. Activation occurs through two main pathways, the canonical/classical pathway and the noncanonical/alternative pathway. The canonical pathway is described as being RelA and IKK-β dependent [5, 14]. In this pathway cell surface receptor binding results in the formation of a cytoplasmic adaptor complex, which recruits an IKK complex composed of IKKα, IKKβ and two molecules of IKKγ [5, 14]. This activates the IKK complex resulting in phosphorylation of IκB [14]. IκB is responsible for maintaining RelA/p50 dimers in the cytoplasm. Phosphorylated IκB is subject to degradation resulting in the release of the NF-κB dimers which enter the nucleus and mediate transcription [14]. The noncanonical pathway however is IKKα dependent, and involves the recruitment of an IKK complex, composed of two IKKα molecules, which is activated via phosphorylation by the NF-κB-inducing kinase (NIK) [5, 14]. Similar to the canonical pathway, activated IKK phosphorylates the IκB complex resulting in its degradation and release of p52/RelB dimers that enter the nucleus and mediate transcription [14].

In both of these pathways, Bcl10 acts upstream of IKK activation to transmit signals from the cell surface, through formation of a multimeric Carma/Bcl10/MALT1 (CBM) complex. The CBM complex is composed of Carma1, a MAGUK family protein containing a CARD domain or Carma 3 in nonlymphoid cells, Bcl10, and MALT1, a paracaspase protein containing a death domain, two immunoglobulin-like domains (Ig-like) and a C-terminal caspase-like domain [10, 12, 15-18]. In general, following signaling at the cell surface

Bcl10 is recruited to modified Carma1/3 (phosphorylated), which interact through their CARD domains [10, 19]. Bcl10 recruits MALT1 and this complex is thought to activate the IKK complex, through lysine-63 ubiquitylation of IKKγ [10, 19]. Experimental evidence has shown that the CARD domain of Bcl10 is essential for NF-κB activation, indicating that Bcl10 is a key adaptor protein in the formation of the CBM complex [1]. The pathway is reviewed in figure 1.0.

Besides this role in NF-κB activation two other functions have been attributed to Bcl10. Bcl10 has been shown in be important for T-cell receptor (TCR) and Fc-γ receptor (FcγR) induced actin polymerization and to act as potential transcription activator in lymphoid cells [20, 21]. Actin polymerization is required for both T-cell and Fc-γ receptor signaling [20]. Interestingly, phosphorylation of serine-138 is critical for Bcl10 to mediate TCR- and Fc-γR induced actin polymerization, indicating a secondary role of Bcl10 is to regulate the assembly of actin matrices [20]. Mutating serine-138 abolishes Bcl10's ability to polymerize actin but does not affect its ability to activate NF-κB [20]. Evidence from *in vitro* studies indicate that Bcl10 may also interact with transcription factor II B (TFIIB) to act as a potential transcriptional transactivator [21]. This study was based on a previous study that identified Bcl10 as a transactivator in yeast and suggests that Bcl10 may perform additional functions in the nucleus [22]. To our knowledge these two studies provide the only evidence that Bcl10 has functions outside the NF-κB pathway.

Figure 1.0 General overview of NF-κB activation through the CBM complex. Following signaling at the cell surface Bcl10 is recruited to phosphorylated Carma1/3, where they interact through their CARD domains and Bcl10 subsequently recruits MALT1. The interaction between MALT1 and Bcl10 is thought to bring about a conformational change in MALT1, which promotes its oligomerization. These MALT1 oligmers recruit and bind the E3 ubiquitin ligase TRAF6, promoting its oligomerization and activating its ligase activity. This complex is recruited to the IKK complex where MALT1 and TRAF6 mediate lysine-63 ubiquitination of IKKγ. This activates the IKK complex, which dissociates from the CBM complex, and phosphorylates the IκB complex targeting it for degradation. Degradation of the IκB complex releases NF-κB dimers, which translocate into the nucleus and promote transcription. [10, 19, 23, 24]

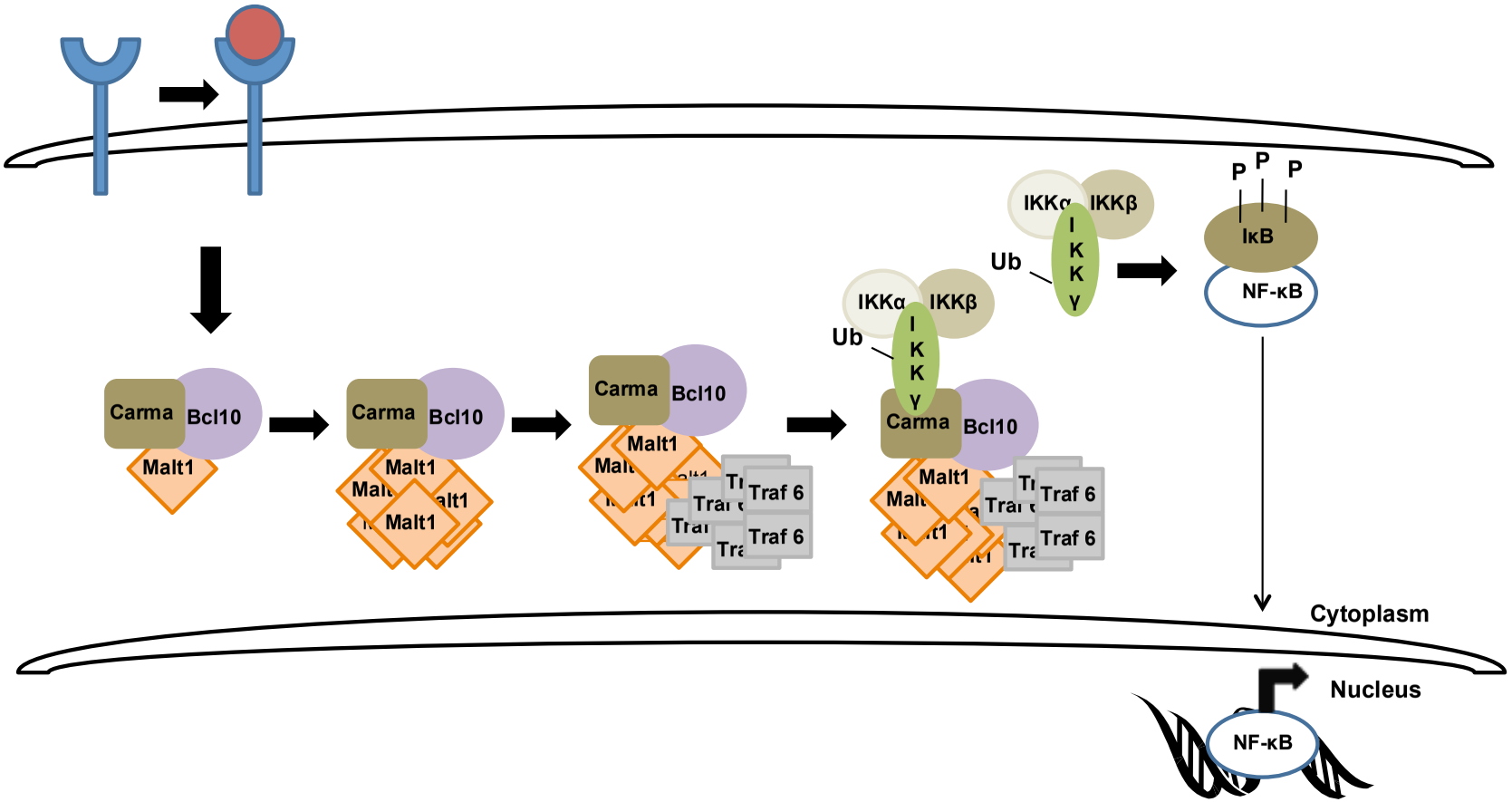
Carma
Bcl10
Malt1
Traf 6
IKKα
IKKβ
IKKγ
Ub
P
IκB
NF-κB
Cytoplasm
Nucleus

All of the functions of Bcl10 except its potential role as a transcriptional transactivator, involve localization to the cytoplasm. However, a number of cancer patient studies have found Bcl10 can localize to the nucleus and that this is linked to tumor aggression and poorer prognosis. Specifically, Bcl10 nuclear expression in primary cutaneous marginal zone B-cell lymphomas correlates with extracutaneous spread of disease and decreased patient survival [25]. Similarly, a study of oral squamous cell carcinomas identify a correlation between nuclear Bcl10 expression and poor patient outcome [26]. Nuclear staining was greatest at the invasive front of the tumor suggesting that nuclear localization correlates with tumor aggressiveness [26]. These studies suggest that Bcl10 may play a very important role in the nucleus that has been overlooked and that aberrant Bcl10 nuclear localization may contribute to cellular transformation and carcinogenesis.

1.2 Bcl10 localization to cryptogenic foci and the double strand break response

Previous studies in our laboratory identified Bcl10 in the nucleus of breast cancer cells where it localizes to a small number of discrete regions enriched in phosphorylated histone variant, H2AX (γH2AX). γH2AX foci mediate the recruitment of chromatin remodeling proteins and DNA repair proteins to sites of DNA damage [27-38]. Interestingly, endogenous γH2AX foci are present in many cancer cells in the absence of induced damage and are referred to as “cryptogenic foci”. The function of these foci is largely unknown. It has been suggested that they are sites of failed DNA repair and more recently that they represent sites of

telomere dysfunction[39, 40]. This finding led us to investigate whether Bcl10 would localize to active sites of DNA repair following treatment with γ-radiation.

Ionizing radiation affects DNA both directly and indirectly by causing chemical modifications [41]. These modifications include sugar damage and base lesions such as apurinic/apyrimidinic sites, single strand breaks (SSB), double strand breaks (DSB), and clustered DNA damage [41]. In fact DNA DSB are the most harmful genotoxic lesions that a cell can accumulate. Therefore a cell's course of action in response to this damage is very important. DNA DSB can arise through several processes such as DNA replication at single strand breaks, treatment with exogenous agents such as bleomycin, and γ-radiation, and repair of clustered DNA damage [42-47]. Following DSB damage, cells respond by activating several DNA repair pathways, cell cycle checkpoints and pro- and anti- survival pathways. If these processes are ineffective, cells can develop further mutations and chromatin aberrations [48]. In normal cells the accumulation of unrepaired DNA strand breaks leads to the activation of cell death pathways. However, cancer cells avoid these pathways, resulting in genetic instability and disease progression.

Following the development of a DSB H2AX is rapidly phosphorylated on serine 139 at the site of damage and accumulates to form sites referred to as γH2AX foci [27, 49, 50]. Accordingly, γH2AX foci are the most commonly used marker for DSB. H2AX is phosphorylated by the serine/threonine protein kinase, ataxia-

telangiectasia mutated (ATM), a member of the phosphatidylinositol 3-kinase family (PI3-K) [51]. Under normal condition ATM is present in the nucleus as an inactive dimer [52, 53]. The protein phosphatase 2A (PP2A) is responsible for maintaining ATM in an inactive, dephosphorylated state [52, 53]. When DSB occur, the interaction between ATM and PP2A is disrupted in a phosphorylation-dependent manner enabling ATM to auto-phosphorylate at a serine-1981 residue, dissociating the ATM dimers and releasing kinase-activated monomers, which are free to phosphorylate several substrates including H2AX [52-54]. These initial steps occur within seconds following DNA damage, to create γH2AX foci [27, 55].

ATM is recruited to sites of damage by the MRE11-RAD50-NBS1 (MRN) complex [56, 57]. The MRN complex, containing a dimer of MRE11, a dimer of RAD50 and a monomer of NBS-1, initially recognizes the DSB and tethers the free DNA ends [42]. The MRE11 proteins bind the free DNA ends, while RAD50 mediates the interaction between the two MRE11 molecules on adjacent DNA-free ends [42, 56-59]. The NBS-1 protein interacts directly with MRE11, and binds ATM monomers in its carboxyl terminus resulting in the phosphorylation of NBS-1 and retention of ATM to maintain high levels of ATM at the damage site and activate ATM-dependent signaling [42, 57]. Apart from H2AX and NBS-1 the ATM signaling cascade involves the phosphorylation of numerous other proteins including mediator of DNA damage checkpoint 1 (MDC1), Artemis, checkpoint kinase 2 (Chk2), breast cancer 1 (BRCA1), protein 53 (p53), DNA-

PKcs kinase, and fanconi anemia complementation group 2 (FANCD2) [60, 61]. These proteins mediate repair, via non-homologous end joining (Artemis and DNA-Pkcs), and homologous recombination (FANCD2), cell-cycle arrest at various checkpoints (Chk2 and MDC1) and the apoptotic response (p53) [60, 61]. This pathway is referred to as the DSB response or the DNA damage response (DDR) and is reviewed in figure 1.1.

Cells repair DSB through two major pathways non-homologous end joining (NHEJ) and homologous recombination (HR). NHEJ is the major pathway used in human cells, particularly in G_0, G_1 and early S phase[48]. Initially Ku70 and Ku80 heterodimers are recruited to break sites where they bind and align the free DNA ends [48, 62, 63]. DNA bound Ku heterodimers are then able to recruit and activate DNA-PK catalytic subunit kinase activity[48, 64]. Artemis along with DNA-PK processes the free DNA ends so that DNA ligase IV-XRCC4 complexes can ligate the free ends and complete repair [48, 65, 66]. Since DSB can result in different free DNA ends, these ends must be processed before the breaks can be re-ligated. Processing of DNA ends can be particularly difficult and result in errors in the DNA code. For this reason NHEJ is considered an error-prone method of repair while HR is considered error-free. Cells repair via HR during late S and G_2 of the cell cycle [67]. HR involves processing of the free DNA ends to create 3' ssDNA overhangs; the MRN complex is believed to be important for this processing [48, 68-70]. RAD51 with the assistance of RPA, BRCA1/BARD1,

Figure 1.1 The DSB response. ATM is maintained in an inactive state by the protein phosphatase PP2A; when a cell is exposed to DNA damaging agent such as γ-irradiation, DSB can occur. When this happens ATM is able to dissociate from PP2A and autophosphoylate itself at a serine-1981 residue, this produces activated monomers. At the same time the MRN complex, composed of a dimer of Mre11, a dimer of Rad50 and a monomer of NBS-1, is recruited to the break site. At the break sites Mre11 binds the free DNA end, Rad50 links the Mre11 proteins and NBS-1 direct binds Mre11 and recruits P-ATM. The interaction between the MRN complex and P-ATM promotes an optimal ATM signaling cascade. P-ATM phosphorylates H2AX, producing γH2AX foci, and various other proteins which lead to repair via NHEJ or HR and the activation of cellular checkpoints, cell cycle arrest and apoptotic pathways.[27, 42, 49-61]

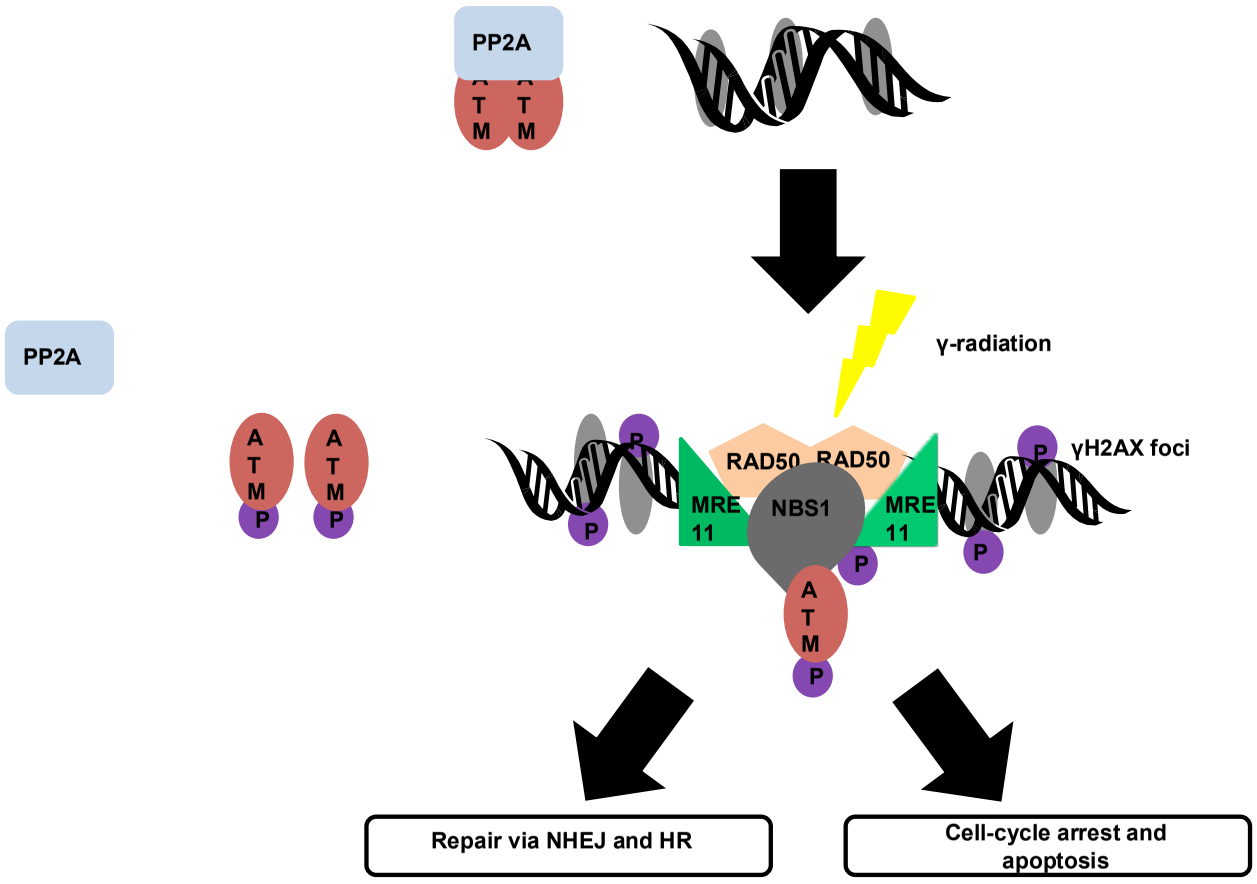
PP2A
ATM
ATM
PP2A
ATMP
ATMP
γ-radiation
P
RAD50
RAD50
MRE 11
NBS1
MRE 11
P
γH2AX foci
P
P
P
ATMP
Repair via NHEJ and HR
Cell-cycle arrest and apoptosis

and BRCA2(FANCD1/DSS1) binds these overhangs and mediates DNA pairing and strand invasion [48, 71]. From this stage on, the specific proteins involved in strand extension and strand resolution are poorly understood. This is a very complex repair process that requires many different proteins for everything to occur properly. However, since this process uses the sister chromatid as a template it is largely error-free. The decision of which repair pathway to use is largely determined by the cell cycle [67].

Pre-existing mutations in many of these key repair proteins have been linked to cancer predisposition. This is because any defects in these repair processes can cause mutations and genomic instability, leading to cancer development. For example, mutation of the breast cancer susceptibility genes BRCA1 and BRCA2 that encode proteins involved in DNA repair, are linked to an increased risk of developing breast and ovarian cancer [72-74]. Not only can mutations in these proteins lead to cancer predisposition, cancer cells develop mechanisms to manipulate these pathways allowing them to become more resistant to genotoxic insults. For example, many cancer cells, in particular cancer stem cells, "hyperactivate" these repair pathways to avoid cell death [75-87]. For these reasons, understanding how cells recognize and repair damage is extremely important for the future development of cancer therapies.

1.3 Cryptogenic foci and cellular senescence

We originally identified Bcl10 in the nucleus of breast cancer cells in cryptogenic

foci; cryptogenic foci are thought to represent sites of failed DNA repair but may also result at sites of telomere dysfunction. The major cellular response to dysfunctional telomeres is cellular senescence, a permanent state of cell cycle arrest [88]. Importantly, cellular senescence is also triggered in response to unrepaired DNA damage [89]. It is of importance that we not only identified a role for Bcl10 in DNA repair but found that it protects cells from cellular senescence, a function associated with dysfunctional telomeres.

Telomere dysfunction can occur through three main mechanisms, direct damage, erosion due to cell proliferation, and disruption due to defective telomere proteins [88]. Like DSB, telomere dysfunction can be detrimental to a cell, leading to chromosome break/fusion cycles, genomic instability, cellular senescence and even cell death [88]. Telomere dysfunction has been linked to an array of different human diseases including cancer. Cells respond to dysfunctional telomeres by triggering the DSB response, which attempts to repair the damage [89-93]. Whether the DSB response is triggered by genuine DSB or by shortened telomeres, senescence is induced through the p53 pathway [89]. p53 is continually degraded by the E3 ubiquitin ligase HDM2 [94-97]. Following DNA damage, p53 is post-translationally modified by ATM and several other proteins, blocking HDM2-mediated degradation [94-97]. The consequent rise in p53 protein levels enhances p53 transcriptional activity and induces transient cell cycle arrest [89, 94, 98]. It is not understood how cells determine whether to transiently arrest the cell cycle or to induce cellular senescence.

Cellular senescence is a very important pathway for preventing continual cell proliferation, especially in the presence of detrimental DNA damage. For this reason cancer cells must mutate or otherwise deactivate this pathway in order to become tumorigenic. Solidifying this idea, a number of preneoplastic cells have been found to maintain the ability to senesce, suggesting that this may halt the progression to malignant disease [89]. Nevertheless, it has been shown that preventing cellular senescence on its own is not sufficient to promote malignant transformation [89]. The majority of mutations in this pathway occur in the p53 response, particularly in p53 itself [89]. However mutating key proteins is not the only way cancer cells overcome senescence; cancer cells can also help prevent telomere-induced senescence by up-regulating telomerase or extending telomeres using the ALT pathway [99, 100]. Telomerase expression or telomere elongation using the ALT pathway prevents senescence by maintaining telomere length so that they do not signal the DSB response. Cellular senescence is a very strong anti-tumor response yet the specific mechanisms by which cancer cells protect themselves from telomere and DSB-induced cellular senescence and death are poorly understood [39, 88].

1.4 Summary

The only well characterized role for Bcl10 is in the activation of NF-κB signaling in the cytoplasm. However, numerous studies have suggested that aberrant Bcl10 nuclear functioning may contribute to cellular transformation and carcinogenesis. To date, no nuclear function has been attributed to Bcl10 that explains these

findings. In this thesis project we investigate the novel roles of Bcl10 in the nucleus of breast cancer cells and identify Bcl10 as a very important anti-cancer target. Specifically we investigated

i) The nuclear localization of Bcl10 to cryptogenic foci and the kinetics of recruitment to ionizing radiation-induced foci (IRIF)

ii) The role of Bcl10 in radiation-induced NF-κB activation

iii) The role of Bcl10 in the repair of radiation-induced DNA damage

iv) Bcl10 and its role in cellular senescence

Chapter 2. Materials and Methods

2.1 Cell Culture

The human breast carcinoma cell line, T47D, was cultured in RPMI-1640 (Gibco, Burlington, ON), supplemented with 2 mM L-glutamine (Gibco), 10 mM HEPES (Gibco), 1.0 mM sodium pyruvate (Gibco), 8 μg/mL bovine insulin (Sigma, Oakville, ONT), 10% (v/v) fetal bovine serum (FBS) (Gibco) and 100 μg/mL penicillin-streptomycin (PS) (Gibco), unless otherwise stated. The human mammary epithelium cell line, hTERT-HME1 (obtained from ATCC, Manassas, VA), was cultured in Dulbecco's Modified Eagle's Medium: Nutrient Mixture F-12 (DMEM/F12) supplemented with 5 mg/mL Albumin from bovine serum (BSA) (Sigma), 10 mM HEPES, 10 ng/mL epidermal growth factor (EGF) (Sigma), 10 ng/mL cholera toxin (List Biological laboratories, Campbell, CA), 10 μg/mL bovine insulin, 500 ng/mL hydrocortisone (Sigma) and 100 μg/mL PS, unless otherwise stated. The human foreskin fibroblast cell line, CRL-2522 (obtained from ATCC), was cultured in DMEM/F12 supplemented with 10% (v/v) FBS and 100 μg/mL PS. All the cells were grown in tissue culture dishes and were incubated at 37 °C and 5% CO_2.

2.2 Bcl10 and MALT1 knockdown

Transient siRNA transfections were performed using lipofection. A scrambled siRNA or mock-transfected and a non-transfected control were included in every experiment. Cells were plated in the appropriate antibiotic-free medium at a density of ~6 x 10^4 cells/mL, and incubated overnight at 37°C and 5% CO_2. The

following day small interfering RNA (siRNA) duplexes were diluted to the appropriate concentration (10-100 nM) in Opti-MEM I reduced serum medium (Gibco). At the same time Lipofectamine RNAiMAX (Invitrogen, Burlington, ON) was diluted at a ratio of 1:50 with Opti-MEM. The siRNA duplex was combined with the diluted Lipofectamine RNAiMAX and incubated at room temperature for 15 min. siRNA-Lipofectamine complexes were then added to the appropriates wells containing the cells plated the previous day. For the non-transfected control an equal volume of Opti-MEM was added to each well. Unless otherwise stated the cells were incubated at 37°C and 5% CO2 for 48 h.

For Bcl10 knockdown we used a 27-mer DsiRNA Dicer-substrate siRNA duplex (Intergrated DNA Technologies, San Diego, CA) at a concentration of 20 nM, with the following sequence:

Sense: 5'-CAAAUUCAGAUGAGAGUAAUUUCTC-3'

Antisense: 5'-GAGAAAUUACUCUCAUCUGAAUUUGAU-3'

A DS Scrambled siRNA (Integrated DNA Technologies) with a similar structure was employed as a mock-transfection control.

For MALT1 knockdown we used a 25-mer StealthRNAi duplex (Invitrogen) at a concentration of 100 nM, with the following sequence:

Sense: 5'-CUGCCUUUGACUCUGGGUUUACAGU-3'

Antisense: 5'-ACUGUAAACCCAGAGUCAAAGGCAG-3'

A StealthRNAi negative universal control with medium GC content (Invitrogen) was used as a mock-transfection control.

2.3 Ionizing Radiation and Bay11 Treatment

Cells were irradiated using a ^{137}Cs irradiator (Shepherd, San Fernando, CA) and were allowed to recovery at 37°C and 5% CO_2 for a specified amount of time. Bay11-7082, referred to as Bay11 (Sigma), was dissolved in dimethyl sulfoxide (DMSO) (Sigma) to create a 50 mM stock solution. Bay11, diluted in media to 3.5 μM, was added to cells two h prior to irradiation and cells were incubated at 37°C and 5% CO_2. Control cells were treated with an equal amount of DMSO.

2.4 Immunofluorescent staining

For indirect immunofluorescent staining cells were grown on 12 mm coverslips in 24-well plates, washed in phosphate buffer solution (PBS) and fixed in 3.7% formaldehyde (Sigma) in PBS for 15 min at room temperature (RT). The fixed cells were washed 3 times with 0.2% (w/v) BSA in PBS and then extracted in CSK extraction buffer (300 mM sucrose (Sigma), 10 mM PIPES (Sigma), 50 mM NaCl (BDH Inc., Edmonton, AB), 3 mM $MgCl_2$ (Sigma), 0.5% (v/v) Triton X-100 (Sigma), 1.2 mM phenylmethylsulfonyl fluroride (PMSF) (Sigma), 0.1mg/mL DNase (Roche, Mississauga, ON), 0.1 mg/mL RNase A (Roche)) on ice for 5 min. The coverslips were blocked in 2% (w/v) BSA in PBS overnight at 4°C. Following block, the coverslips were washed in 0.2% (w/v) BSA in PBS x3 and incubated with 1:600 rabbit anti-Bcl10 (B-0431, Sigma), and/or 1:1000 mouse anti-phospho-Histone H2A.X (JBW301, Millipore, Billerica, MA), and/or 1:1000 mouse anti-ATM Protein Kinase pS1981 (200-301-400, Rockland, Gilbertsville, PA), and/or 1:50 rabbit anti-MALT1 (28246, Santa Cruz, Santa

Cruz, CA), and/or 1:500 mouse anti-Mre11 (214-100, Abcam, Cambridge, MA), and/or 1:100 mouse anti-NF-κB p65 (sc-8008, Santa Cruz), for 1 hour at RT. Once again the coverslips were washed in 0.2% (w/v) BSA in PBS x3 and then incubated with 1:100 Alexa Fluor 488 goat anti-mouse IgG (A11029, Invitrogen) and 1:100 Alexa Fluor 555 goat anti-rabbit IgG (A21429, Invitrogen) for 20 min at RT. The coverslips were rinsed with PBS and stained with 1ug/mL 4,6-Diamidino-2-phenylindole dihydrochloride (DAPI) (Sigma) for 5 min at RT and then mounted onto slides using anti-fade mount. Slides were allowed to dry overnight and then were imaged using a Zeiss LSM 710 confocal microscope and a Zeiss plan-ApoChromat 40X/1.3 numerical aperture (NA) oil immersion lens. Images are representative of at least three separate experiments.

2.5 Image Analysis

Average nuclear intensity was measured using Metamorph (Molecular Devices Inc., Downington, PA). Optical sections were obtained for a minimum of 25 cells per experiment; a nuclear mask was created using the Dapi channel and overlaid onto the FITC channel where the average intensity was measured within each area. Graphs represent a pool of at least three separate experiments.

γH2AX foci quantification was done using Imaris (Bitplane AG, Saint Paul, MN). Z-stacks were obtained, 0.3 μM per slice, for ~50 cells from two separate experiments. Images were reconstructed on a 3-demenisional scale and noise was subtracted using a 3x3x3 median filter. The spots function was used to count the

foci above a 0.5 μM size filter and a minimum intensity filter of 800, unless otherwise stated.

2.6 Comet Assay for the detection and quantitation of DNA damage

Cells growing in 6-well plates were washed with PBS, trypsinized with 0.25% Trypsin-EDTA (Gibco) and transferred to centrifuge tubes. Cells were centrifuged at 1000 rpm for 10 min at 4°C (Beckman GS-6KR Centrifuge), resuspended in 1 mL ice-cold PBS and counted using a hemocytometer. Counted cells were centrifuged at 1000 rpm for 5 min at 4°C and resuspended at a density of 2x 10^5 cells/mL in ice-cold PBS, cells were combined with molten LMAgarose (Trevigen, Gaithersburg, MD) at a ratio of 1:10 and 75 μl was immediately pipetted onto CometSlides (Trevigen). Slides were placed at 4°C in the dark for 20 min to allow for gelling, and then were immersed in pre-chilled lysis solution (Trevigen) for 30 min at 4°C. Excess buffer was gently tapped off and slides were immersed in freshly prepared alkaline solution pH >13 (300 mM NaOH (Fisher, Ottawa, ON), 1 mM Ethylenedinitrilo tetracetic Acid, Disodium salt, Dihydrate (EDTA) (EMD Bioscience, Gibbstown, NJ) at RT for 30 min. Prior to electrophoresis slides were neutralized by washing twice in 1X TBE buffer (89 mM Tris Base (Invitrogen), 89 mM Boric Acid (EMD Bioscience, Gibbstown, NJ), 2 mM EDTA) for 5 min at RT. Electrophoresis was carried out in 1X TBE buffer at 26 V for 15 min at 4°C. Slides were dipped in 70% Ethanol (Commercial Alcohols) for 5 mins at RT and then were allowed to dry overnight in the dark. 50 μl of SYBR green (Trevigen), diluted to 1:3000 in TE buffer (10

mM Tris-HCl (Sigma) pH 7.5, 1 mM EDTA), was added to each circle of dried agarose and slides were visualized using a Zeiss Image.Z.1 upright microscope with a Cooke SensiCam High performance camera and a 10X/0.3 NA Zeiss EC-Plan-NEOFluor dry lens. At least 20 images were obtained for each treatment in a single experiment. Comets were analyzed using CometScore software (TriTek Corp., Sumerduck, VA). Each experiment was performed a minimum of three times and graphs were obtained by pooling the data from each experiment. Representative images for figures where obtained using a 20X/0.8 NA Zeiss Plan-ApoChromat dry lens.

2.7 Western Blot Analysis

Whole cell lysates were isolated in 1X SDS sample buffer (2% w/v Sodium dodecyl sulfate (SDS) (Bio-rad, Mississauga, ON), 40 mM Tris pH 6.8, 7.5% v/v Glycerol (Invitrogen), Sodium Fluoride (Sigma), Sodium orthovanadate (Sigma), Phenylmethylsulfonyl fluroride (Sigma)). Just prior to electrophoresis 50 mM Dithiothreitol (DTT) (Sigma) and 0.1% v/v Bromophenol Blue (J.T Baker Chemical, Phillipsburg, NJ) was added to the samples and the samples were separated on either a 10% or 12% SDS-polyacrylamide gel. Proteins were transferred to a nitrocellulose membrane and blocked in 10% milk (Bio-rad) in TBST (0.1M Tris, 0.15M NaCl) for at least 30 min at room temperature. Blots were immunostained with primary antibody diluted in 4% BSA in TBST (Table 1) overnight at 4°C. The primary antibody was removed, the blots were washed three times in TBST for 10 mins at room temperature, and 1/16000 goat anti-

rabbit IgG-Peroxidase (A9169, Sigma) or 1/16000 goat anti-mouse IgG-Peroxidase (A4416, Sigma) was added to detect the primary antibody and incubated for at least an hour at room temperature. Antibodies were detected using Amersham ECL Western Blotting Detection Reagent (GE healthcare, Fairfield, CT) or SuperSignal West Pico Chemiluminescent Substrate (Thermo Scientific, Ottawa, ON). Blots were exposed to X-ray film (Fuji medical X-ray film Super RX) and the films were developed using a Kodak X-omat 2000A processor. Relative intensity was calculated using ImageJ (NIH). Scanned blots were opened in ImageJ, background values were subtracted, and blots were inverted, each band was selected and the integrated density was measured. IκBα values were normalized to the actin loading control to give the final relative intensity values.

2.8 Cell Survival

Cells were transfected according to the above protocol. At 48 h post-transfection the culture medium was removed and the cells were washed with PBS and trypsinized. 1.5X-2X volume of complete growth media was added to stop trypsinization and the cells were added to a 50 mL centrifuge tube and centrifuged at 1000 rpm and 4°C for 5 min. Cells were kept on ice until ready to plate, pelleted cells are resuspended in 1 mL of growth medium. 100 µl of cells was added to 9.9 mL of isoton (Beckman coulter, Mississauga, ON) and the cells were counted using the coulter counter (Beckman coulter), at least four measurements were taken, the high and low value were eliminated and the average was taken of

the remaining two. Cells were diluted to the desired cell number (0 Gy-150 cells, 0.2 Gy-150, 0.5 Gy-150, 1 Gy-200, 2 Gy-200, 4 Gy-500, 6 Gy-1000, 8 Gy-5000, 10 Gy-5000), and 1 mL of cells was added to the appropriate plates containing 2.5 mL of complete growth media. 6 replicates were plated for each treatment condition. Plates were incubator overnight at 37°C and 5%CO_2 to allow for the cells to attach. The next day cells were irradiated using a ^{137}Cs irradiator (Shepherd, San Fernando, CA) and then incubated for ~14 days to allow for colony formation. When colony were big enough to visualized by the naked eye, ~14 days after irradiation, the medium was removed and the colonies were stained with crystal violet (1% crystal violet (Fisher), 30% Ethyl Alcohol) for at least 1 h at room temperature, the stain was removed and the plates were washed in warm water and allowed to dry. The colonies were counted manually and the data was graphed using GraphPad Prism (GraphPad software Inc., San Diego, CA). Graphs are an average of three separate experiments.

2.9 Senescence-associated β-galactosidase

Cells were washed twice in PBS and fixed in 3.7% formaldehyde in PBS for 15 min at room temperature (RT). Fixed cells were washed twice with PBS and then freshly prepared senescence-associated β-galactosidase staining solution (1.84 mM Citric acid (Sigma)/6.3 mM Sodium Phosphate (Sigma) pH 6.0, 150 mM NaCl (BDH Inc), 2 mM $MgCl_2$ (Sigma), 5 mM Potassium Ferricyanide (EM Science, Gibbstown, NJ), 5 mM Potassium Ferrocyanide (EM Science), 1mg/mL 5-Bromo-4-Chloro-3-indolyl β-D-galactopyranoside (Sigma)) was added to each

plate, such that the cells were completely covered. The plates were incubated at 37°C without CO_2 until staining was detectable, ~6 h for T47D cells and ~8 h for hTERT-HME1 cells. Plates were imaged using an Olympus microscope equipped with a Zeiss axiocam MRC and an Olympus UPlanFL 20X/0.50 N.A dry lens. Images were analyzed using Metamorph (Molecular Devices Inc.); positively stained cells were counted by setting a color threshold and counting cells above said threshold, total cell number was counted manual in Metamorph or ImageJ. Graphs represent a pool of at least three separate experiments. 48 h β-galactosidase experiments represent cells 48 h post-transfection. 5-day β-galactosidase experiments were performed by trypsinizing cells at 48 h post-transfection and re-plating them in a p100 tissue culture dish with fresh medium and allowing them to grow for another 72 h.

Table 1. Antibodies used for western blot analysis

Antibody	**Dilution**	**Company and Catalogue #**
Rabbit anti-IκBα	1/1000	Cell Signaling: 9242
Rabbit anti-Bcl10	1/600	Sigma: B-0431
Mouse anti-actin	1/16000	Sigma: A5441
Rabbit anti-MALT1	1/500	Santa Cruz: sc-28246
Mouse anti-P-ATM	1/1000	Rockland: 200-301-400

Chapter 3. Results

3.1 Nuclear Bcl10 accumulates at endogenous γH2AX foci and nascent sites of DNA-damage

3.1.1 Bcl10 associates with γH2AX foci in resting cells which are equivalent to "cryptogenic foci"

We had observed that Bcl10 co-localizes with endogenous γH2AX foci. Endogenous γH2AX foci are present in many cancer cells in the absence of induced damage and are referred to as "cryptogenic foci". The function of these foci is largely unknown, however these foci have been found to be enriched in DNA repair proteins, suggesting that they represent sites of failed DNA repair [40, 101]. To investigate whether the Bcl10 foci we observed had a similar composition, we used indirect immunofluorescent staining to look for the presence of double strand break (DSB) repair proteins. In T47D cells, we found that Mre11 and P-ATM co-localize with endogenous Bcl10 foci (Figure 3.0). This supports the concept that these Bcl10 foci are equivalent to "cryptogenic foci". In the cytoplasm Bcl10 associates with MALT1. Nevertheless, MALT1 has not been described in nuclear foci. We stained for MALT1 and discovered that MALT1 also localizes to these foci (Figure 3.0).

3.1.2 Bcl10 is recruited to nascent sites of DNA-damage

The observation that Bcl10 co-localizes with the DSB repair proteins, Mre11 and P-ATM, in the nucleus of resting T47D cells, prompted us to look at Bcl10 localization following treatment with γ-radiation, which will induce DNA DSB.

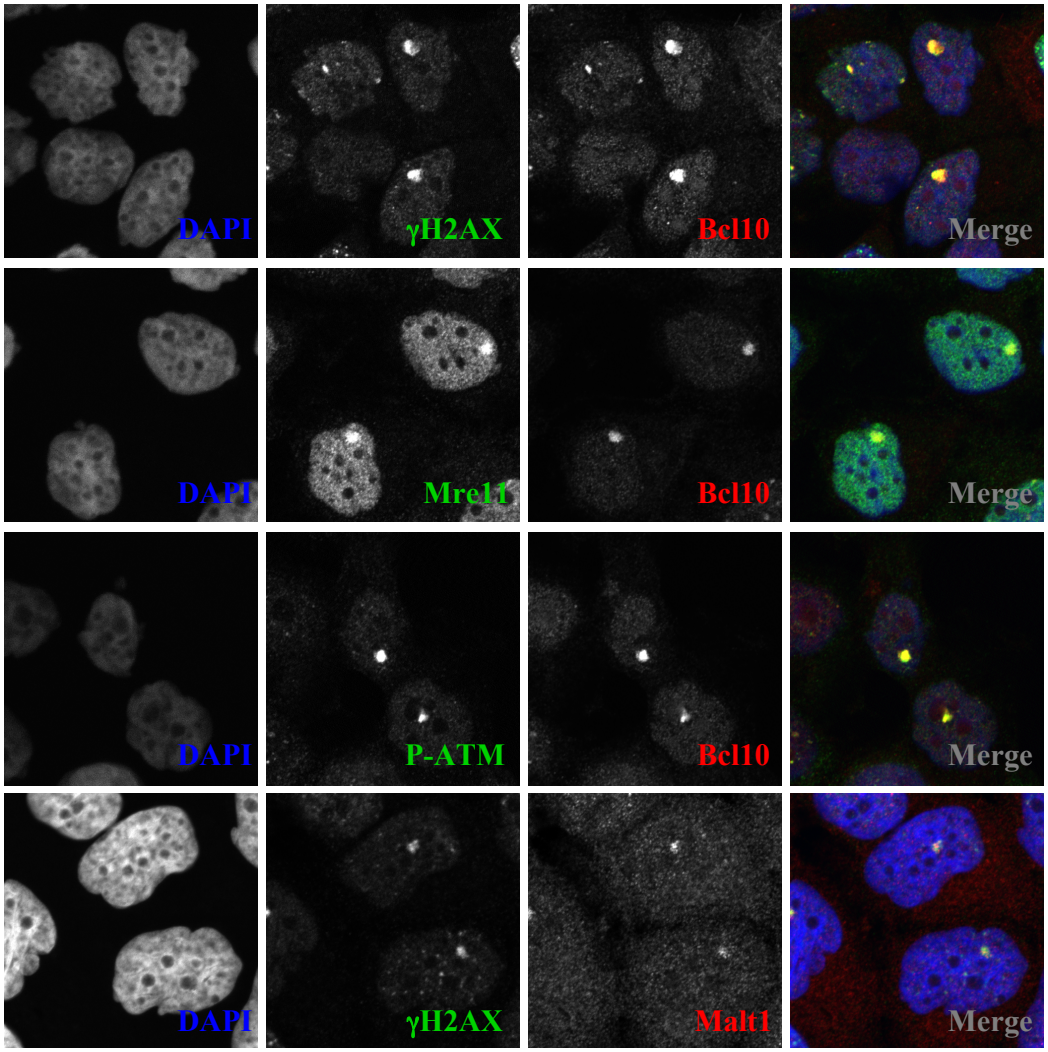

Figure 3.0 Bcl10 localizes to cryptogenic foci in T47D cells. Resting T47D cells were fixed in 3.7% formaldehyde and immunostained, all images were counterstained with DAPI (blue). The top column of images shows T47D cells stained with mouse anti-γH2AX (FITC, green) and rabbit anti-Bcl10 (Cy3, red); the final frame (merge) shows that γH2AX and Bcl10 co-localize (yellow) in large nuclear foci. The second column shows T47D cells stained with mouse anti-Mre11 (FITC, green) and rabbit anti-Bcl10 (Cy3, red) the final frame (merge) shows that Mre11 and Bcl10 co-localize (yellow). The third column shows T47D cells stained with mouse anti-P-ATM (FITC, green) and rabbit anti-Bcl10 (Cy3, red); the final frame (merge) shows that P-ATM and Bcl10 co-localize (yellow). The final column shows T47D cells stained with mouse anti-γH2AX (FITC, green) and rabbit anti-MALT1 (Cy3, red); the final frame (merge) shows that γH2AX and MALT1 co-localize (yellow). Images are representative of at least 3 separate experiments.

We used radiation time course experiments in combination with immunofluorescence to study the localization of Bcl10 to DSB/IRIF. Following treatment with 2 Gy, in T47D cells, we observe that Bcl10 quickly co-localizes with γH2AX at 5 mins post-ionizing radiation (IR), by 30 min post-IR Bcl10 co-localizes with ~100% of the γH2AX foci and then builds up and becomes more substantial in these foci at the later time points, 1 h, 4 h, and 8 h (Figure 3.1A). To verify that these sites represent radiation-induced DSB, we monitored Bcl10 co-localization with P-ATM. Activated ATM (P-ATM) is recruited to DSB sites where it mediates the phosphorylation of a number of key proteins involved in DNA repair and cell cycle arrest [60, 61]. Therefore, P-ATM should be present at all DSB sites. Similar to γH2AX, we observe that Bcl10 co-localizes with P-ATM as early as 5 mins post-IR (Figure 3.1B). By 30 min post-IR we observe that Bcl10 co-localizes with ~100% of the P-ATM foci and builds up to become very substantial in these foci at the later time points, 1 h, 4 h, and 8 h (Figure 3.1B).

3.1.3 Bcl10 recruitment to ionizing radiation-induced foci is dose-dependent

Determining the kinetics of Bcl10 recruitment to IRIF can provide clues as to the function of Bcl10 at these sites. To better understand Bcl10 recruitment kinetics we wanted to determine if recruitment occurs in a dose-dependent manner. We approached this by also observing recruitment following treatment with 5 Gy. As shown in Figure 3.2A, Bcl10 is quickly recruited to some of the γH2AX foci at 5 min post-IR, showing a much stronger association with the foci at 1 h post-IR and accumulating in the foci at 4 h and 8 h post-IR. This is different from the kinetics

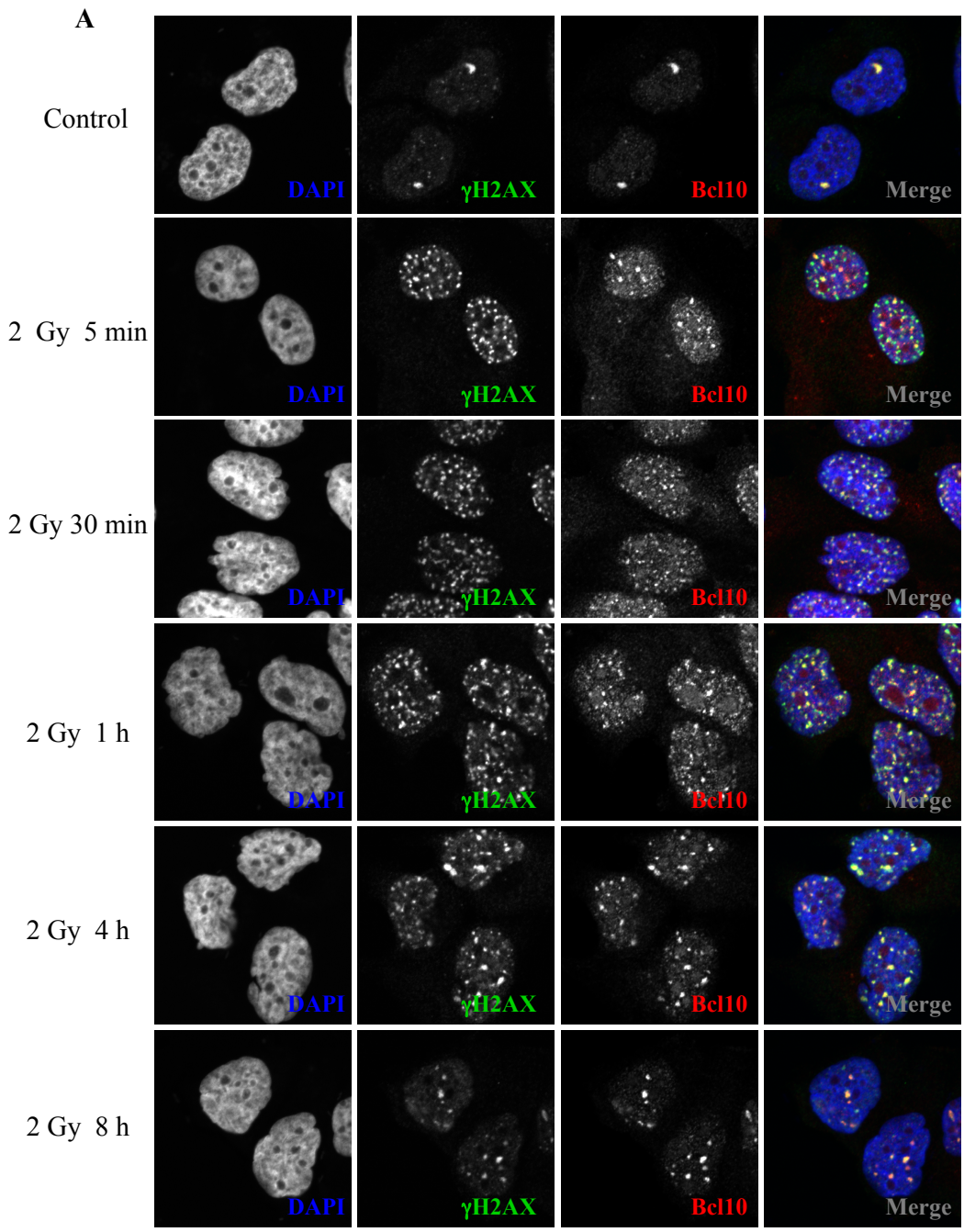

Figure 3.1 Bcl10 is recruited to ionizing radiation-induced foci in T47D cells (2 Gy). T47D cells were irradiated at 2 Gy and fixed in 3.7% formaldehyde after 5 mins, 30 mins, 1 h, 4 h, and 8 h, unirradiated cells were fixed and stained as a control. (A) Fixed cells were stained with mouse anti-γH2AX (FITC, green), rabbit anti-Bcl10 (Cy3, red), and counterstained with DAPI. (B) Fixed cells were stained with mouse anti-P-ATM (FITC, green), rabbit anti-Bcl10 (Cy3, red), and counterstained with DAPI.

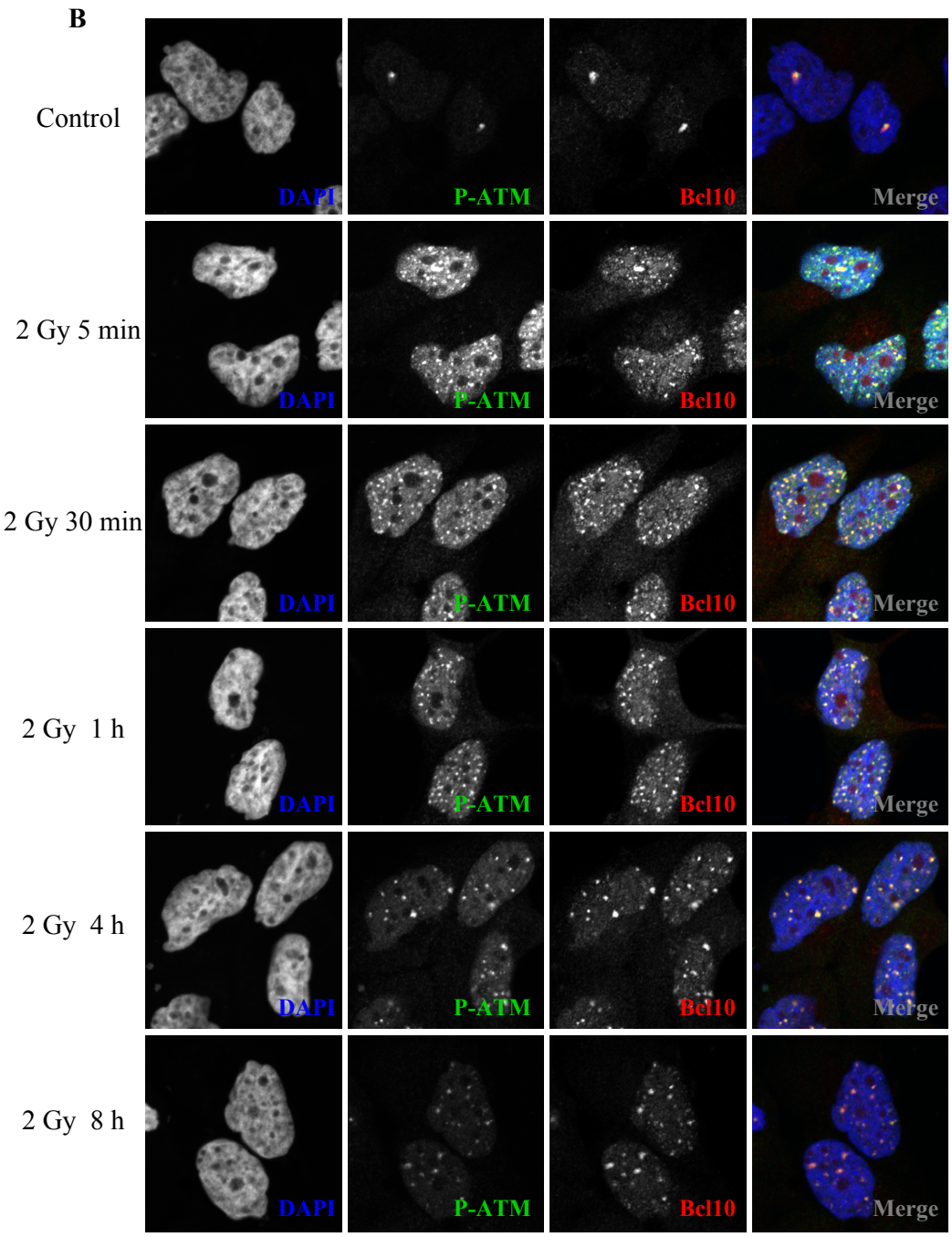
B
Control
2 Gy 5 min
2 Gy 30 min
2 Gy 1 h
2 Gy 4 h
2 Gy 8 h
DAPI
P-ATM
Bcl10
Merge

we observed when cells were treated with 2 Gy, suggesting a dose-dependent response. Bcl10 and P-ATM show a much stronger association throughout the time course; Bcl10 co-localizes with most of the P-ATM foci at 5 mins post-IR, co-localizing with 100% of the foci by 30 mins post-IR and remaining strongly associated out until 8 h post-IR (Figure 3.2B). Bcl10 foci closely resemble P-ATM, both in terms of the number of foci and the apparent quantity of the proteins in the foci at each time point (Figure 3.2B).

3.1.4 Bcl10 recruitment to ionizing radiation-induced foci is a wide spread phenomenon that is not restricted to breast cancer cells

In order to fully understand the role of Bcl10 in the nucleus, we wanted to determine if this descriptive phenomenon was an aberrant function of cancer cells or if it also occurred in normal human cells. Therefore, similar experiments were carried out in the human mammary epithelial cell line, hTERT-HME1, and the normal human foreskin fibroblast cell line, CRL-2522. hTERT-HME1 cells contain very few endogenous γH2AX/Bcl10 and P-ATM/Bcl10 foci (Figure 3.3A and 3.3B). We observed that following 2 Gy ionizing radiation Bcl10 is quickly recruited to IRIF co-localizing with 100% of the γH2AX and P-ATM foci at 30 mins post-IR, and becoming more prominent in the foci at later time points when the foci reduce in number (Figure 3.3A and 3.3B). Bcl10 is also rapidly recruited to IRIF following 5 Gy ionizing radiation, but does not co-localize with 100% of the γH2AX foci until 1 h post-IR, building up in the remaining foci at 4 h and 8 h post-IR (Figure 3.4A). Bcl10 shows a robust association with P-ATM co-

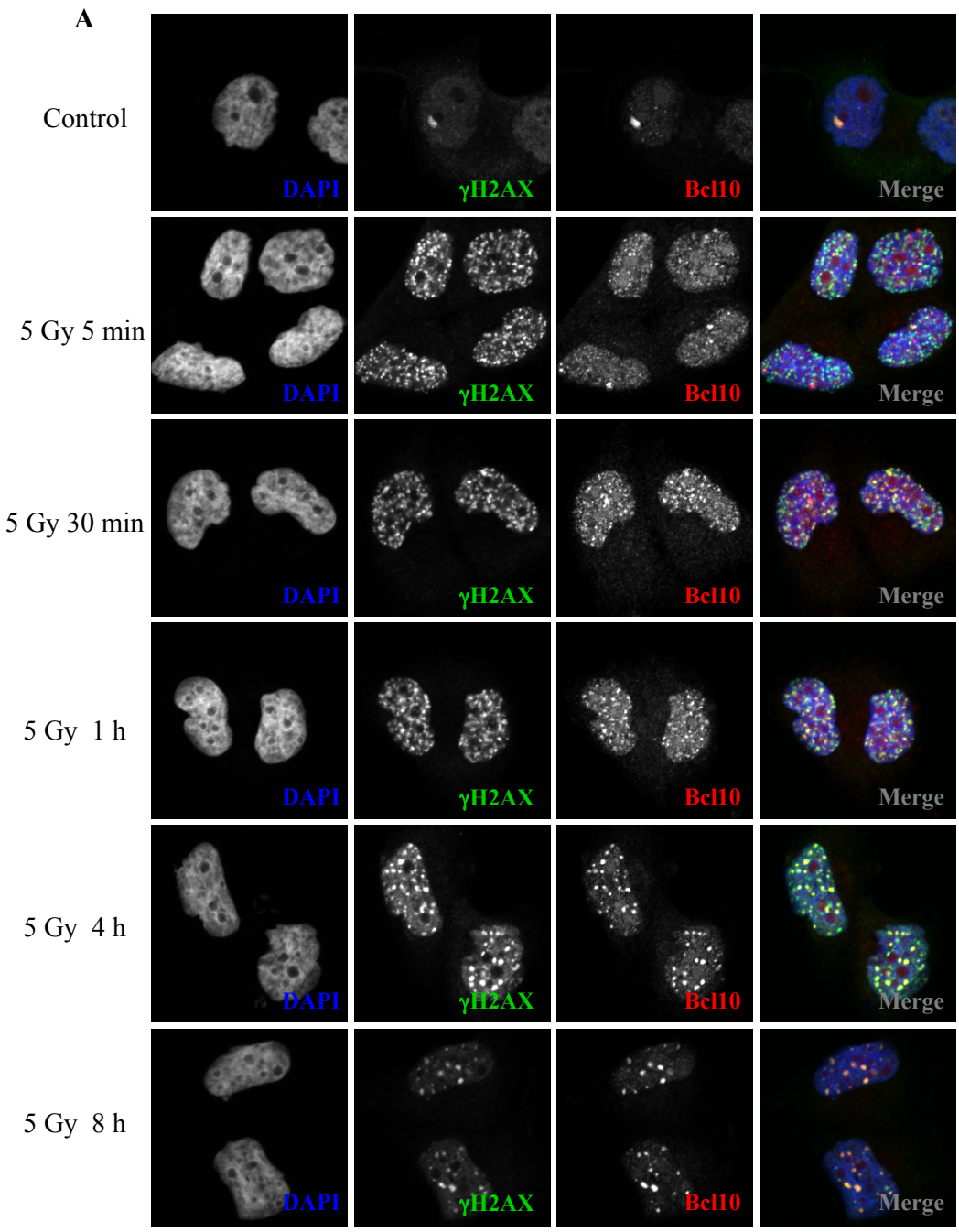

Figure 3.2 Bcl10 is recruited to ionizing radiation-induced foci in T47D cells (5 Gy). T47D cells were irradiated at 5 Gy and fixed in 3.7% formaldehyde after 5 mins, 30 mins, 1 h, 4 h, and 8 h, unirradiated cells were fixed and stained as a control. (A) Fixed cells were stained with mouse anti-γH2AX (FITC, green), rabbit anti-Bcl10 (Cy3, red), and counterstained with DAPI. (B) Fixed cells were stained with mouse anti-P-ATM (FITC, green), rabbit anti-Bcl10 (Cy3, red), and counterstained with DAPI.

B

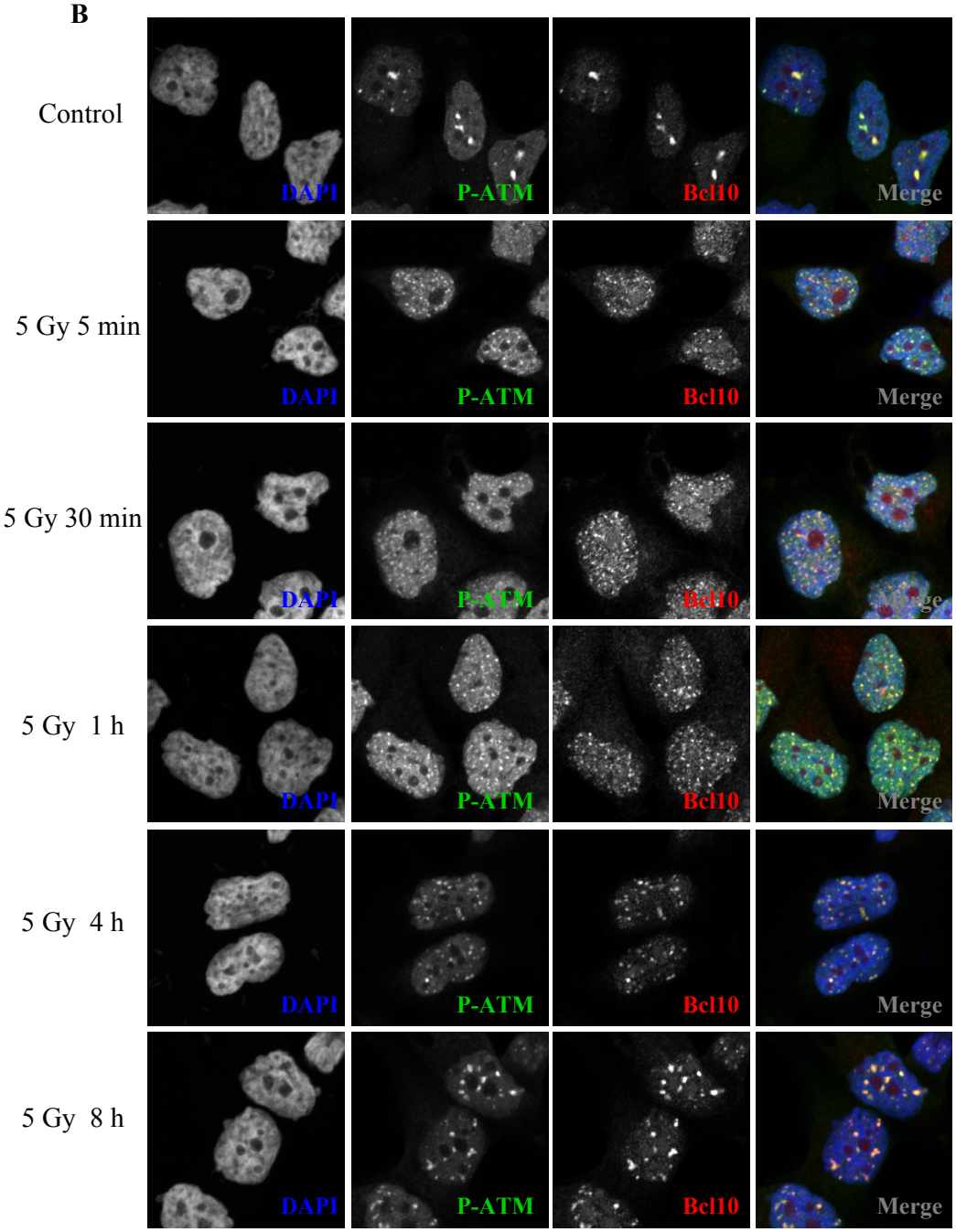
Control
5 Gy 5 min
5 Gy 30 min
5 Gy 1 h
5 Gy 4 h
5 Gy 8 h
DAPI
P-ATM
Bcl10
Merge

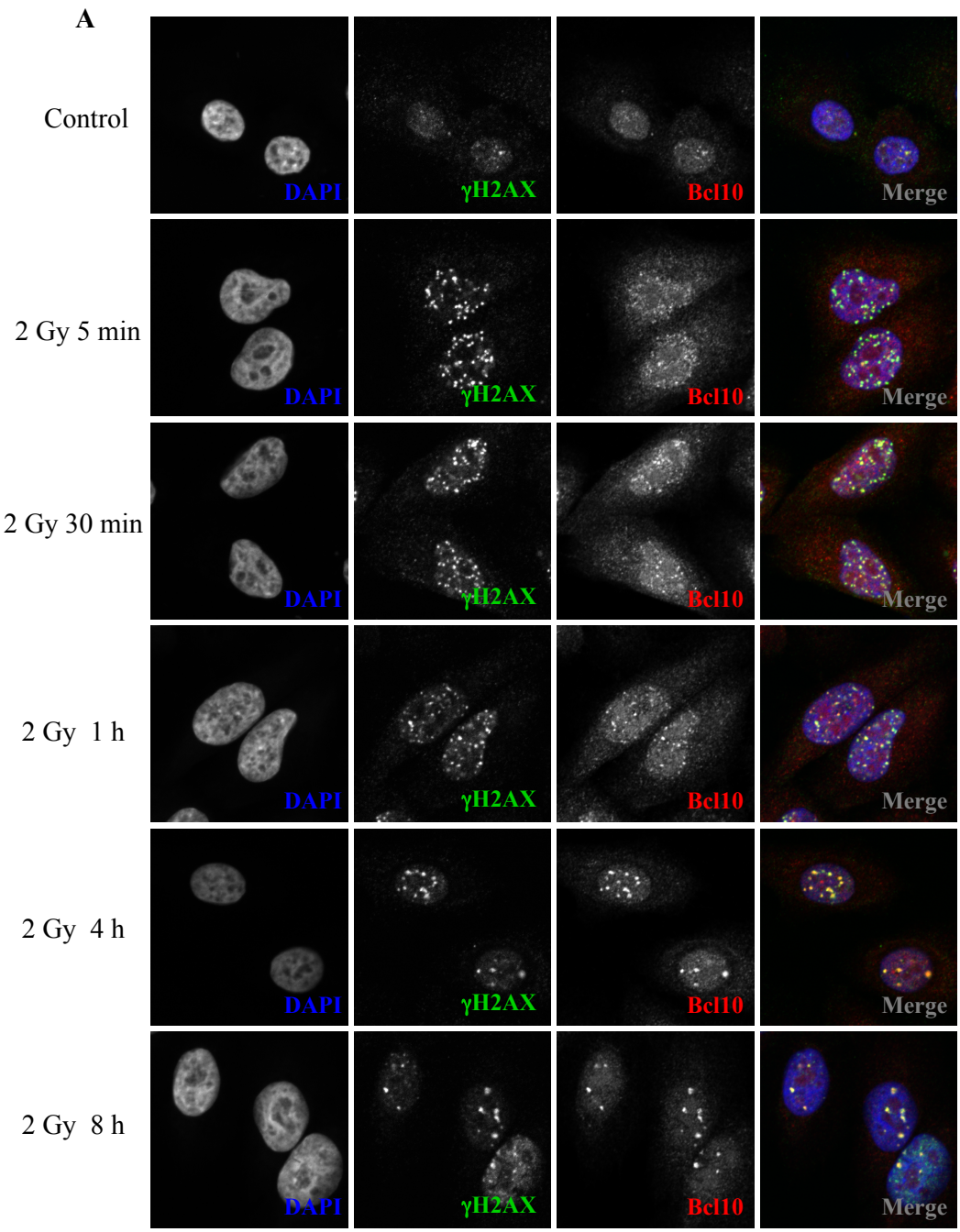

Figure 3.3 Bcl10 is recruited to ionizing radiation-induced foci in hTERT-HME1 cells (2 Gy). hTERT-HME1 cells were irradiated at 2 Gy and fixed in 3.7% formaldehyde after 5 mins, 30 mins, 1 h, 4 h, and 8 h, unirradiated cells were fixed and stained as a control. (A) Fixed cells were stained with mouse anti-γH2AX (FITC, green), rabbit anti-Bcl10 (Cy3, red), and counterstained with DAPI. (B) Fixed cells were stained with mouse anti-P-ATM (FITC, green), rabbit anti-Bcl10 (Cy3, red), and counterstained with DAPI.

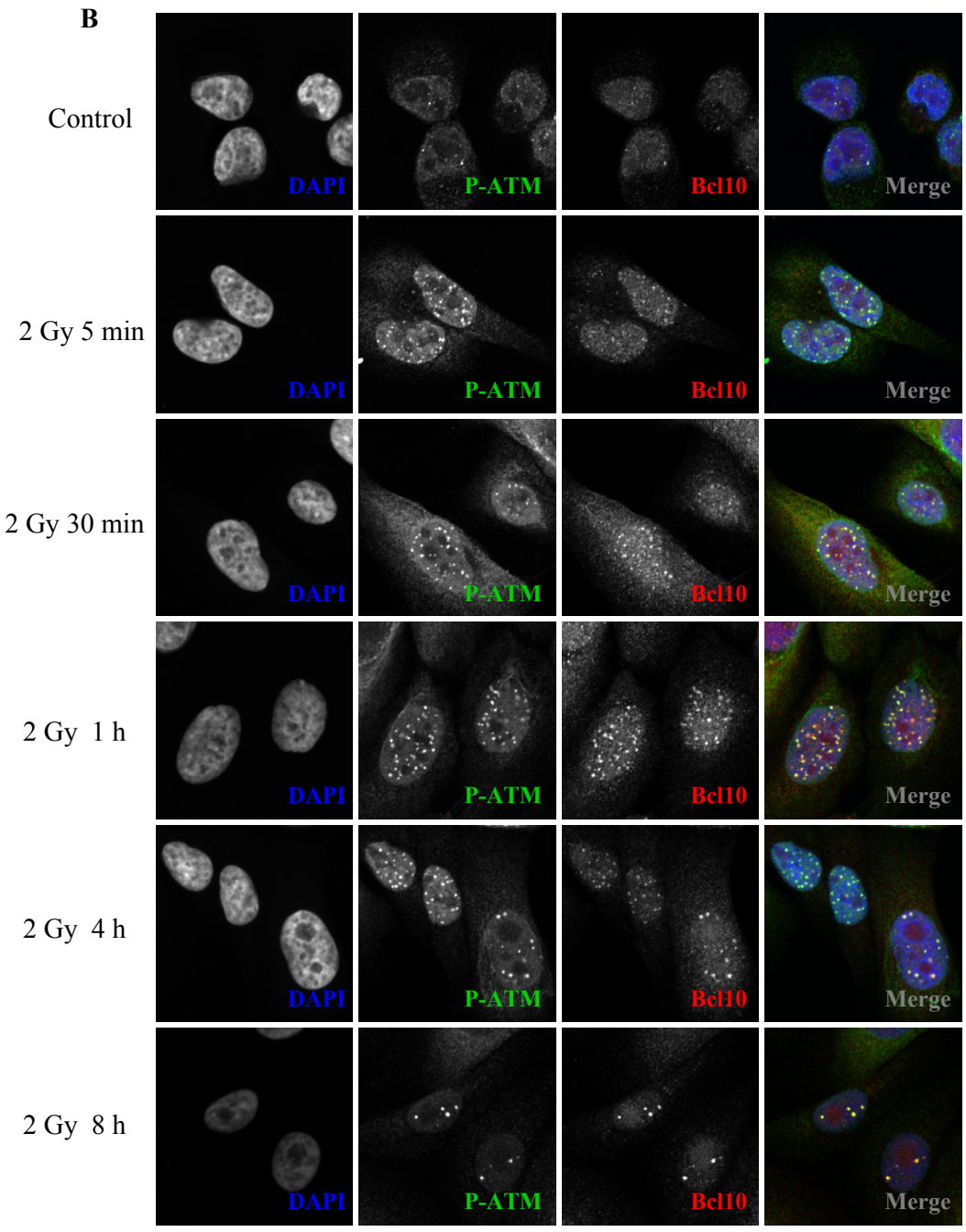
B
Control
2 Gy 5 min
2 Gy 30 min
2 Gy 1 h
2 Gy 4 h
2 Gy 8 h
DAPI
P-ATM
Bcl10
Merge

localizing with 100% of the P-ATM foci even at 30 mins post-IR (Figure 3.4B). Bcl10 therefore appears to be particularly important in stabilizing foci that contain activated ATM.

Similar to hTERT-HME1 cells, normal skin fibroblasts (CRL-2522 cells) contain very few endogenous γH2AX/Bcl10 and P-ATM/Bcl10 foci (Figure 3.5). In these cells Bcl10 is recruited to 100% of the γH2AX foci by 5 mins post-IR with 2 Gy and remains associated with these foci at the later time points (Figure 3.5). This trend is maintained when the cells are treated with 5 Gy (Figure 3.6).

3.2 Bcl10 plays a minor role in radiation-induced NF-κB activation while MALT1 is absolutely required

It has been extensively demonstrated that Bcl10 and MALT1 are important for NF-κB activation in the cytoplasm of lymphoid cells in response to various types of stimuli. We wanted to investigate whether Bcl10 and MALT1 are important for radiation-induced NF-κB activation in breast cancer cells. NF-κB proteins, such as p65, are held in the cytoplasm by an IκB inhibitory complex [14]. When activation occurs, the IκB complex is targeted for degradation and the NF-κB proteins are released, allowing them to translocate into the nucleus and mediate transcription [14]. We used RNA interference to transiently knockdown Bcl10 and MALT1 in T47D cells (a scrambled siRNA control was included in every experiment) and then monitored NF-κB activation in response to radiation using two different approaches: i) measuring NF-κB p65 translocation from the

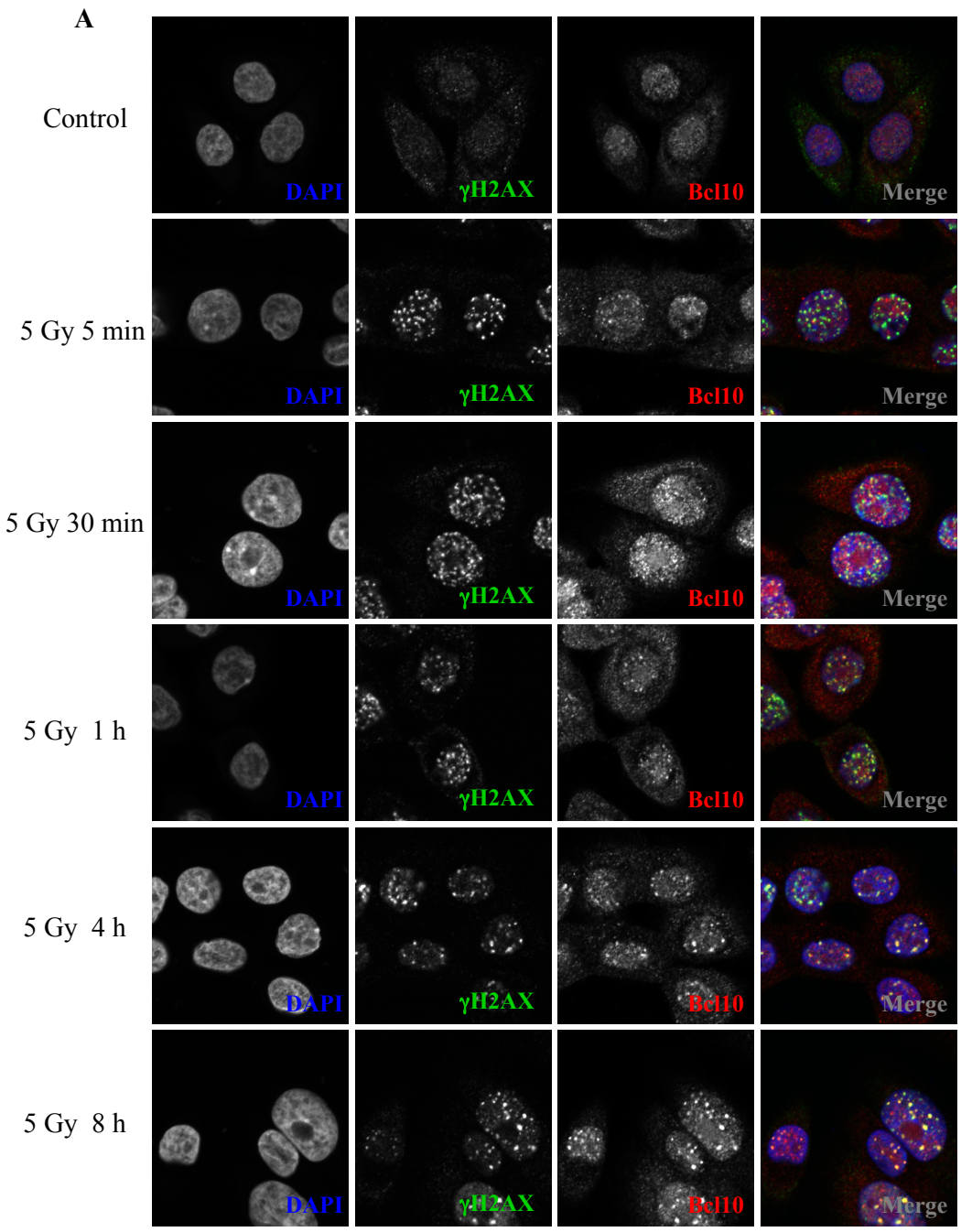

Figure 3.4 Bcl10 is recruited to ionizing radiation-induced foci in hTERT-HME1 cells (5 Gy). hTERT-HME1 cells were irradiated at 5 Gy and fixed in 3.7% formaldehyde after 5 mins, 30 mins, 1 h, 4 h, and 8 h, unirradiated cells were fixed and stained as a control. (A) Fixed cells were stained with mouse anti-γH2AX (FITC, green), rabbit anti-Bcl10 (Cy3, red), and counterstained with DAPI. (B) Fixed cells were stained with mouse anti-P-ATM (FITC, green), rabbit anti-Bcl10 (Cy3, red), and counterstained with DAPI.

B

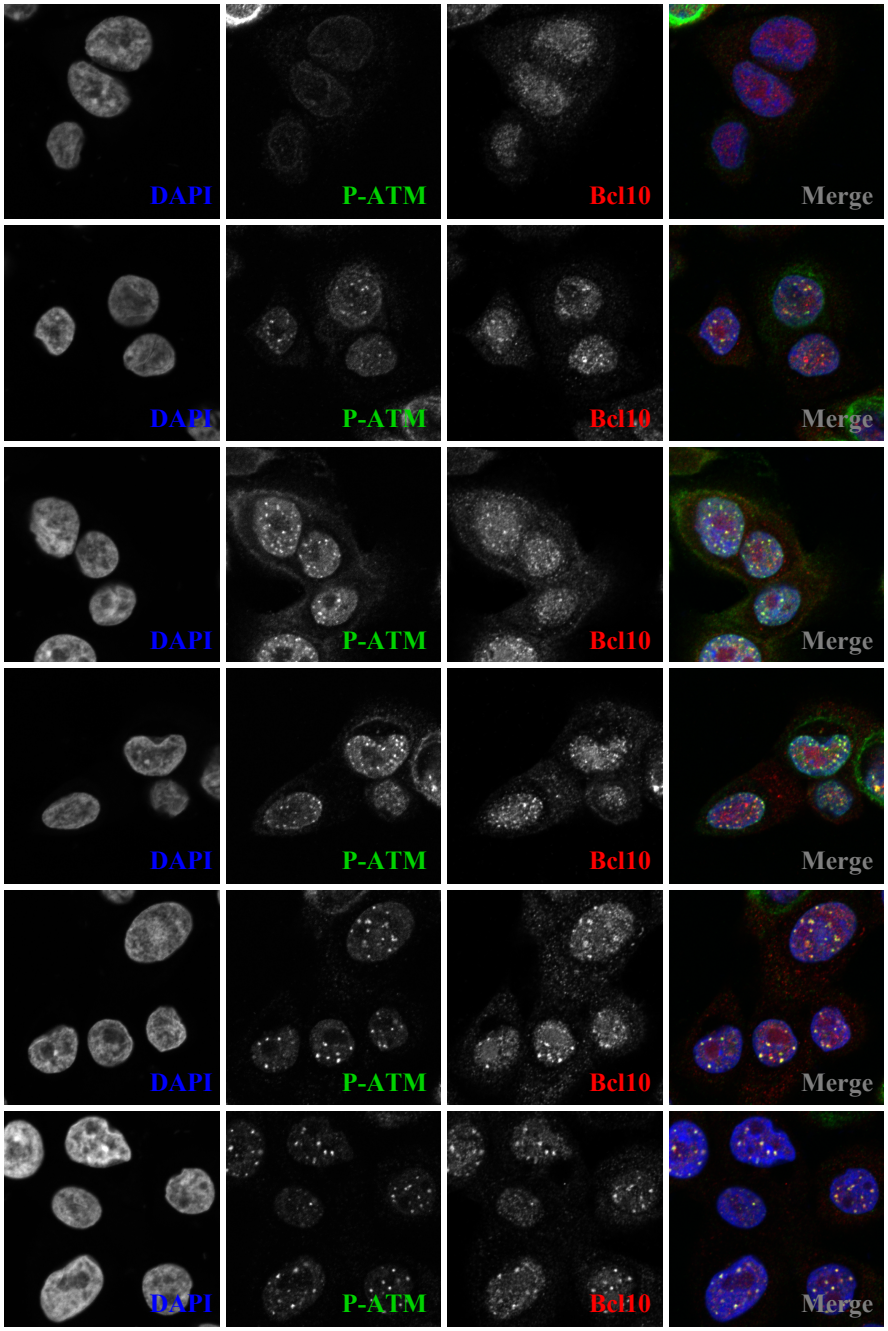
Control
5 Gy 5 min
5 Gy 30 min
5 Gy 1 h
5 Gy 4 h
5 Gy 8 h
DAPI
P-ATM
Bcl10
Merge

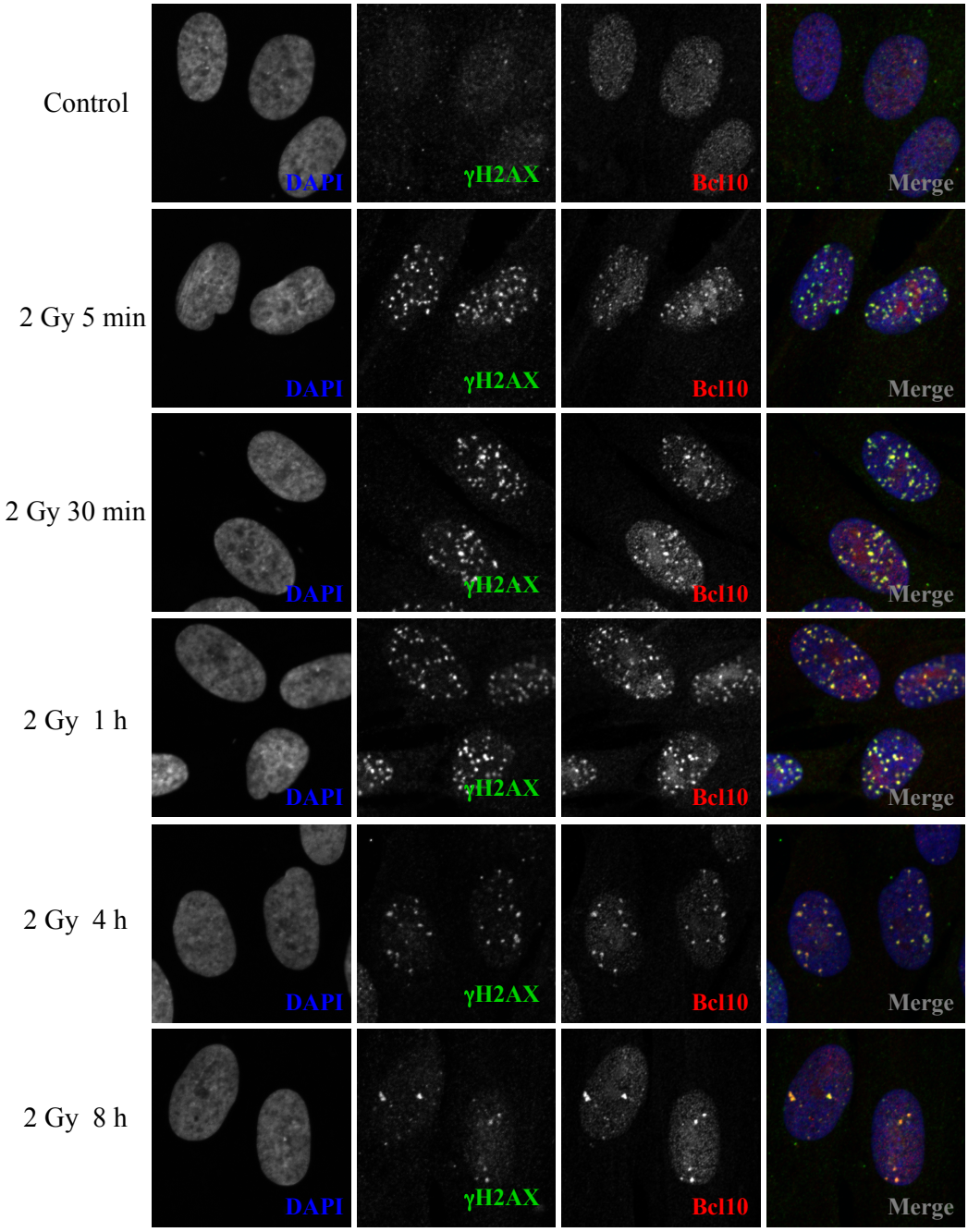

Figure 3.5 Bcl10 is recruited to ionizing radiation-induced foci in CRL-2522 cells (2 Gy). CRL-2522 cells were irradiated at 2 Gy and fixed in 3.7% formaldehyde after 5 mins, 30 mins, 1 h, 4 h, and 8 h, unirradiated cells were fixed and stained as a control.Fixed cells were stained with mouse anti-γH2AX (FITC, green), rabbit anti-Bcl10 (Cy3, red), and counterstained with DAPI

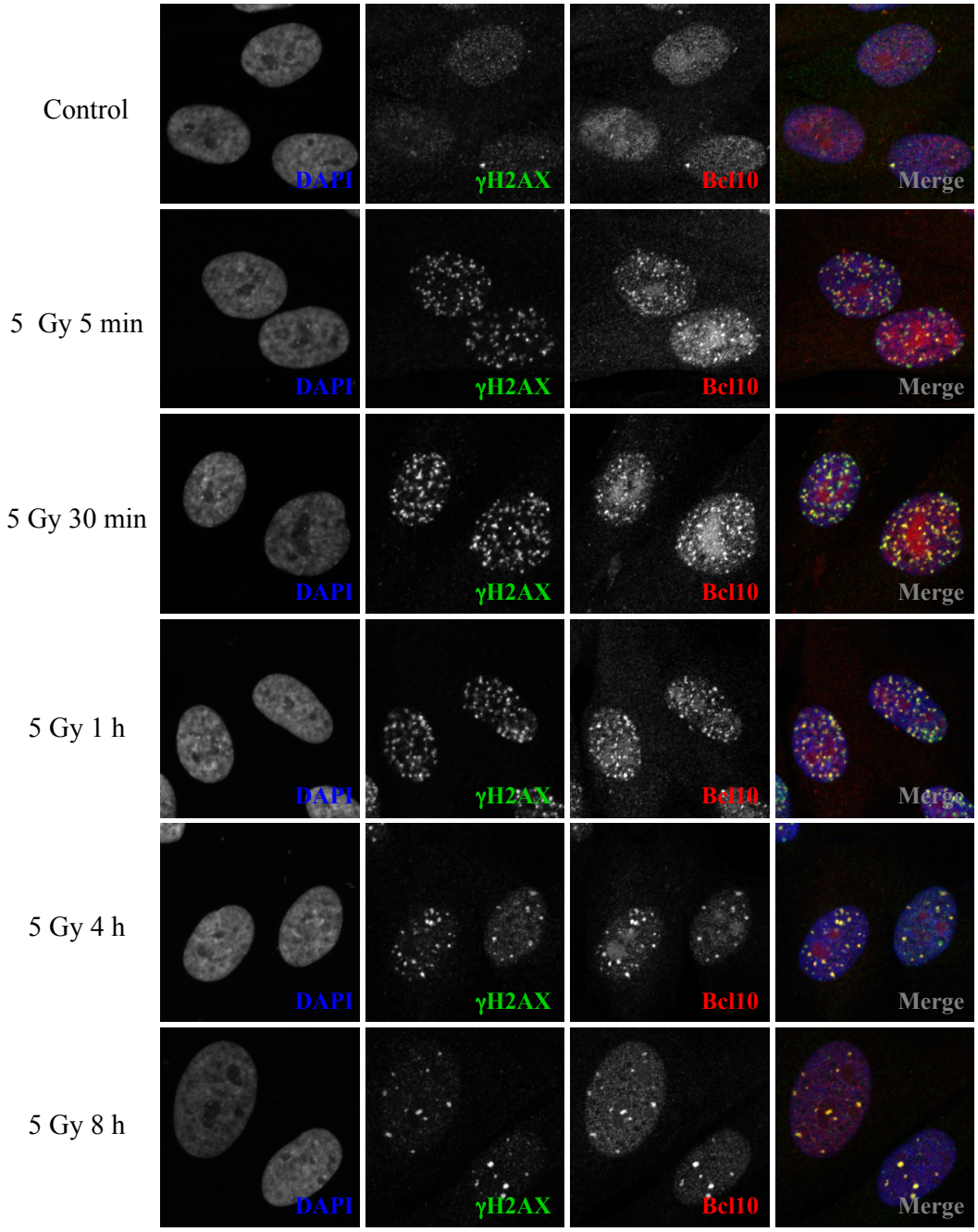

Figure 3.6 Bcl10 is recruited to ionizing radiation-induced foci in CRL-2522 cells (5 Gy). CRL-2522 cells were irradiated at 5 Gy and fixed in 3.7% formaldehyde after 5 mins, 30 mins, 1 h, 4 h, and 8 h, unirradiated cells were fixed and stained as a control.Fixed cells were stained with mouse anti-γH2AX (FITC, green), rabbit anti-Bcl10 (Cy3, red), and counterstained with DAPI.

cytoplasm to the nucleus using immunofluorescence, and ii) by monitoring the degradation of the NF-κB inhibitory protein, IκBα, via western blot.

3.2.1 Bcl10 knockdown slightly impairs radiation-induced p65 nuclear translocation

T47D cells were transfected with Bcl10 siRNA and at 48 h post-transfection cells were subjected to 5 Gy and NF-κB p65 nuclear localization was monitored at 15, 30, 60, 90, and 120 mins post-IR. In cells with reduced Bcl10 levels, we see a slight increase in nuclear p65 staining at 15 mins post-IR. This level remains constant at 30 and 60 mins post-IR and then decreases to levels that are similar to the unirradiated control at 90 and 120 mins (Figure 3.7A). In the cells transfected with the scrambled siRNA (Mock), we see a slight increase in nuclear p65 at 15 and 30 mins post-IR, and then a significant increase at 60 mins with maintenance of these levels out to 120 mins post-IR (Figure 3.7B).

The average nuclear intensity of p65 staining for ~100 cells (25 cells per experiment; pool of 4 separate experiments) was quantified using Metamorph. At all the time points, cells treated with Bcl10 siRNA have a lower average nuclear p65 intensity then the mock-transfected cells. The difference in average nuclear p65 intensity between Bcl10 siRNA and mock-transfected cells was significantly different at 90 and 120 mins post-IR, as assessed by a one-tail T-test ($p<0.05$) (Figure 3.7C).

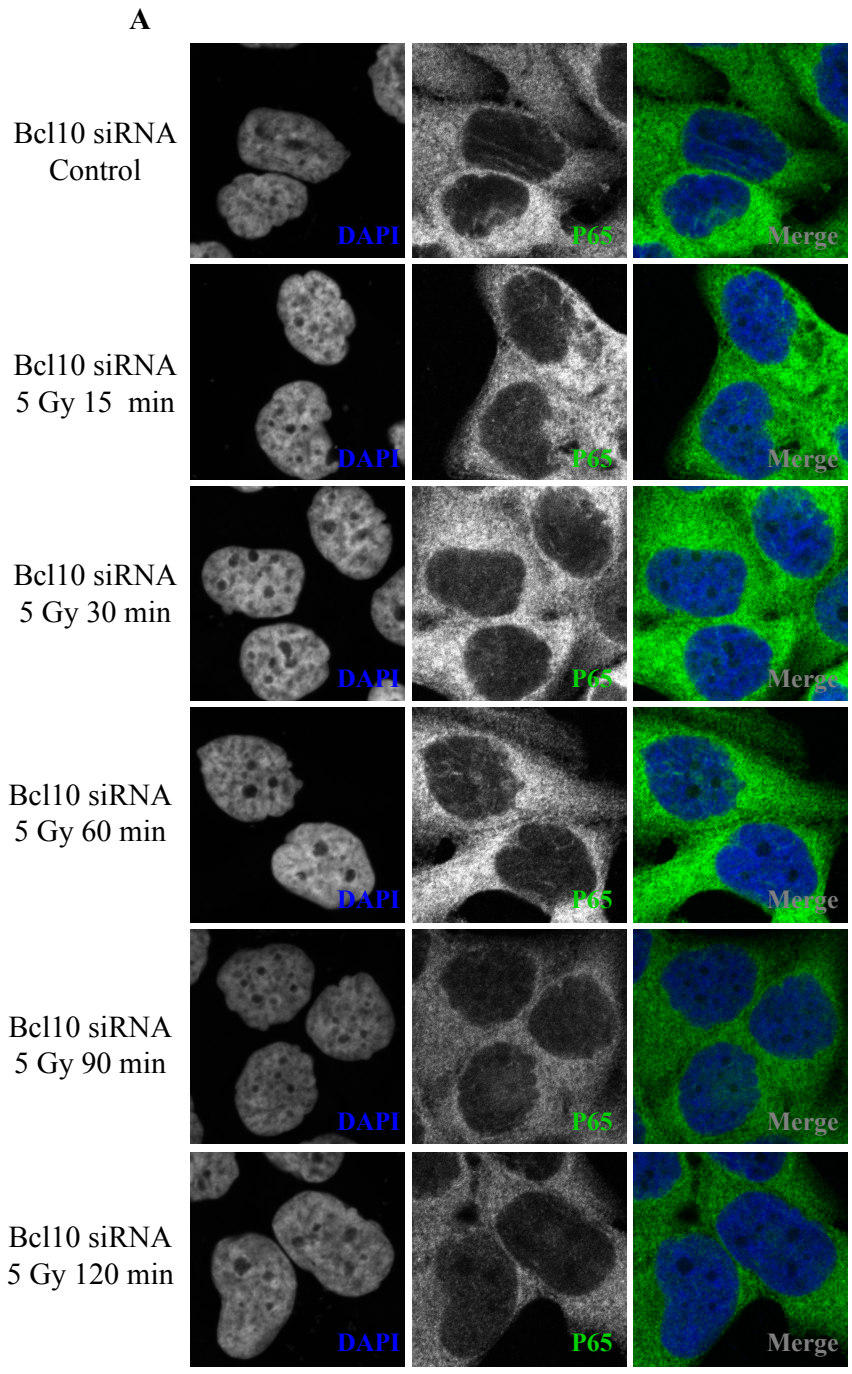

Figure 3.7 Bcl10 knockdown inhibits DNA damage-induced NF-κB p65 nuclear translocation. T47D cells were transfected with Bcl10 siRNA (A) or a scrambled siRNA (B); 48 h post-transfection cells were exposed to 5 Gy ionizing radiation and fixed in 3.7% formaldehyde 15, 30, 60, 90, and 120 mins post-IR. Unirradiated cells were fixed as a control. Fixed cells were stained with mouse anti-p65 (FITC, green) and counterstained with DAPI. (C) Average nuclear p65 intensity was measured using Metamorph. Error bars represent SEM.

B

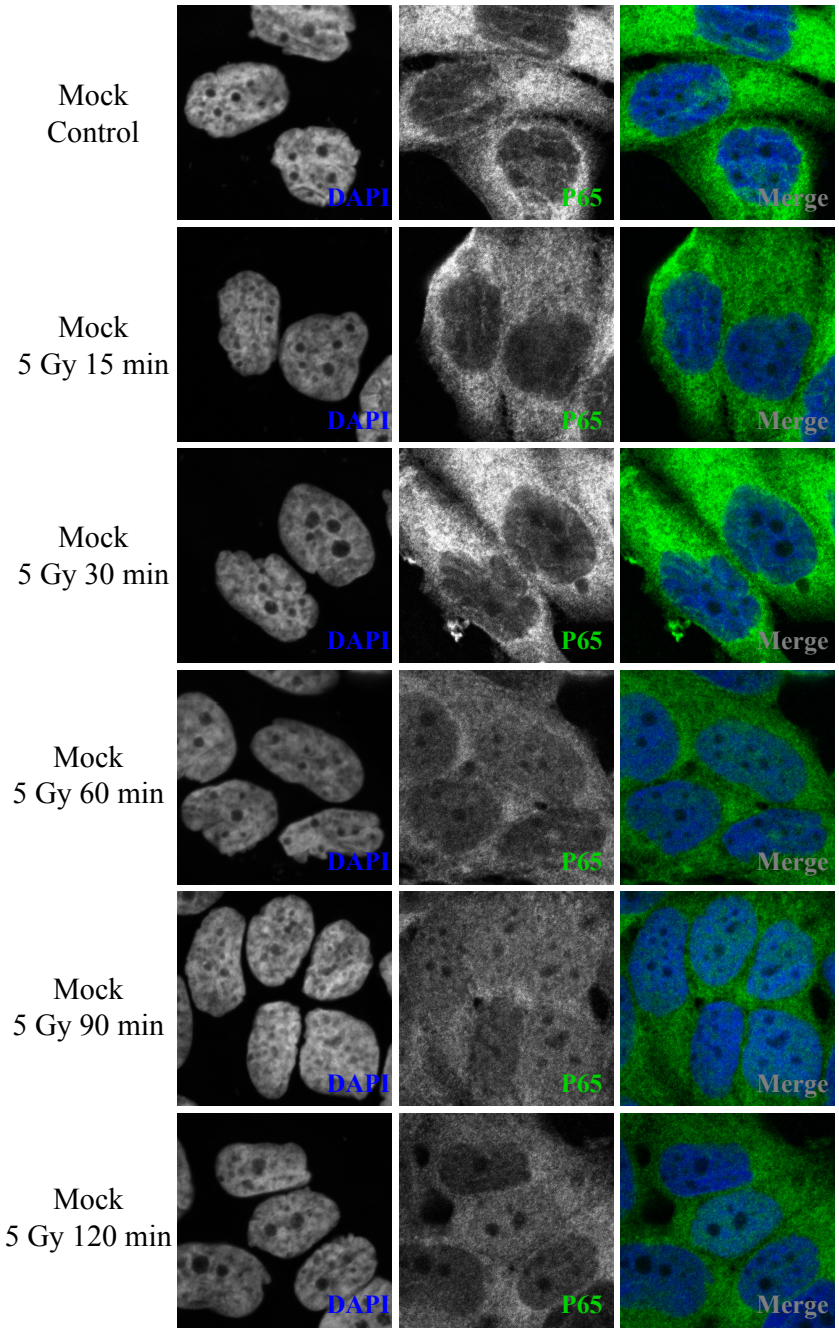
Mock
Control
Mock
5 Gy 15 min
Mock
5 Gy 30 min
Mock
5 Gy 60 min
Mock
5 Gy 90 min
Mock
5 Gy 120 min
DAPI
P65
Merge

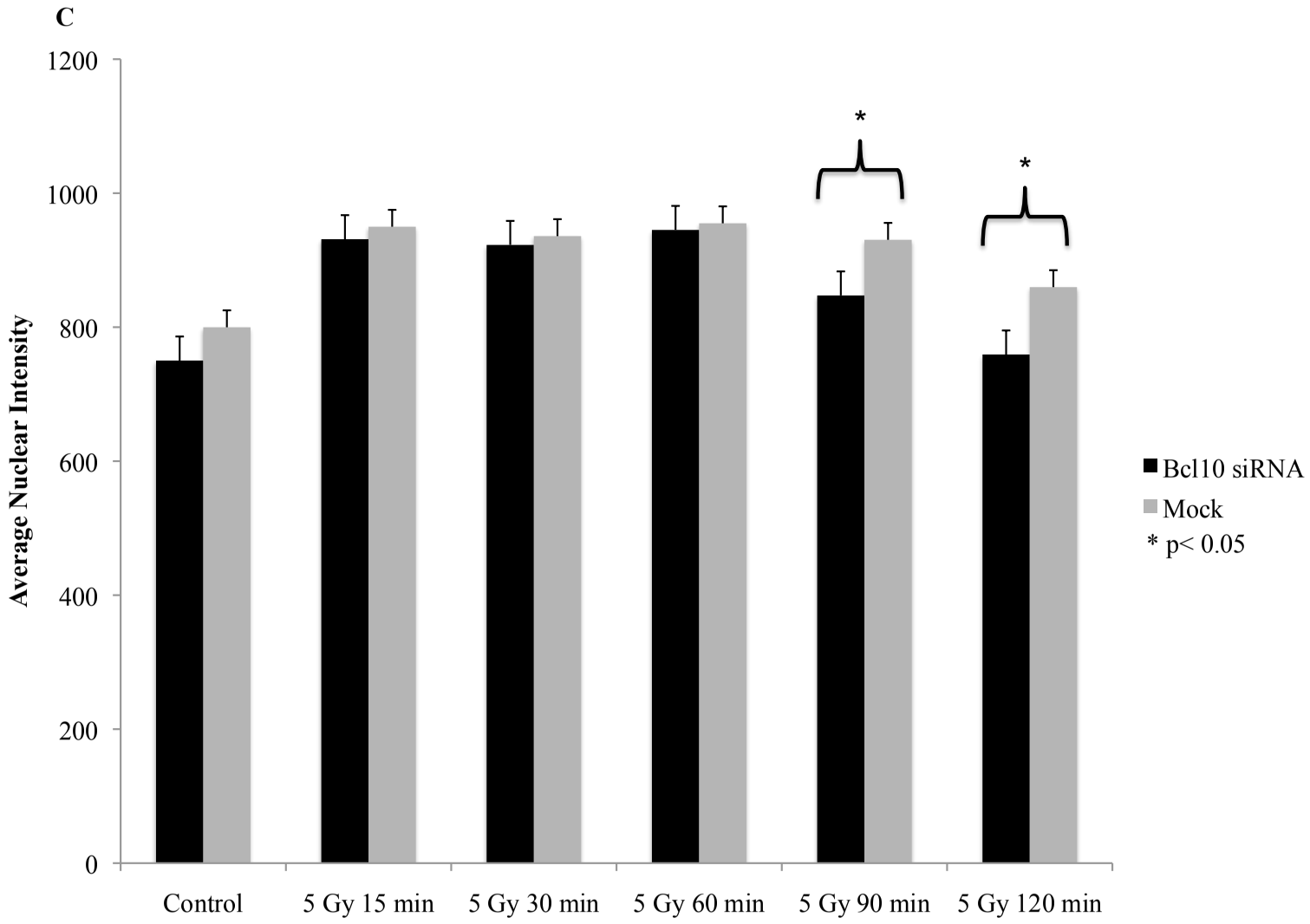
C
1200
1000
800
600
400
200
0
Average Nuclear Intensity
*
*
Control
5 Gy 15 min
5 Gy 30 min
5 Gy 60 min
5 Gy 90 min
5 Gy 120 min
Bcl10 siRNA
Mock
* p< 0.05

3.2.2 Bcl10 knockdown delays radiation-induced IκBα degradation

To confirm the p65 results, we also monitored NF-κB activation by measuring IκBα degradation. At 48 h post-transfection cells were irradiated at 5 Gy and the protein was isolated at 15, 30, 60, 90 and 120 mins post-IR and analyzed by western blot. As shown in Figure 3.8, cells transfected with Bcl10 siRNA maintain fairly constant IκBα levels until 120 mins post-IR where we begin to see a decrease. In comparison, the mock-transfected cells show a continual decrease in IκBα protein levels from the unirradiated control to 90 mins post-IR and then a slight increase at 120 mins (Figure 3.8). This is reflected in the relative intensity of the IκBα protein band normalized to the actin control (Figure 3.8).

3.2.3 MALT1 knockdown significantly compromises radiation-induced p65 nuclear translocation

Transient knockdown of MALT1 has a more dramatic effect on NF-κB activation in response to irradiation than Bcl10 knockdown. Following treatment with 5 Gy, MALT1 siRNA transfected cells show very little p65 nuclear translocation at 15, 30, 60, 90 and 120 mins post-IR (Figure 3.9A). In mock-transfected cells however, nuclear p65 levels begin to increase at 30 mins post-IR, hitting a maximum at 60 mins, with maintenance of these levels up to 120 mins (Figure 3.9B). Quantitation of these images revealed that cells treated with MALT1 siRNA have significantly lower p65 nuclear intensities than the mock-transfected cells at 15 ($p<0.01$), 30, 60, 90 and 120 mins post-IR and significantly higher levels in the unirradiated control ($p<0.0001$) (Figure 3.9C)

Figure 3.8 Bcl10 knockdown inhibits DNA damage-induced NF-κB IκBα degradation. T47D cells were transfected with Bcl10 siRNA or a scrambled siRNA; 48 h post-transfection cells were exposed to 5 Gy ionizing radiation and whole cell lysates were isolated 15, 30, 60, 90, and 120 mins post-IR. Whole cell lysates was isolated from unirradiated cells as a control. Samples were electrophoresed in a 10%, (the top two bands, IκBα and actin) or 12% (bottom two bands, Bcl10 and actin) SDS-polyacrylamide gel. The samples were transferred to a nitrocellulose membrane and immunostained with rabbit anti-IκBα, mouse anti-actin, and rabbit anti-Bcl10. Primary antibodies were detected with goat anti-mouse IgG-peroxidase or goat anti-rabbit IgG-peroxidase and developed with Amersham ECL Western Blotting Detection Reagent.

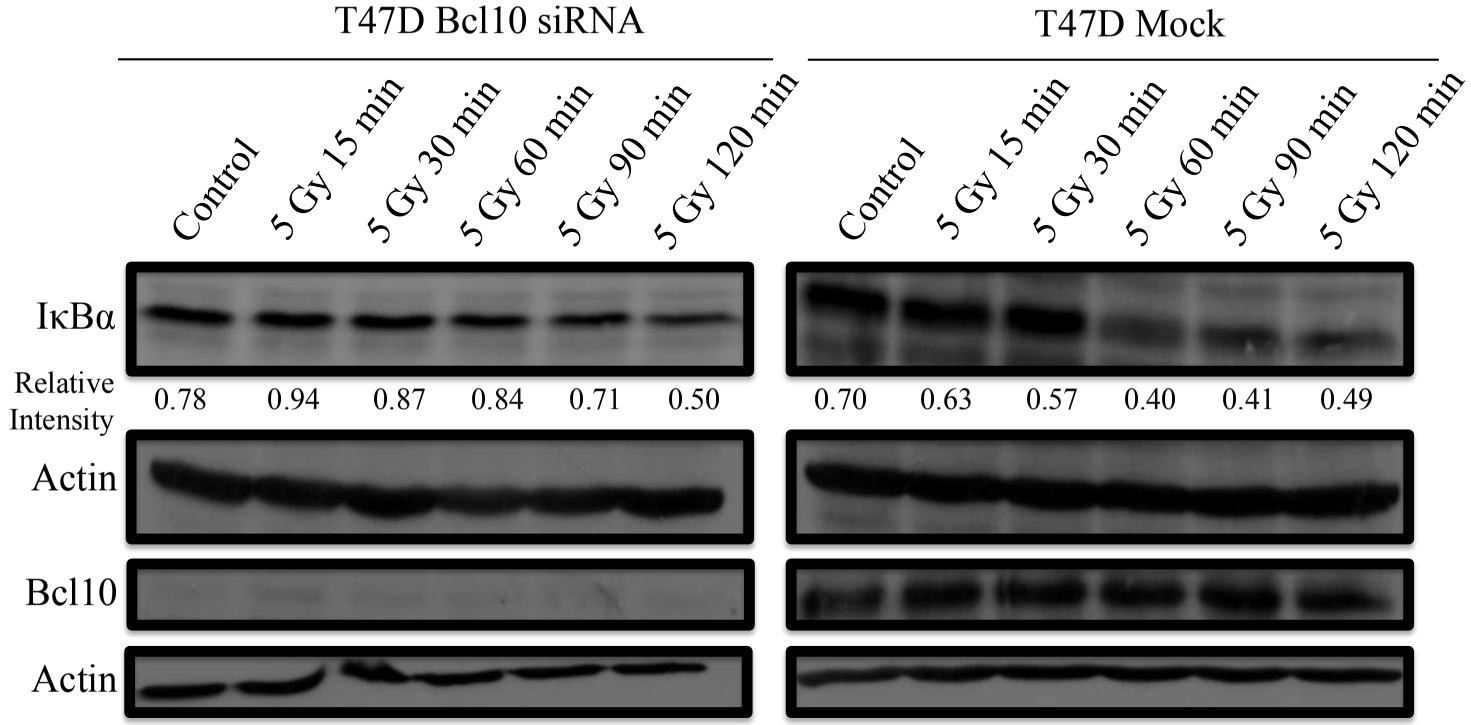
T47D Bcl10 siRNA
T47D Mock
Control
5 Gy 15 min
5 Gy 30 min
5 Gy 60 min
5 Gy 90 min
5 Gy 120 min
IκBα
Relative Intensity
0.78 0.94 0.87 0.84 0.71 0.50
0.70 0.63 0.57 0.40 0.41 0.49
Actin
Bcl10
Actin

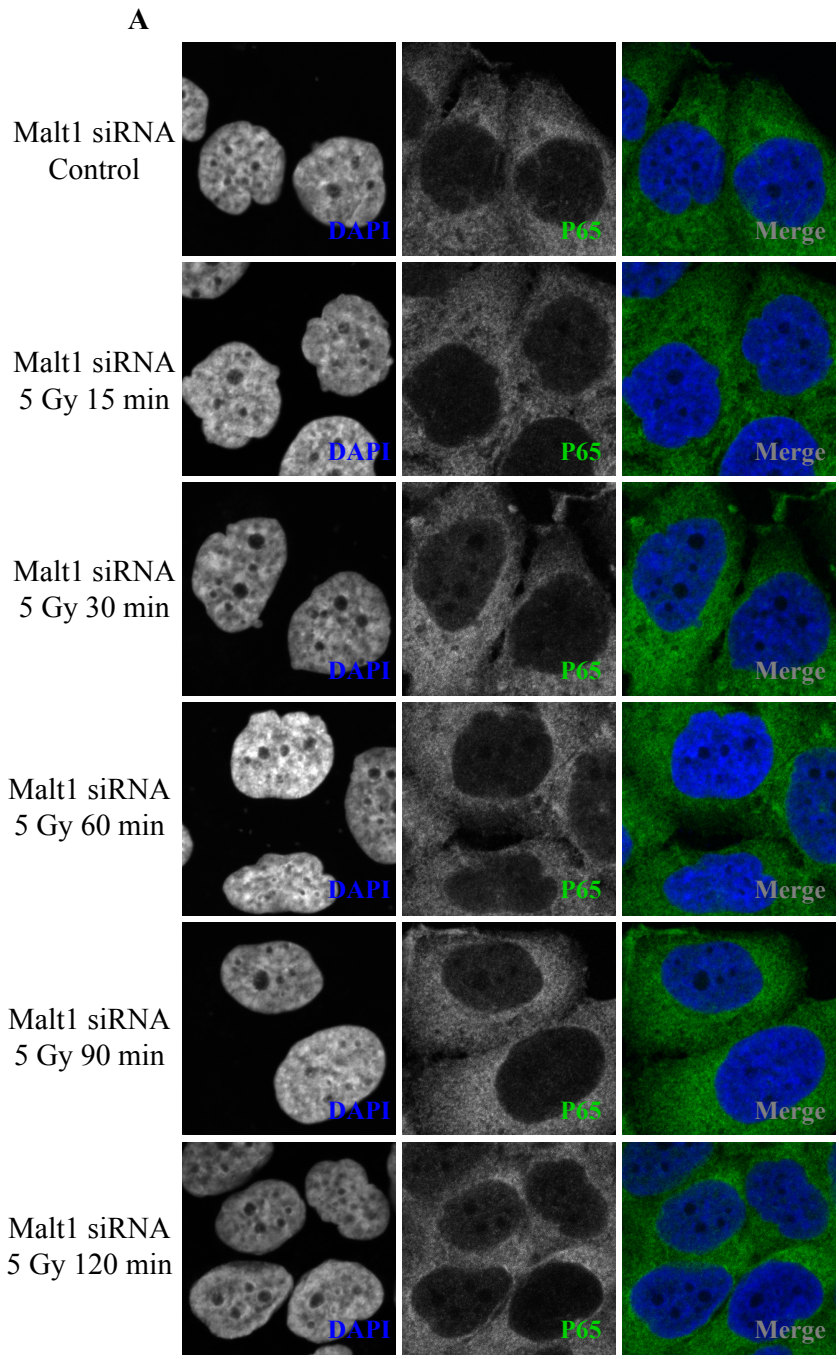

Figure 3.9 MALT1 knockdown inhibits DNA damage-induced NF-κB p65 nuclear translocation. T47D cells were transfected with MALT1 siRNA (A) or a scrambled siRNA (B); 48 h post-transfection cells were exposed to 5 Gy ionizing radiation and fixed in 3.7% formaldehyde 15, 30, 60, 90, and 120 mins post-IR. Unirradiated cells were fixed as a control. Fixed cells were stained with mouse anti-p65 (FITC, green) and counterstained with DAPI. (C) Average nuclear p65 intensity was measured using Metamorph. Error bars represent SEM.

B

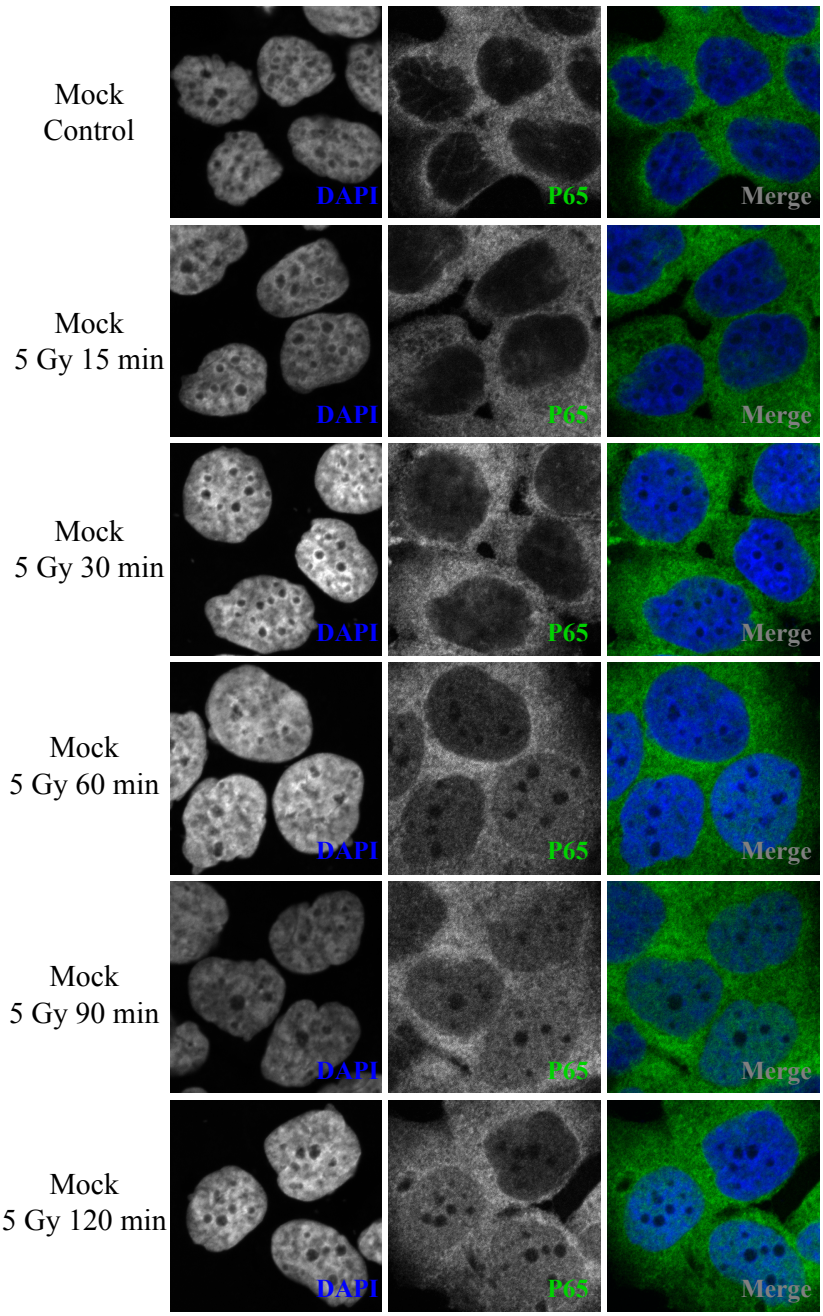
Mock Control
DAPI
P65
Merge
Mock 5 Gy 15 min
DAPI
P65
Merge
Mock 5 Gy 30 min
DAPI
P65
Merge
Mock 5 Gy 60 min
DAPI
P65
Merge
Mock 5 Gy 90 min
DAPI
P65
Merge
Mock 5 Gy 120 min
DAPI
P65
Merge

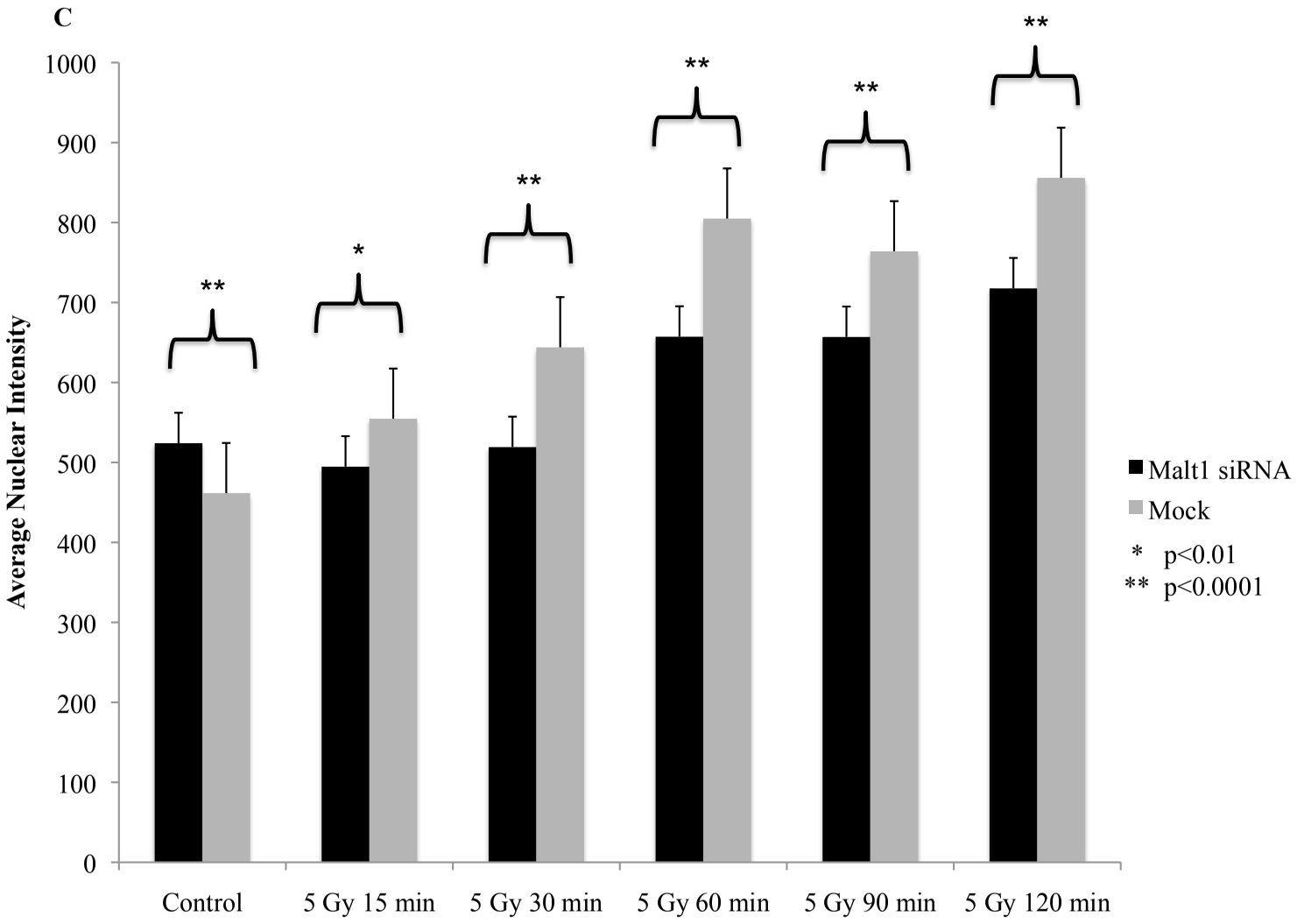
C
Average Nuclear Intensity
1000
900
800
700
600
500
400
300
200
100
0
**
*
**
**
**
**
Control
5 Gy 15 min
5 Gy 30 min
5 Gy 60 min
5 Gy 90 min
5 Gy 120 min
Malt1 siRNA
Mock
* p<0.01
** p<0.0001

3.2.4 MALT1 knockdown inhibits radiation-induced IκBα degradation

IκBα degradation analysis confirmed the p65 results. Mock-transfected cells begin to show a decrease in IκBα levels at 30 mins post-IR with 5 Gy, a further decrease at 60 mins and maintenance out to 120 mins (Figure 3.10). In contrast, MALT1 siRNA transfected cells show fairly constant IκBα levels comparable to the unirradiated control to 120 mins post-IR, an indication that there is no NF-κB activation. These observations are supported by the relative intensities of the IκBα protein bands normalized to the actin control (Figure 3.10).

3.3 Bcl10 is required for efficient repair of radiation-induced DNA Damage

3.3.1 Bcl10 knockdown significantly diminishes the repair of radiation-induced DNA damage in T47D cells

We observed that Bcl10 plays only a minimal role in radiation-induced NF-κB activation, so we wanted to determine if it had an alternative function in the nucleus. In particular, we wanted to determine if Bcl10 is important for the repair of radiation-induced DNA damage. To assess this, we performed comet assays with electrophoresis under neutral pH, conditions that allow the detection of mostly DSB. With this assay, DNA damage is assessed by the amount of DNA present in the tails of the comets, where more DNA damage results in a higher percentage of DNA being present in the tail. We observed that T47D Bcl10 siRNA transfected cells have larger comet tails at 48 h post-transfection than the mock-transfected and non-transfected controls prior to irradiation (Figure 3.11A). At 2 h post-IR with 5 Gy, all the treatments have similar length comet tails, at 4

Figure 3.10 MALT1 knockdown inhibits DNA damage-induced NF-κB IκBα degradation. T47D cells were transfected with MALT1 siRNA or a scrambled siRNA; 48 h post-transfection cells were exposed to 5 Gy ionizing radiation and whole cell lysates were isolated 15, 30, 60, 90, and 120 mins post-IR. Whole cell lysates was isolated from unirradiated cells as a control. Samples were electrophoresed in a 10%, SDS-polyacrylamide gel. The samples were transferred to a nitrocellulose membrane and immunostained with rabbit anti-IκBα, mouse anti-actin, and rabbit anti-Bcl10. Primary antibodies were detected with goat anti-mouse IgG-peroxidase or goat anti-rabbit IgG-peroxidase and developed with Amersham ECL Western Blotting Detection Reagent.

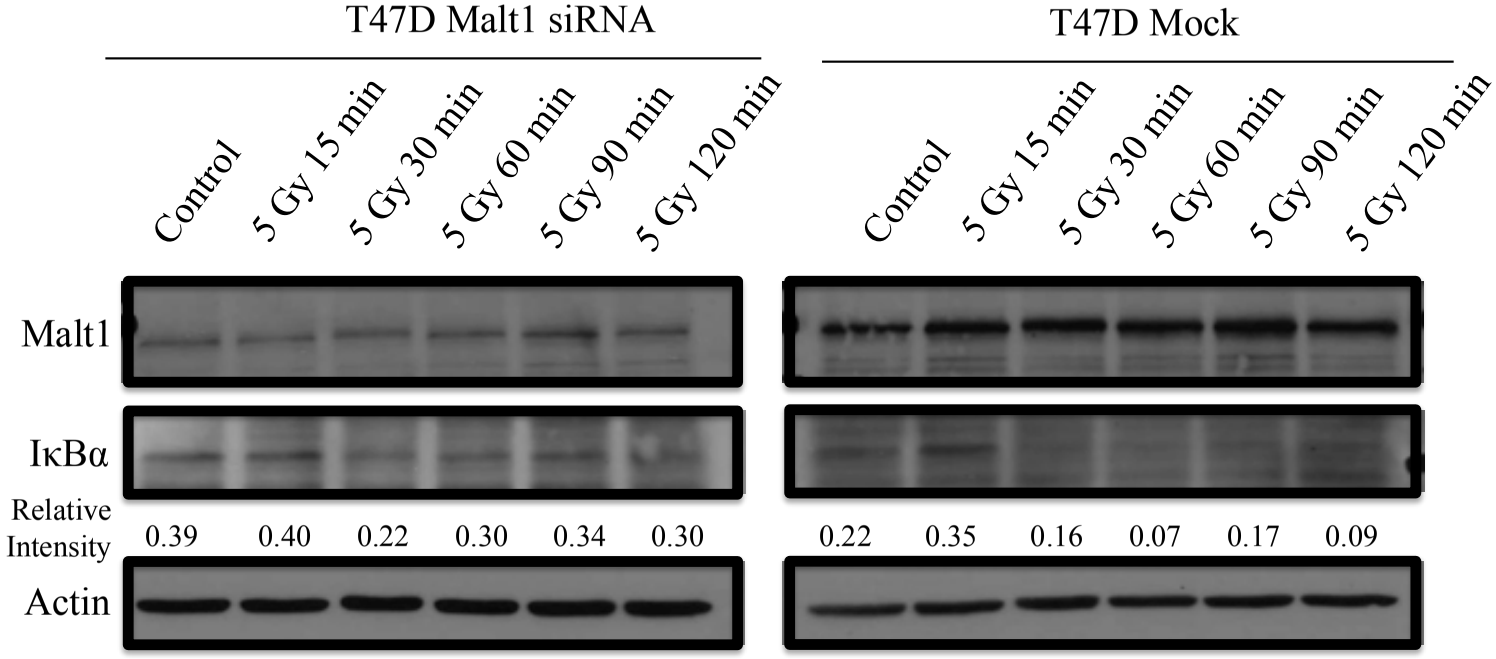
T47D Malt1 siRNA
T47D Mock
Control
5 Gy 15 min
5 Gy 30 min
5 Gy 60 min
5 Gy 90 min
5 Gy 120 min
Malt1
IκBα
Relative Intensity
0.39 0.40 0.22 0.30 0.34 0.30
0.22 0.35 0.16 0.07 0.17 0.09
Actin

h post-IR mock-transfected and non-transfected cells begin to show a reduction in tail length and by 24 h have tail lengths similar to their unirradiated controls (Figure 3.11A). The Bcl10 siRNA transfected cells however, show an increase in tail length from 2 h to 4 h and a further increase at 24 h post-IR (Figure 3.11A). The percent of DNA in the tail was quantified using CometScore (TriTek Corp.). Bcl10 siRNA treated cells have a statistically significant higher percentage of DNA in the tail compared to the mock and non-transfected cells in the unirradiated control and at 4 h and 24 h post-IR ($p<0.00001$) (Figure 3.11B). This is indicative that these cells have a repair defect, and suggests that Bcl10 is important for the repair of radiation-induced DNA damage. Figure 3.11C shows a graph of the earlier time points; for all treatments the most DNA damage is apparent at 0 mins post-IR, with Bcl10 siRNA-treated cells containing significantly more damage than mock transfected cells ($p<0.05$). The percent of DNA in the tail decreases from 0 mins post-IR to 1 h post-IR in the Bcl10 siRNA, mock and non-transfected cells (Figure 3.11C).

Radiation causes many different types of DNA damage, the most deleterious being DNA DSB. We can monitor DNA DSB and their repair by quantifying γH2AX foci. To confirm our comet assay results, we quantified γH2AX foci in Bcl10 siRNA, mock siRNA and non-transfected T47D cells, by gathering Z-stacks and using Imaris software to create 3-D reconstructions. We quantitated ~50 cells for each time point (25 cells per experiments; pool of 2 experiments). Unirradiated Bcl10 siRNA-treated cells contain 1.48 γH2AX foci per nucleus, 1

Figure 3.11 Bcl10 knockdown inhibits the repair of radiation-induced DNA damage in T47D cells. T47D cells were transfected with Bcl10 siRNA or a scrambled siRNA, non-transfected cells were included as a control. 48 h post-transfection cells were exposed to 5 Gy ionizing radiation and introduced into the comet assay 0 mins, 30 mins, 1 h, 2 h, 4 h and 24 h post-IR. Unirradiated cells were served as a control. (A) Images were taken using a Zeiss Image.Z.1 upright microscope with a Cooke SensiCam High performance camera and a 20X/0.8 NA Zeiss Plan-ApoChromat dry lens. (B+C) Comet tails were measured using CometScore. Error bars represent SEM.

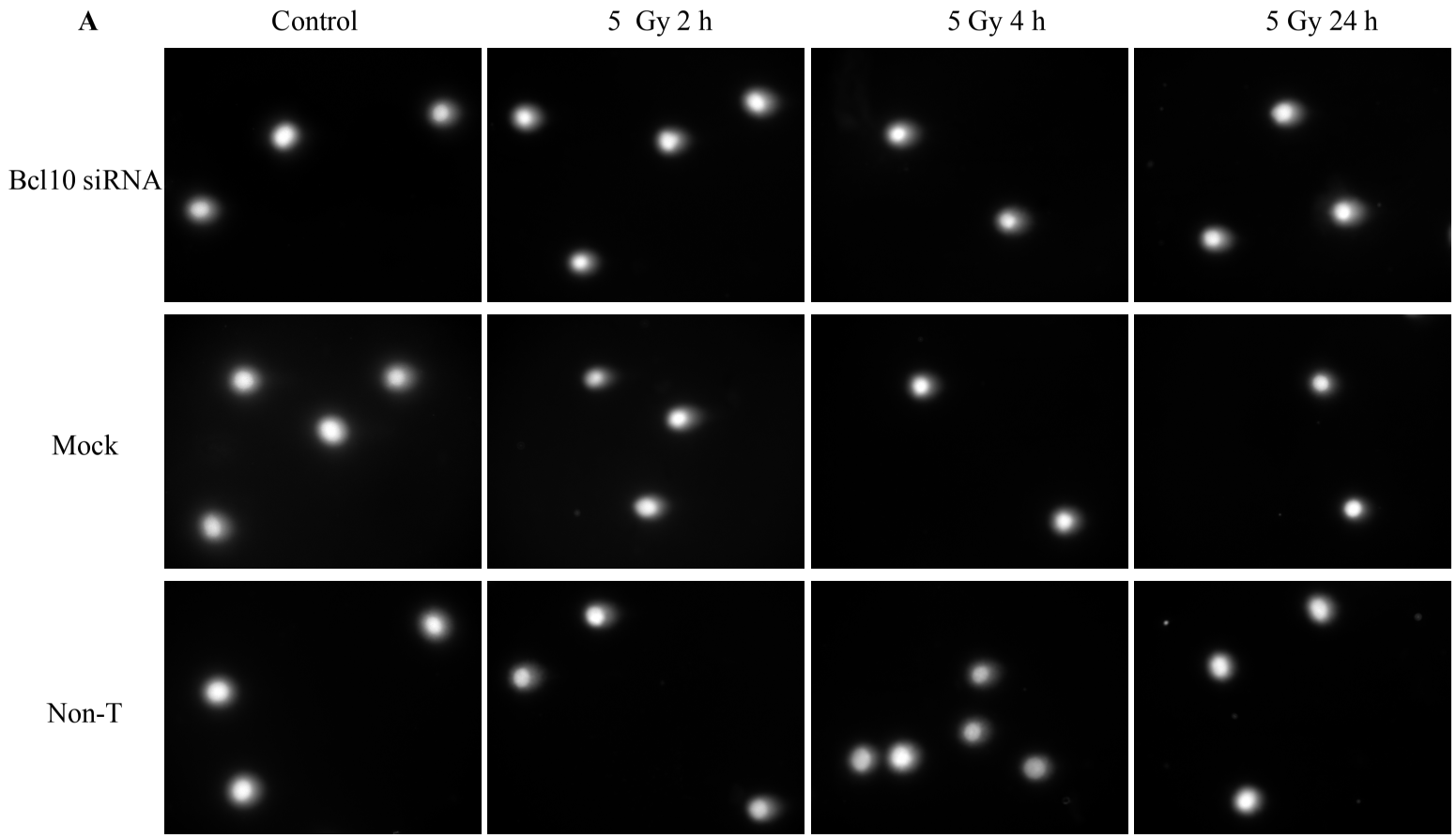
A
Control
5 Gy 2 h
5 Gy 4 h
5 Gy 24 h
Bcl10 siRNA
Mock
Non-T

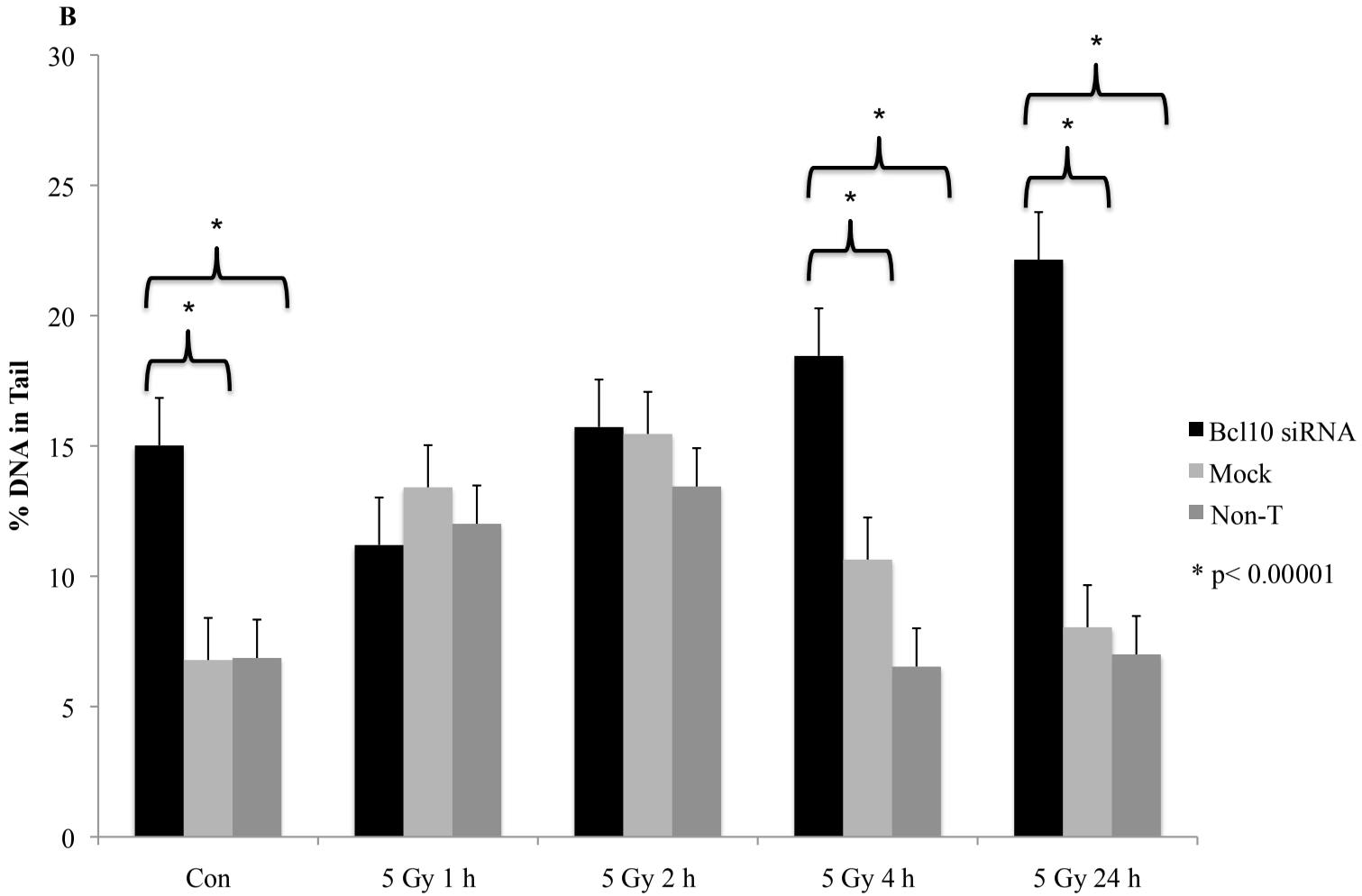
B
% DNA in Tail
30
25
20
15
10
5
0
Con
5 Gy 1 h
5 Gy 2 h
5 Gy 4 h
5 Gy 24 h
Bcl10 siRNA
Mock
Non-T
* p< 0.00001

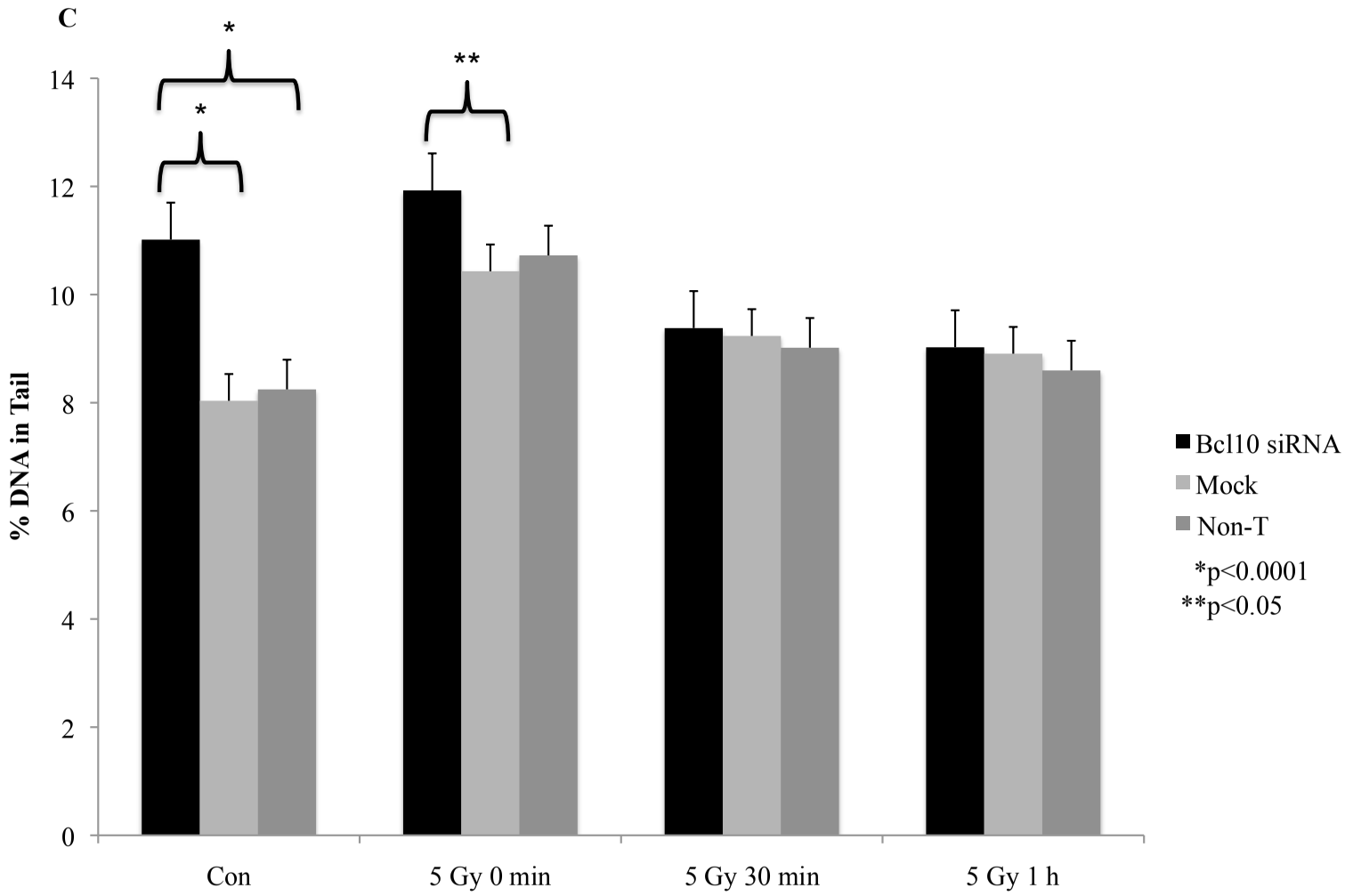
C
*
**
*
14
12
10
8
6
4
2
0
% DNA in Tail
Con
5 Gy 0 min
5 Gy 30 min
5 Gy 1 h
Bcl10 siRNA
Mock
Non-T
*p<0.0001
**p<0.05

h after treatment with 5 Gy 87.25 nuclear γH2AX foci are present and at 4 h post-IR 71.98 foci are remaining (Figure 3.12A and 3.12D). Mock-transfected and non-transfected cells contain 5.21 and 3.10 γH2AX foci in the unirradiated control, 112.2 and 116.7 at 1 h post-IR and 51.7 and 57.6 at 4 h post-IR, respectively (Figures 3.12B, 3.12C and 3.12D). As shown in Figure 3.12D Bcl10 siRNA-treated cells contain significantly fewer γH2AX foci than the mock and non-transfected cells in the unirradiated control (non-transfected $p< 0.05$)(mock-transfected $p<0.001$) and at 1 h post-IR ($p<0.001$) and significantly more γH2AX foci at 4 h post-IR (non-transfected $p<0.01$)(mock-transfected $p<0.001$).

3.3.2 NF-κB inhibition delays Bcl10 recruitment to IRIF at higher doses in T47D cells

Since Bcl10 has no known functions apart from its role in the activation of NF-κB in the cytoplasm of lymphoid cells, it was important to determine if this new role in DNA repair was independent of NF-κB. To investigate this, we used the NF-κB inhibitor, Bay-11, which specifically blocks the degradation of IκBα. Before looking at repair, we examined the effect of Bay-11 treatment on the recruitment of Bcl10 to IRIF. T47D cells were treated with 3.5 μM Bay-11 or DMSO (control) 2 h prior to irradiation and then analyzed using indirect immunofluorescent staining. Figure 3.13A shows that, following treatment with 2 Gy, Bcl10 is rapidly recruited to γH2AX foci 5 mins post-IR, co-localizing with ~100% of the foci by 30 mins and then building up in the foci at 1 h, 4 h and 8

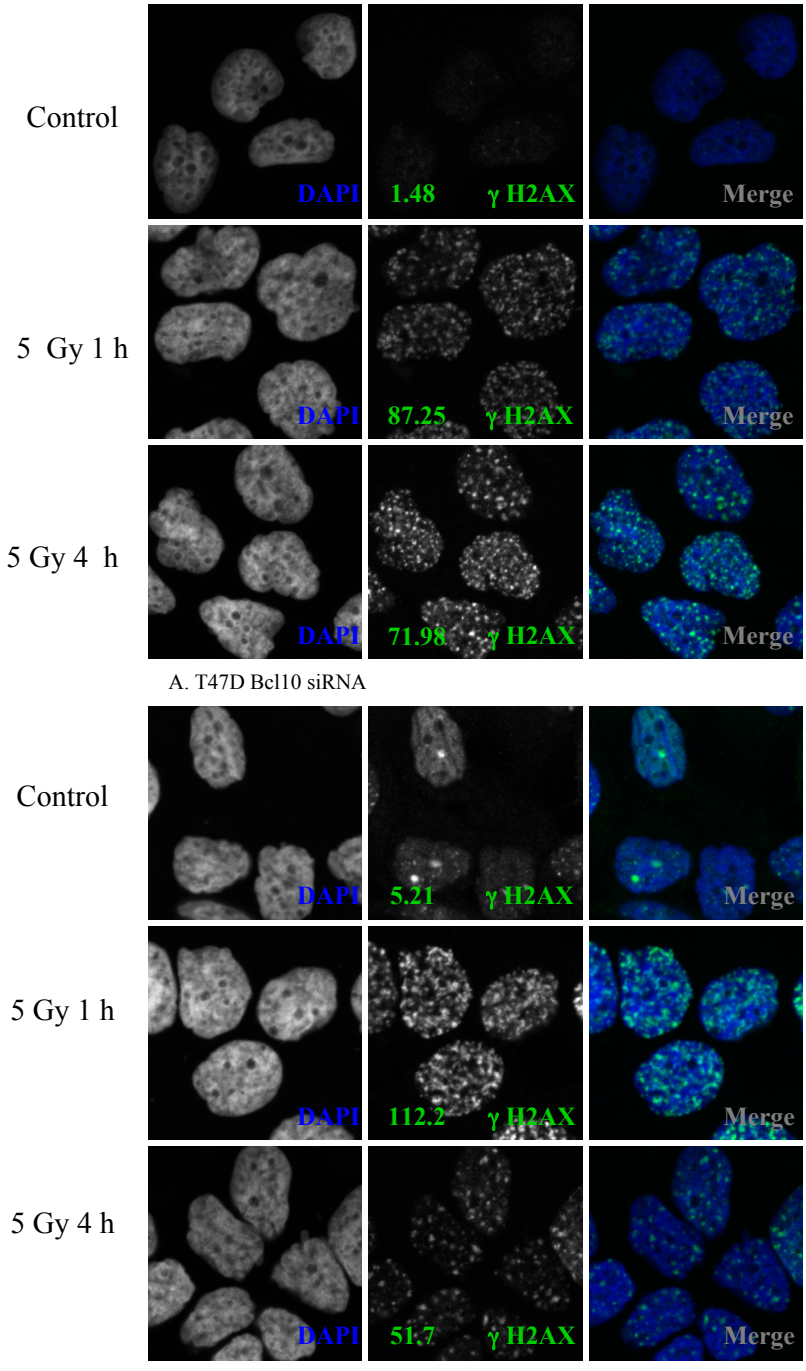

Figure 3.12 Bcl10 knockdown alters γH2AX foci formation in T47D cells. T47D cells were transfected with Bcl10 siRNA (A) scrambled siRNA (B), or non-transfected (C). 48 h post-transfection cells were exposed to 5 Gy ionizing radiation and fixed after 1 h and 4 h post-IR. Unirradiated cells were fixed as a control. Fixed cells were stained with mouse anti-γH2AX and counterstained with DAPI. Numbers represent average γH2AX foci per nuclei. (D) Foci were quantified using Imaris. Error bars represent SEM.

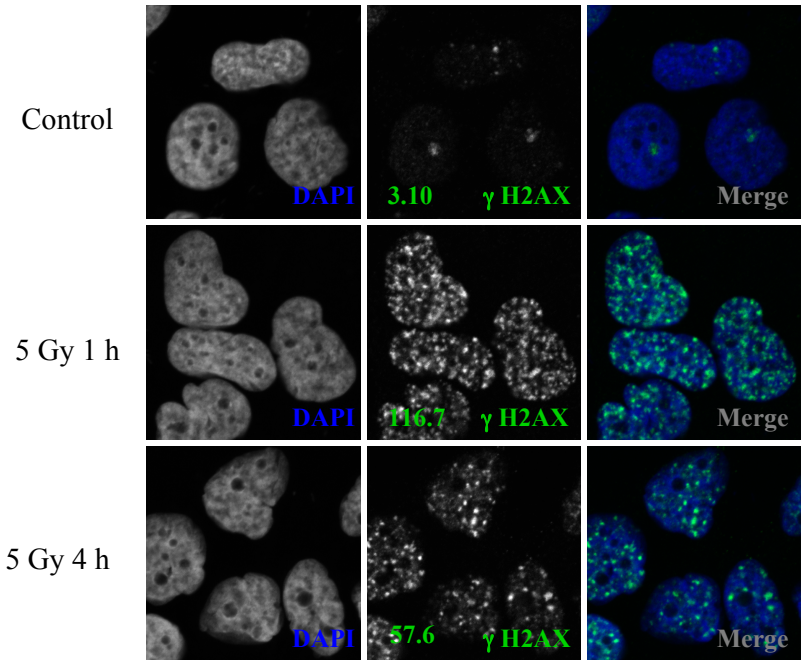

C. T47D Non-Transfected

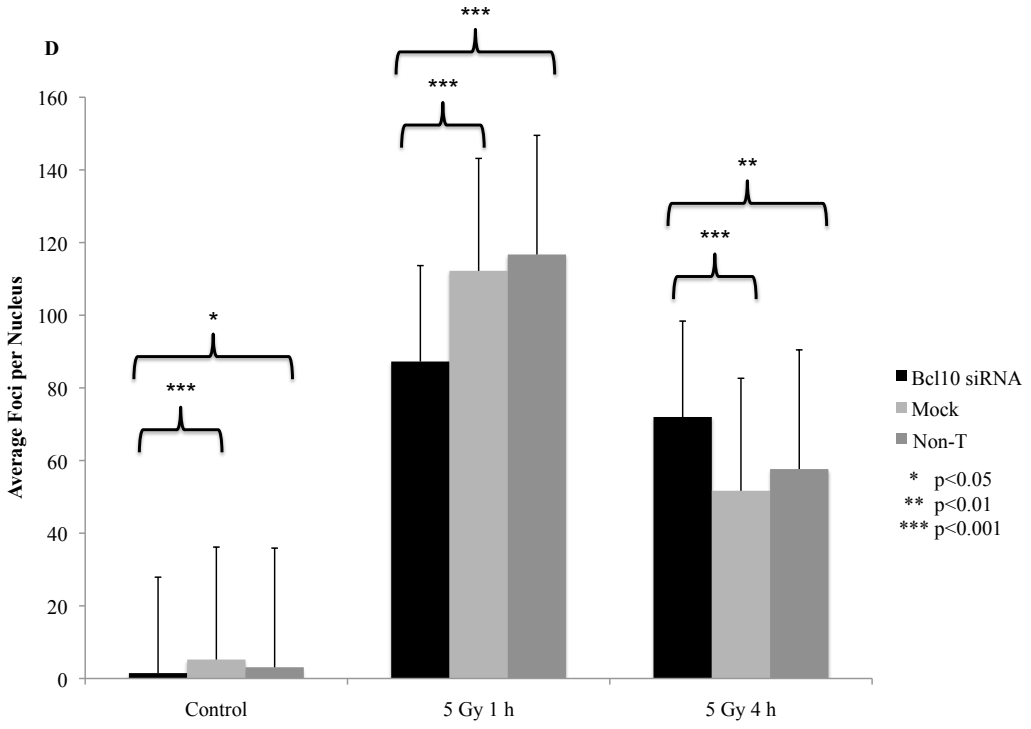

h, in T47D cells treated with Bay-11. We observe the same recruitment kinetics in DMSO-treated cells (Figure 3.13B). Both Bay-11 and DMSO-treated cells contain large cryptogenic foci. We also monitored Bcl10 co-localization with P-ATM; in Bay-11-treated cells, we see that Bcl10 is strongly associated with P-ATM throughout the 2 Gy time course, co-localizing with 100% of the foci at 5 mins post-IR and building up at later time points (Figure 3.13C). This is also true for DMSO-treated cells (Figure 3.13D).

To ensure that Bay-11 was effectively inhibiting NF-κB activation, we monitored p65 nuclear localization. As shown in figure 3.13E Bay-11 treatment inhibits p65 nuclear localization, with p65 being completely absent from the nucleus in the unirradiated control and 1 h and 4 h post-IR with 2 Gy. DMSO-treated cells however show an increase in nuclear p65 at 1 h post-IR and then a further increase at 4 h (Figure 3.13F). This indicates that Bay-11 is effectively blocking NF-κB activation.

We performed the same experiments at 5 Gy, to determine if there are any dose-dependent responses. When we irradiated T47D Bay-11-treated cells at 5 Gy, we found that Bcl10 recruitment to γH2AX foci was significantly impaired; at 5 mins, 30 mins and 1 h post-IR, we see Bcl10 present at only a couple of foci, not until 4 h post-IR do we see Bcl10 co-localizing with 100% of the foci and then building up in these foci at 8 h (Figure 3.14A). DMSO-treated cells however, show rapid recruitment of Bcl10 at 5 min and 30 mins post-IR, 100% co-

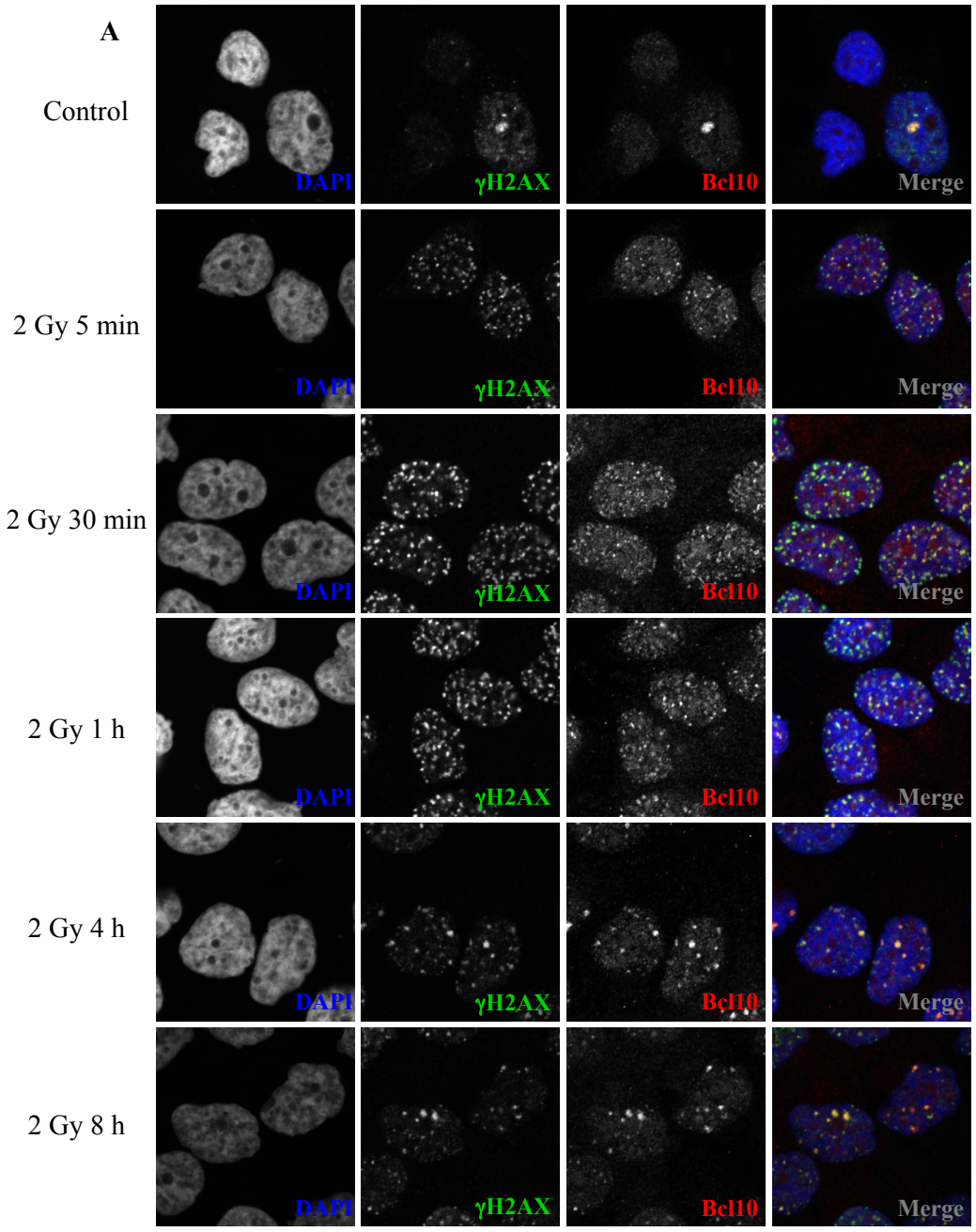

Figure 3.13 Bcl10 is recruited to ionizing radiation-induced foci in T47D cells treated with Bay-11 (2 Gy). T47D cells were treated with 3.5 μM Bay-11 (A, C, E) or DMSO (B, D, F) 2 h prior to irradiation with 2 Gy, cells were fixed after 5 mins, 30 mins, 1 h, 4 h, and 8 h, unirradiated cells were fixed as a control. DAPI was used as a counterstain. (A+B) Fixed cells were stained with mouse anti-γH2AX (FITC, green), rabbit anti-Bcl10 (Cy3, red). (C+D) Fixed cells were stained with mouse anti-P-ATM (FITC, green), rabbit anti-Bcl10 (Cy3, red). (E+F) Fixed cells were stained with mouse anti-p65 (FITC, green).

B

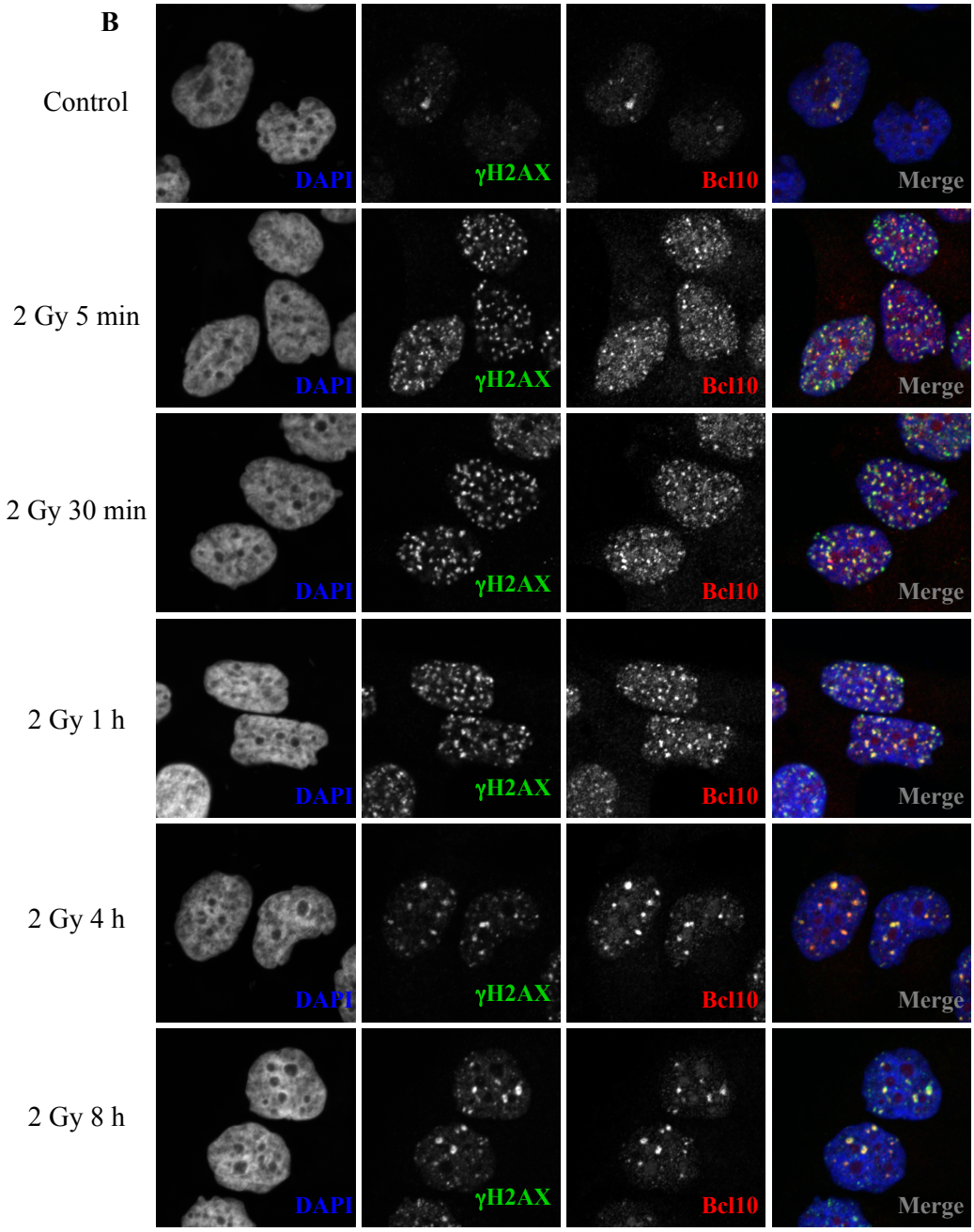
Control
DAPI
γH2AX
Bcl10
Merge
2 Gy 5 min
DAPI
γH2AX
Bcl10
Merge
2 Gy 30 min
DAPI
γH2AX
Bcl10
Merge
2 Gy 1 h
DAPI
γH2AX
Bcl10
Merge
2 Gy 4 h
DAPI
γH2AX
Bcl10
Merge
2 Gy 8 h
DAPI
γH2AX
Bcl10
Merge

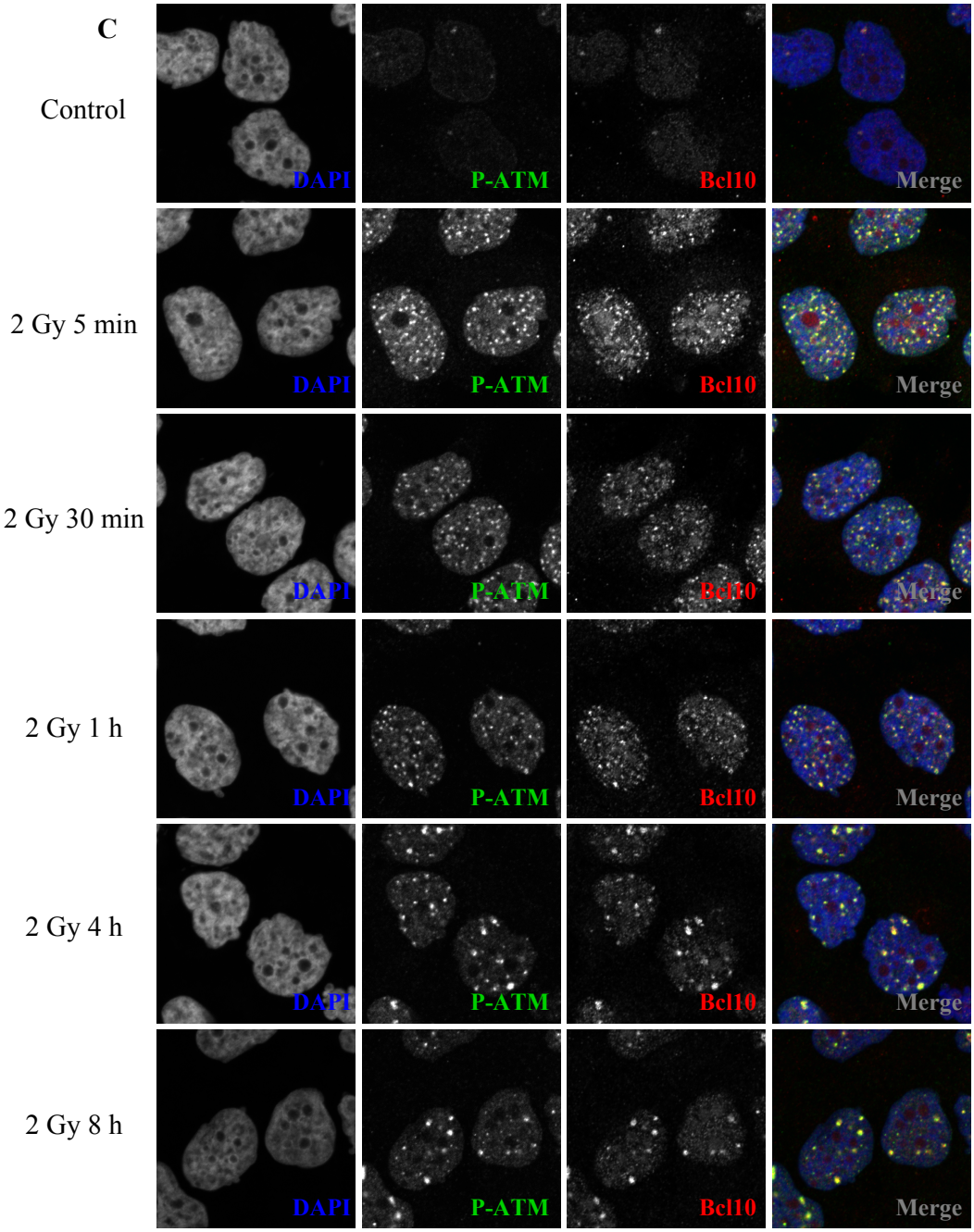
C
Control
2 Gy 5 min
2 Gy 30 min
2 Gy 1 h
2 Gy 4 h
2 Gy 8 h
DAPI
P-ATM
Bcl10
Merge

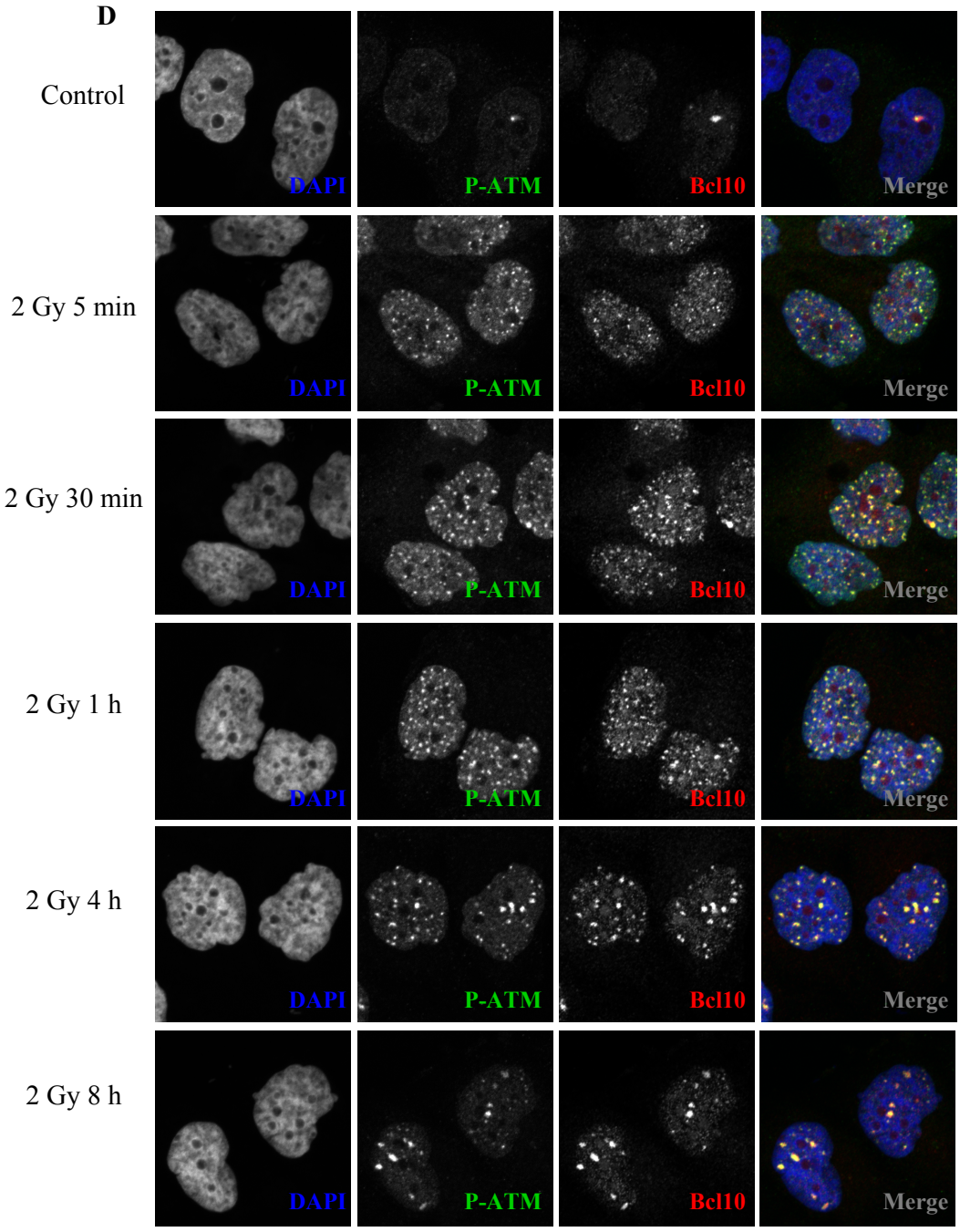
D
Control
2 Gy 5 min
2 Gy 30 min
2 Gy 1 h
2 Gy 4 h
2 Gy 8 h
DAPI
P-ATM
Bcl10
Merge

E

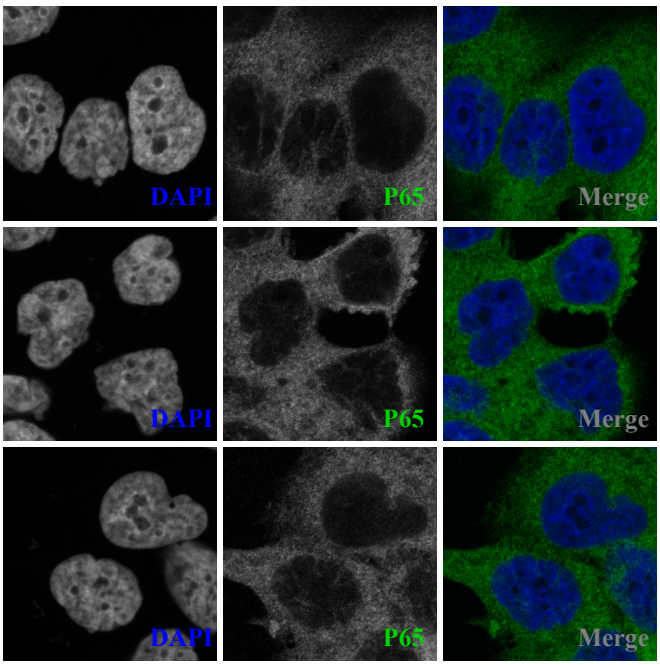

T47D Bay11 Treatment

F

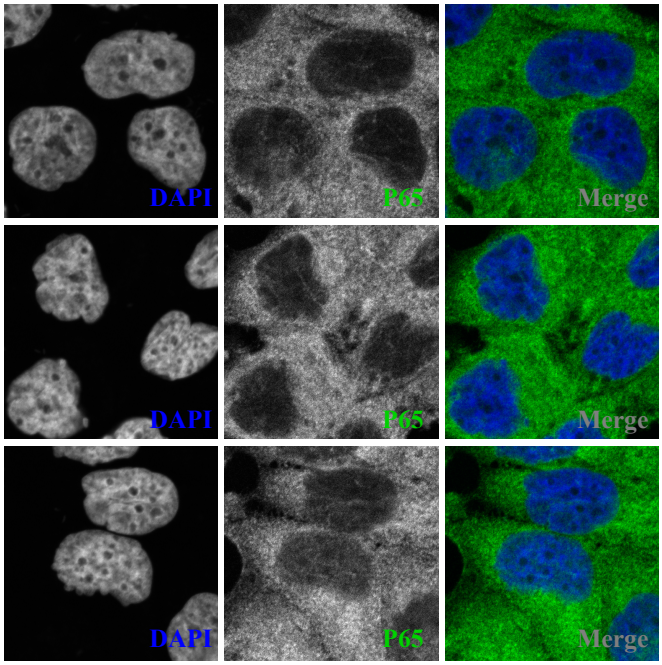

T47D DMSO Treatment

localization at 1 h and build-up at 4 and 8 h (Figure 3.14B). Bcl10 shows a slightly strongly association with P-ATM in Bay-11-treated cells, though we do not see 100% co-localization until 4 h post-IR (Figure 3.14C). This stronger association with P-ATM compared to γH2AX suggests that Bay-11 treatment may alter the formation of P-ATM foci. Figure 3.14D shows that in DMSO-treated cells Bcl10 is rapidly recruited to P-ATM foci following ionizing radiation, co-localizing with 100% of the foci at 1 h post-IR, and becoming very abundant in the foci at 4 h and 8 h.

Bay-11 remains an effective inhibitor at 5 Gy. The nucleus of Bay-11-treated T47D cells is devoid of p65 at 1 h and 4 h post-IR with 5 Gy as well as in the unirradiated control (Figure 3.14E). In DMSO-treated cells, we see an increase in nuclear p65 from the unirradiated control to 1 h post-IR with 5 Gy and then a further increase at 4 h post-IR (Figure 3.14D).

3.3.3 NF-κB inhibition has a minimal effect on the repair of radiation-induced DNA damage in T47D cells

To determine if the role of Bcl10 in DNA repair is independent of its role in NF-κB activation, we performed comet assays' with T47D cells treated with Bay-11 or DMSO (control). Bay-11 unirradiated cells contain almost no DNA in the tail of the comets, while DMSO cells contain a more visible amount; by 2 h post-IR DMSO cells show a prominent increase in the amount of DNA in the tail, while Bay-11 cells show only a slight increase (Figure 3.15A). The amount of DNA in

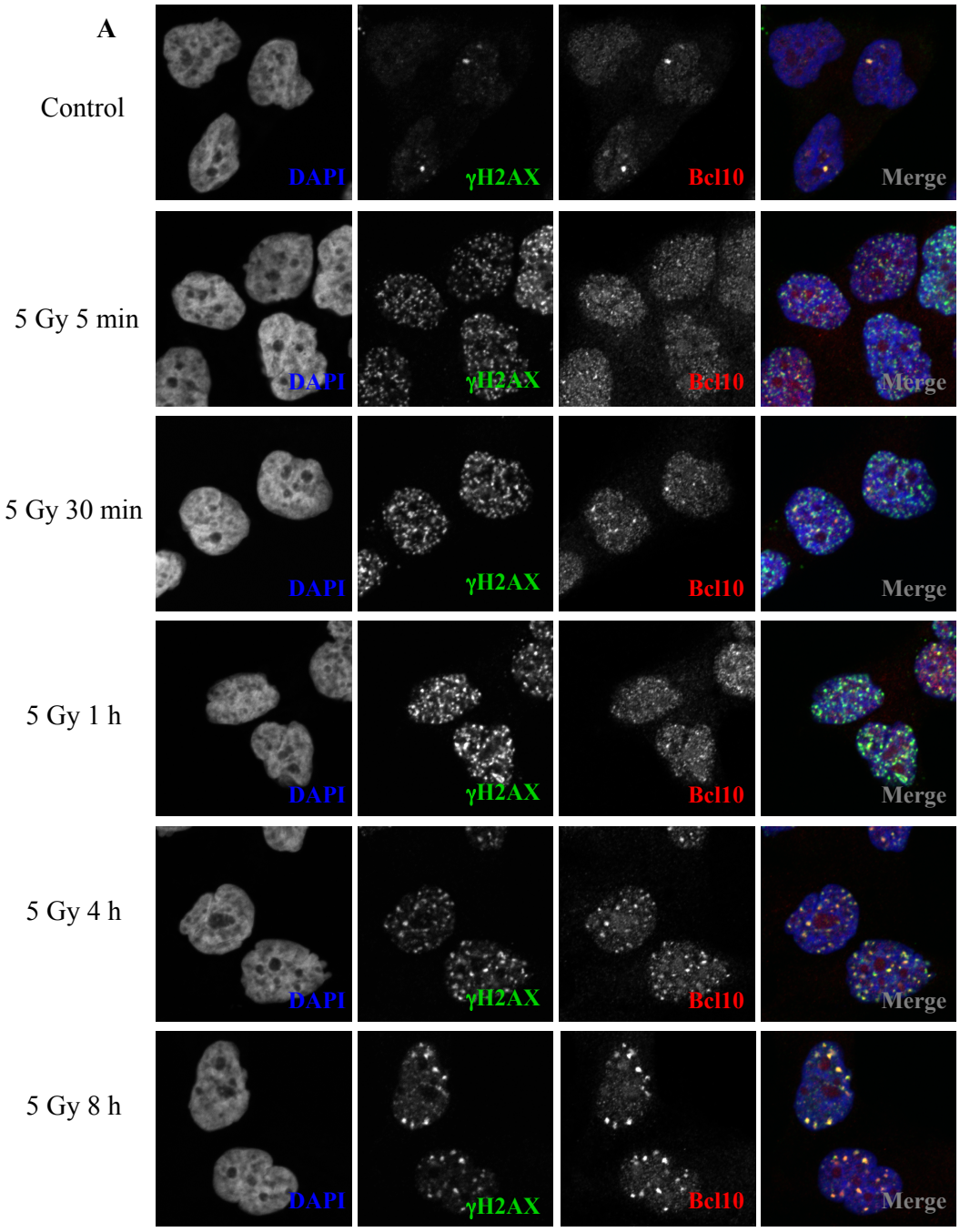

Figure 3.14 Bcl10 recruitment to ionizing radiation-induced foci in T47D cells treated with Bay-11 is delayed at 5 Gy. T47D cells were treated with 3.5 μM Bay-11 (A, C, E) or DMSO (B, D, F) 2 h prior to ionizing radiation with 5 Gy, cells were fixed after 5 mins, 30 mins, 1 h, 4 h, and 8 h, unirradiated cells were fixed as a control. DAPI was used as a counterstain. (A+B) Fixed cells were stained with mouse anti-γH2AX (FITC, green), rabbit anti-Bcl10 (Cy3, red). (C+D) Fixed cells were stained with mouse anti-P-ATM (FITC, green), rabbit anti-Bcl10 (Cy3, red). (E+F) Fixed cells were stained with mouse anti-p65 (FITC, green).

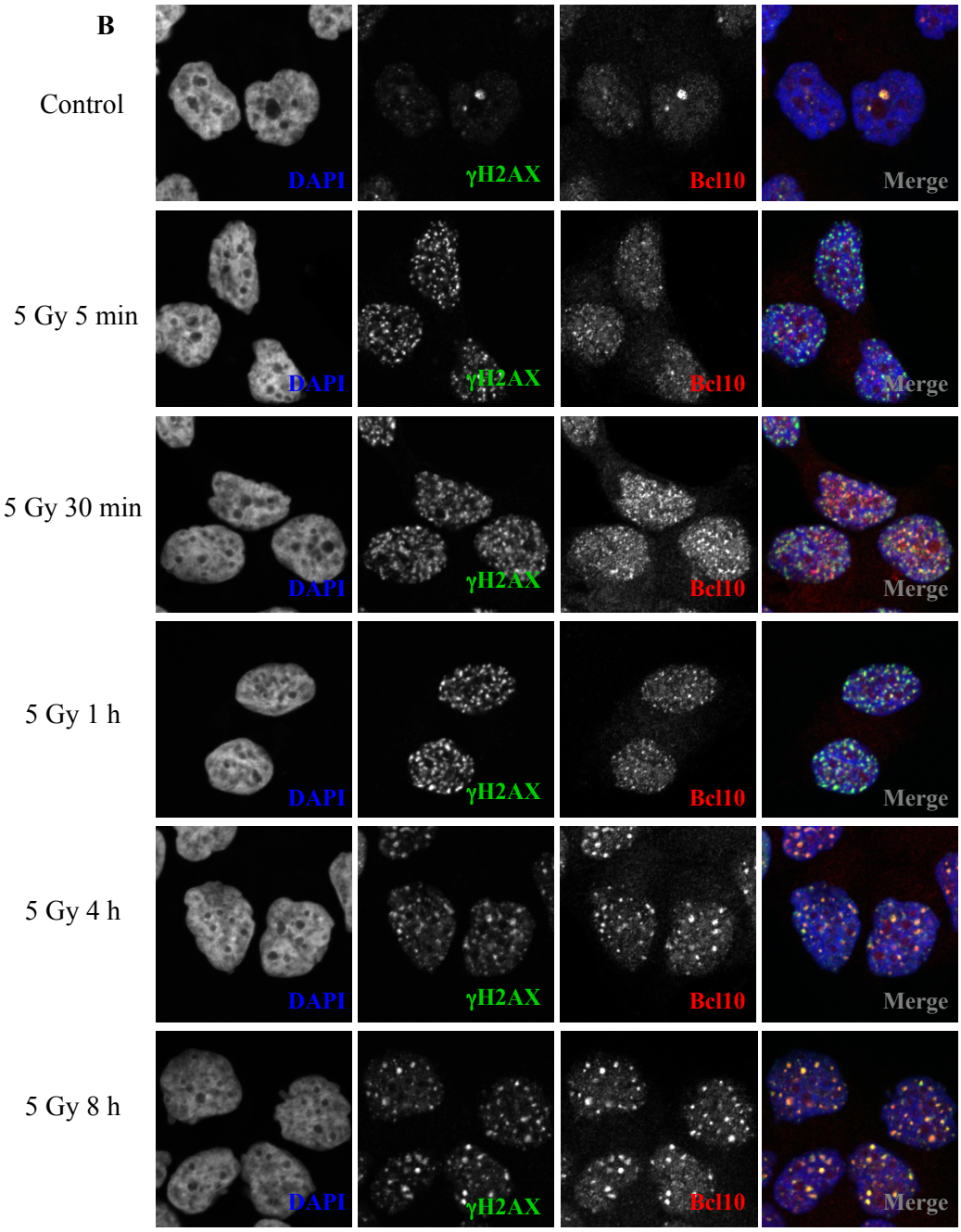
B
Control
5 Gy 5 min
5 Gy 30 min
5 Gy 1 h
5 Gy 4 h
5 Gy 8 h
DAPI
γH2AX
Bcl10
Merge

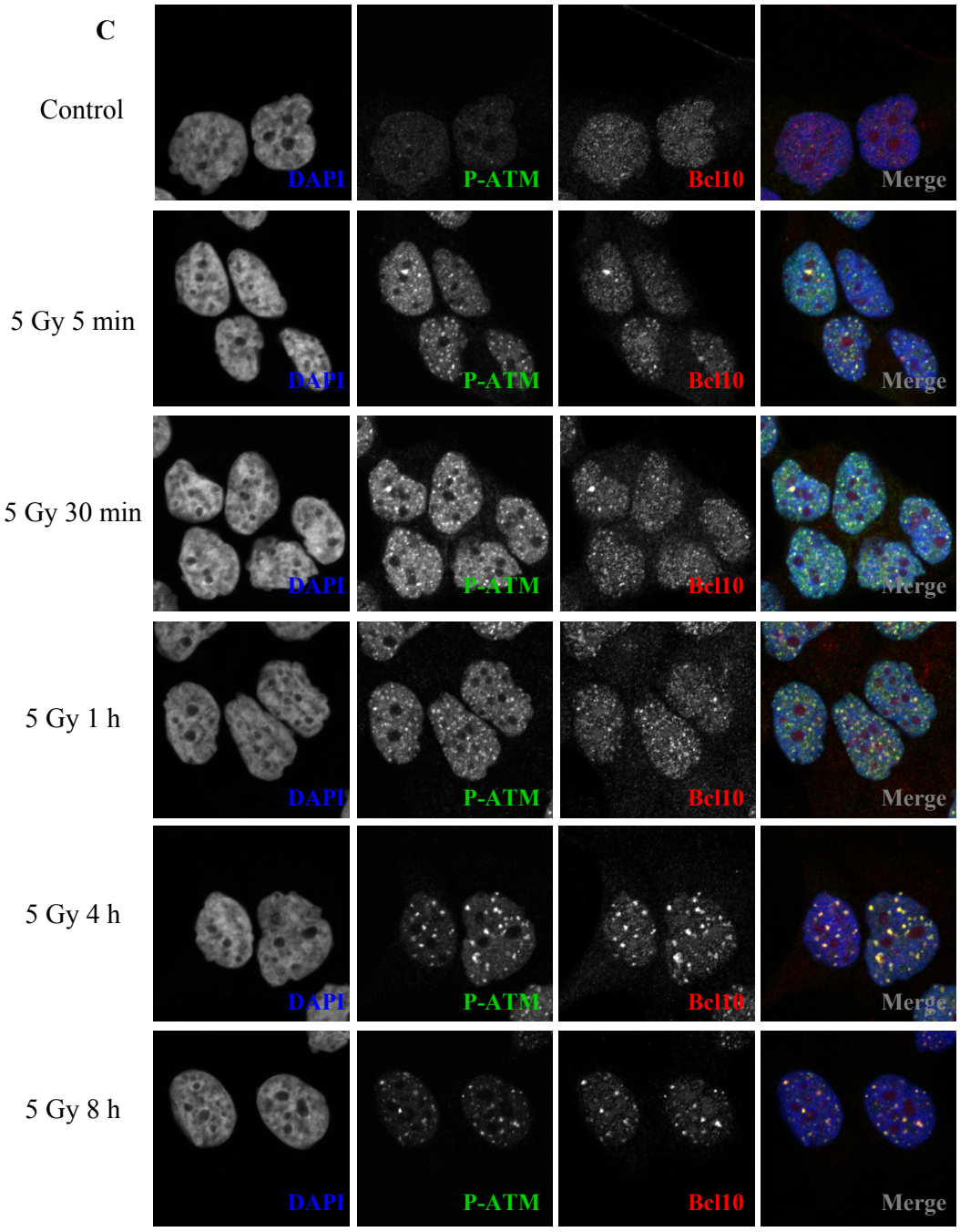
C
Control
5 Gy 5 min
5 Gy 30 min
5 Gy 1 h
5 Gy 4 h
5 Gy 8 h
DAPI
P-ATM
Bcl10
Merge

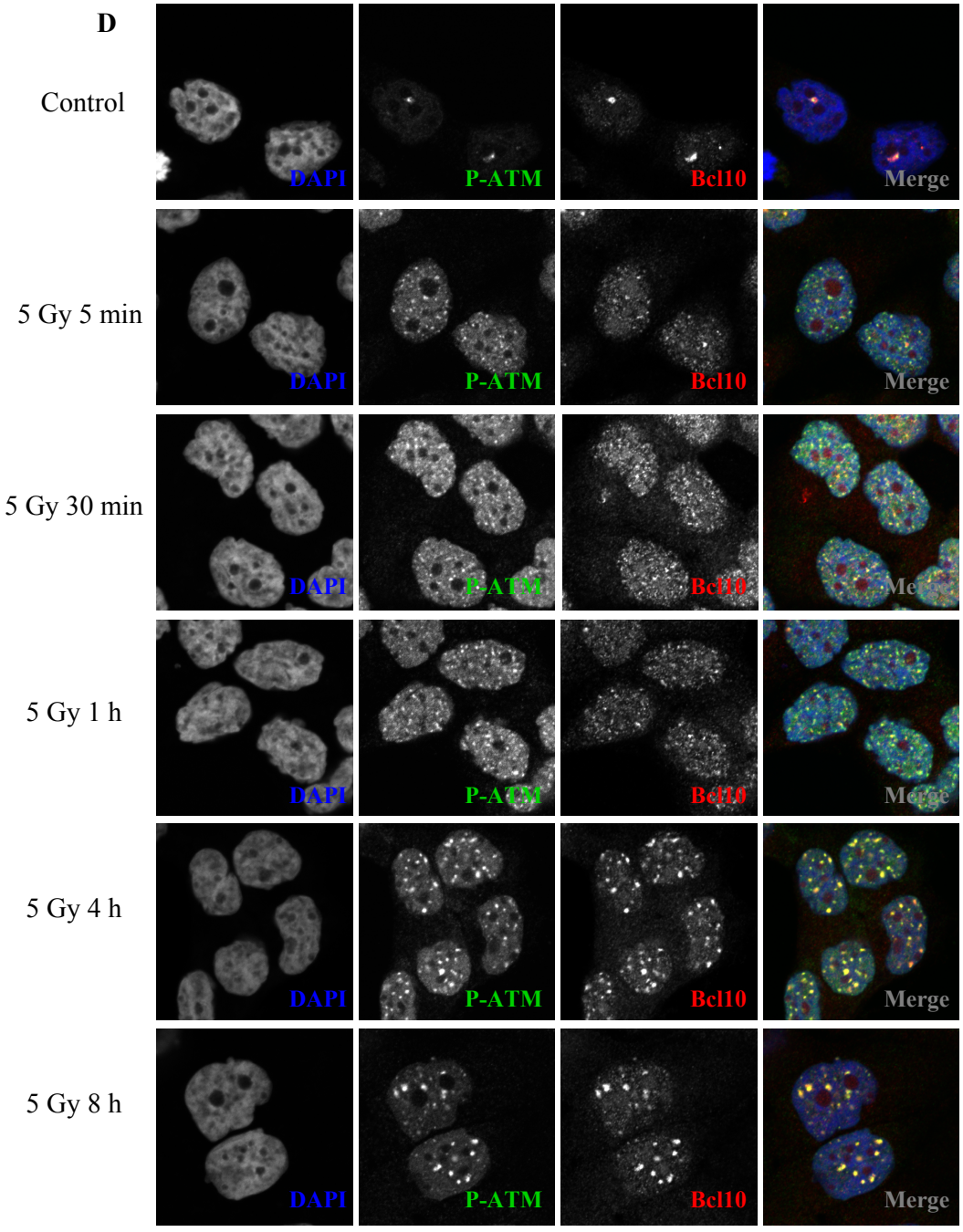
D
Control
5 Gy 5 min
5 Gy 30 min
5 Gy 1 h
5 Gy 4 h
5 Gy 8 h
DAPI
P-ATM
Bcl10
Merge

E

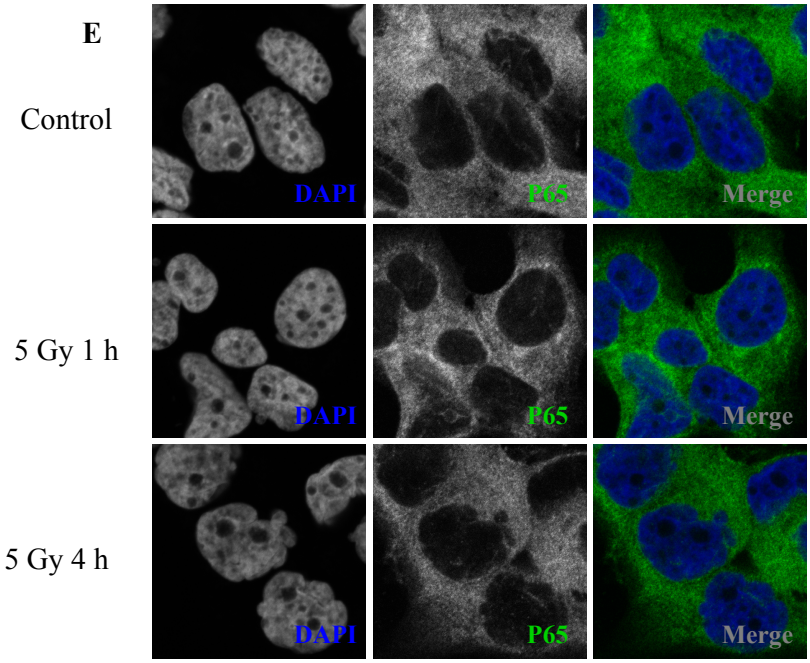

T47D Bay11 Treatment

F

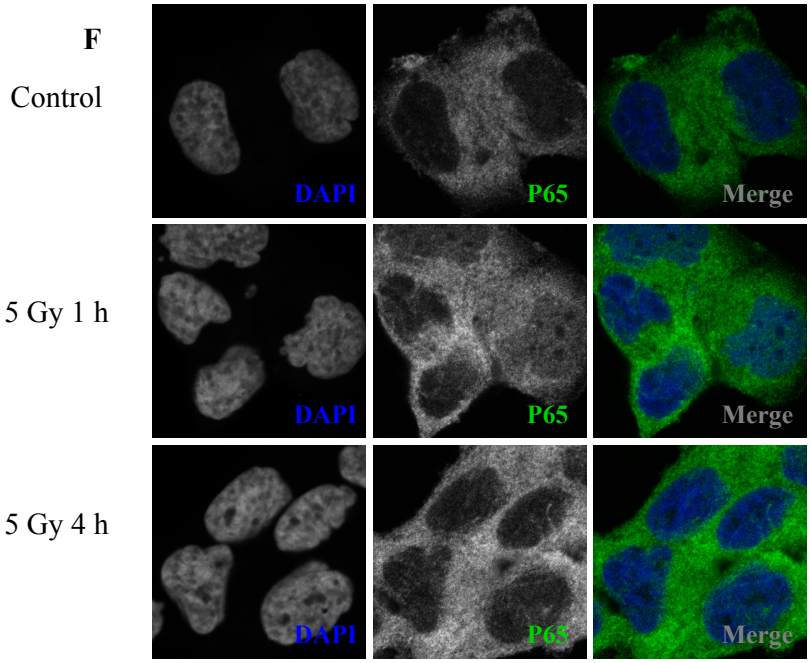

T47D DMSO Treatment

tail begins to decrease in DMSO-treated cells at 4 h post-IR and further decreases at 24 h, conversely in Bay-11-treated cells this amount begins to increase at 4 h and further increase at 24 h post-IR (Figure 3.15A). We quantified the percent of DNA in the tail and found that at 1 h, 2 h, and 4 h post-IR as well as in the unirradiated control, DMSO-treated cells have a higher percentage of DNA in the tail than the Bay-11-treated cells, at 24 h however, Bay-11-treated cells have significantly more DNA in the tail than DMSO-treated cells ($p < 0.001$) (Figure 3.15B).

We also monitored DNA DSB repair by quantifying γH2AX foci. Unirradiated Bay-11-treated cells contain significantly fewer γH2AX foci, 10 per nuclei, compared to DMSO-treated cells, 22 per nuclei (Figure 3.16). At 1 h post-IR with 5 Gy, Bay-11-treated cells contain 157 foci per nuclei while DMSO-treated cells contain 144 foci (Figure 3.16). By 4 h post-IR, DMSO-treated cells have 108 foci remaining whereas Bay-11-treated cells have 90 foci remaining (Figure 3.16). Indicating no repair defect in Bay-11-treated cells.

3.3.4 Bcl10 knockdown significantly diminishes the repair of radiation-induced DNA damage in hTERT-HME1 cells

In order to fully understand the role of Bcl10 in DNA repair, we wanted to determine whether this was a normal function of Bcl10 or an aberrant function in cancer cells, in particular breast cancer cells. To approach this, we repeated the same experiments in the normal breast epithelium cell line, hTERT-HME1. We

Figure 3.15 Bay-11 treatment slightly inhibits the repair of radiation-induced DNA damage in T47D cells. T47D cells were treated with Bay-11 or DMSO. 2 h after treatment cells were exposed to 5 Gy ionizing radiation and introduced into the comet assay 1 h, 2 h, 4 h and 24 h post-IR. Unirradiated cells served as a control. (A) Images were taken using a Zeiss Image.Z.1 upright microscope with a Cooke SensiCam High performance camera and a 20X/0.8 NA Zeiss Plan-ApoChromat dry lens. (B) Comet tails were measured using CometScore. Error bars represent SEM.

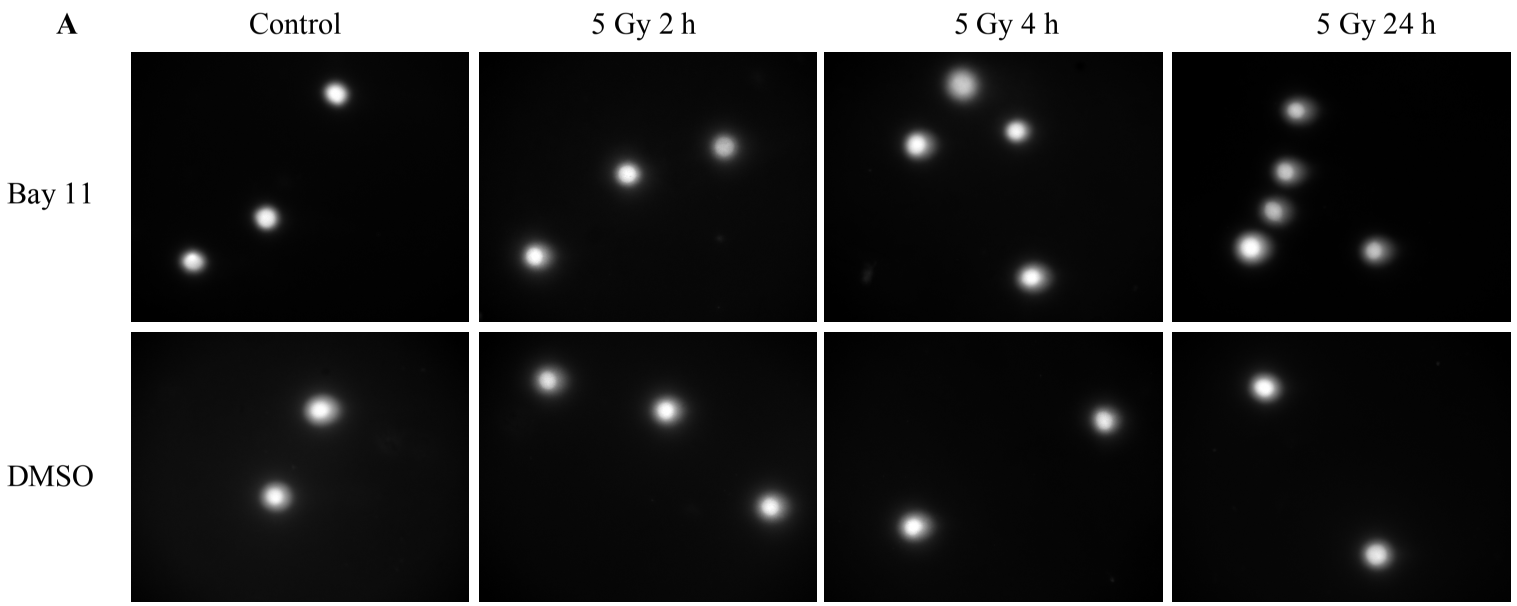
A
Control
5 Gy 2 h
5 Gy 4 h
5 Gy 24 h
Bay 11
DMSO

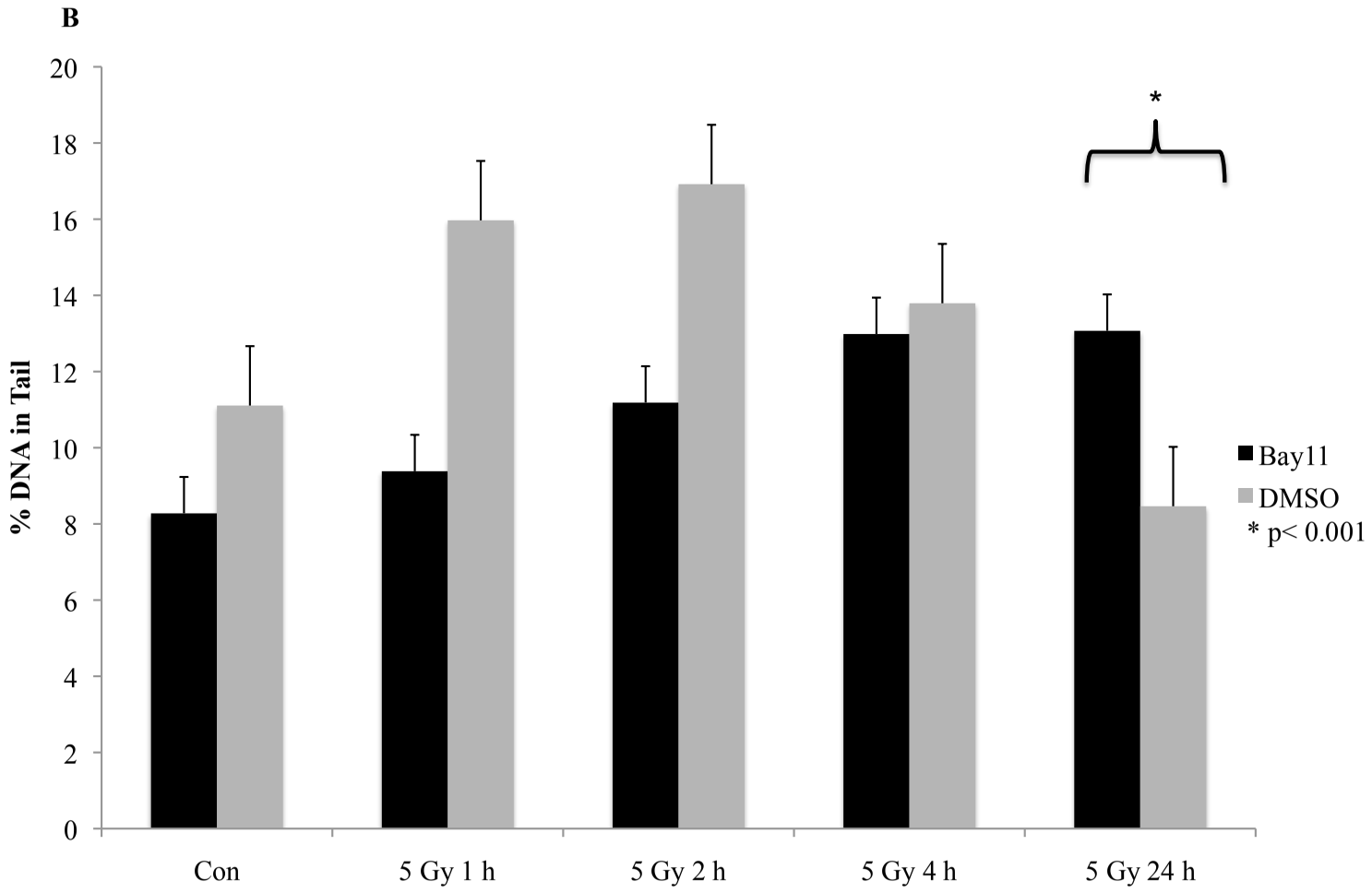
B
% DNA in Tail
20
18
16
14
12
10
8
6
4
2
0
Con
5 Gy 1 h
5 Gy 2 h
5 Gy 4 h
5 Gy 24 h
*
Bay11
DMSO
* p< 0.001

Figure 3.16 Bay-11 treatment does not alter ionizing radiation-induced γH2AX foci formation in T47D cells. T47D cells were treated with 3.5 μM Bay-11 or DMSO. After 2 h cells were exposed to 5 Gy ionizing radiation and fixed in 3.7% formaldehyde 1 h and 4 h post-IR. Unirradiated cells were fixed as a control. Fixed cells were stained with mouse anti-γH2AX and counterstained with DAPI. Foci were quantified using Imaris. Error bars represent SEM.

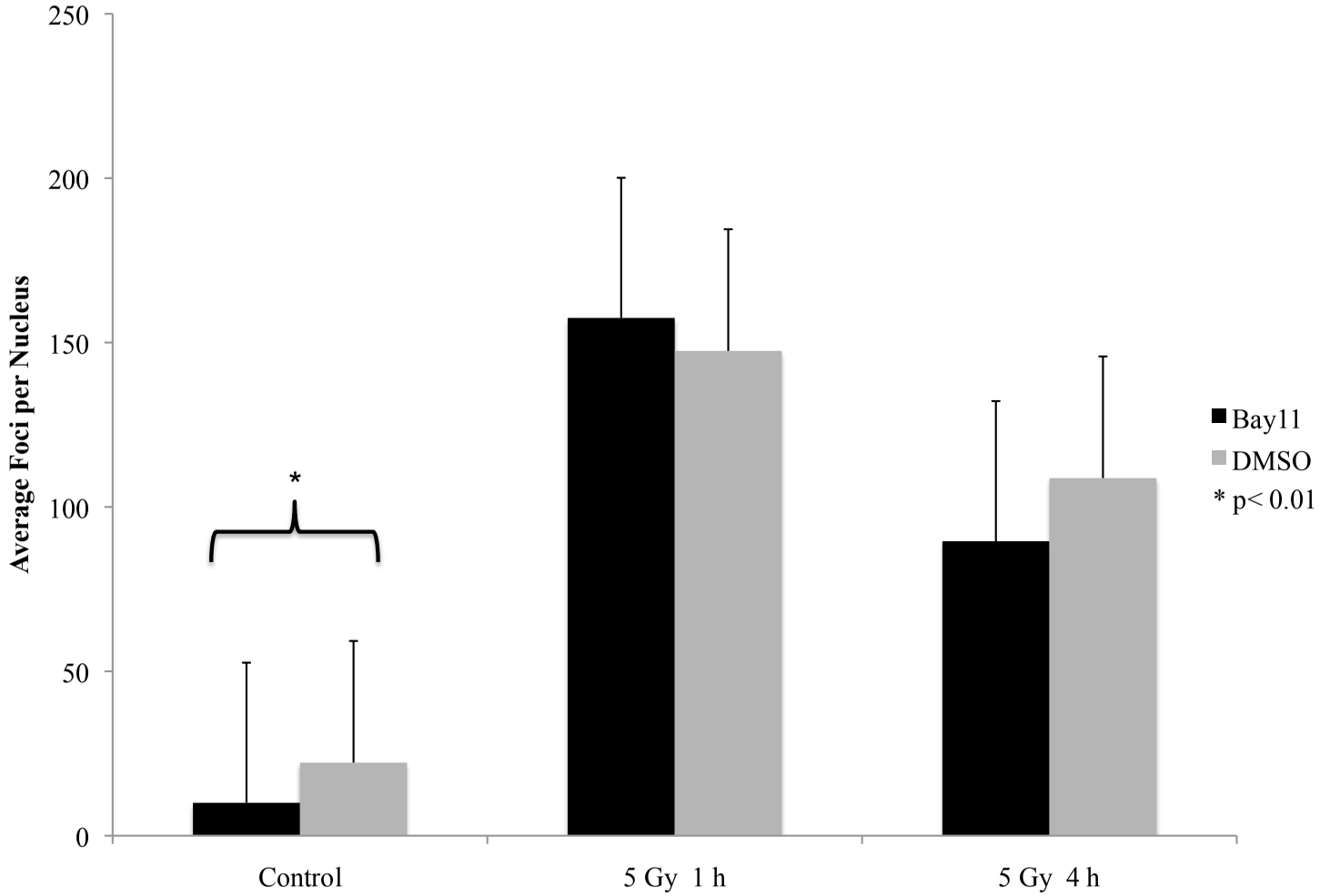
250
200
150
100
50
0
Average Foci per Nucleus
*
Control
5 Gy 1 h
5 Gy 4 h
Bay11
DMSO
* p< 0.01

first assessed DNA repair using the neutral comet assay and transient Bcl10 knockdown. Bcl10 siRNA-treated cells have a large portion of DNA present in the tail of the comets in the unirradiated control compared to mock and non-transfected comets (Figure 3.17A). By 2 h post-IR with 5 Gy, Bcl10 siRNA comets look very similar to mock and non-transfected comets; by 4 h post-IR, the amount of DNA in the tail decreases in mock and non-transfected comets, while it increases in Bcl10 siRNA comets (Figure 3.17A). We see a further increase in the amount of DNA present in the tail of Bcl10 siRNA comets at 24 h post-IR, whereas the mock and non-transfected comets begin to resemble their unirradiated controls (Figure 3.17A). Figure 3.17B shows that Bcl10 siRNA-treated cells contain significantly more DNA in the tail than non-transfected cells in the unirradiated control, at 5 Gy 1 h, 2 h, 4 h, and 24 h; while Bcl10 siRNA-treated cells contain significantly more DNA in the tail than mock-transfected cells in the unirradiated control and at 4 h and 24 h post-IR ($p < 0.00001$). This suggests that Bcl10 is important for proper DNA repair. Figure 3.17C shows a graph of the earlier time points; we observe that the most DNA damage occurs at 0 mins post-IR with Bcl10 siRNA-treated cells containing significantly more DNA damage than non-transfected cells ($p<0.001$). The percent of DNA in the tail decreases from 0 min to 30 mins post-IR, with Bcl10 siRNA-treated cells still containing significantly more damage than non-transfected cells ($p<0.05$) (Figure 3.17C). The percent of DNA in the tail begins to increase at 1 h post-IR, mock transfected cells contain significantly more damage than Bcl10 siRNA-treated cells ($p<0.05$),

while Bcl10 siRNA transfected cells contain significantly more DNA in the tail than non-transfected cells ($p<0.001$) (Figure 3.17C).

We also assessed DNA DSB repair by quantifying γH2AX foci in Bcl10 siRNA, mock and non-transfected cells. Unirradiated Bcl10 siRNA-treated cells have an average of 0.72 foci per nucleus, by 1 h post-IR with 5 Gy, these cells have 46.2 foci, and then by 4 h post-IR they contain 25.1 γH2AX foci (Figure 3.18A). As shown in figure 3.18B, mock-transfected cells contain 1.15, 40.3, and 27.8 foci per nucleus in the unirradiated control, at 1 h post-IR, and 4 h post-IR, respectively. Finally, non-transfected cells possess 0.90 foci in the unirradiated control, 52.6 foci at 1 h post-IR, and 29.1 foci at 4 h post-IR (Figure 3.18C). Figure 3.18D shows that there is no significant difference in the average number of γH2AX in Bcl10 siRNA-treated cells, mock and non-transfected cells in the unirradiated control, at 1 h post-IR or at 4 h post-IR.

3.3.5 NF-κB inhibition does not alter Bcl10 recruitment to IRIF in hTERT-HME1 cells

Once again, we used the NF-κB inhibitor, Bay-11, to determine if the role of Bcl10 in DNA repair is independent of NF-κB. Initially, we looked at the effect of Bay-11 treatment on the recruitment of Bcl10 to IRIF. Following 2 Gy irradiation to Bay-11-treated hTERT-HME1 cells, we observed that Bcl10 is rapidly recruited to γH2AX foci, co-localizing with 100% of the foci by 30 mins post-IR; at the later time points, 1 h, 4 h, and 8 h post-IR, Bcl10 builds up in the foci, as

Figure 3.17 Bcl10 knockdown inhibits the repair of radiation-induced DNA damage in hTERT-HME1 cells. hTERT-HME1 cells were transfected with Bcl10 siRNA or a scrambled siRNA, non-transfected cells were included as a control. 48 h post-transfection cells were exposed to 5 Gy ionizing radiation and introduced into the comet assay 0 mins, 30 mins 1 h, 2 h, 4 h and 24 h post-IR. Unirradiated cells served as a control. (A) Images were taken using a Zeiss Image.Z.1 upright microscope with a Cooke SensiCam High performance camera and a 20X/0.8 NA Zeiss Plan-ApoChromat dry lens. (B+C) Comet tails were measured using CometScore. Error bars represent SEM. (C) Graph represents an average of two separate experiments.

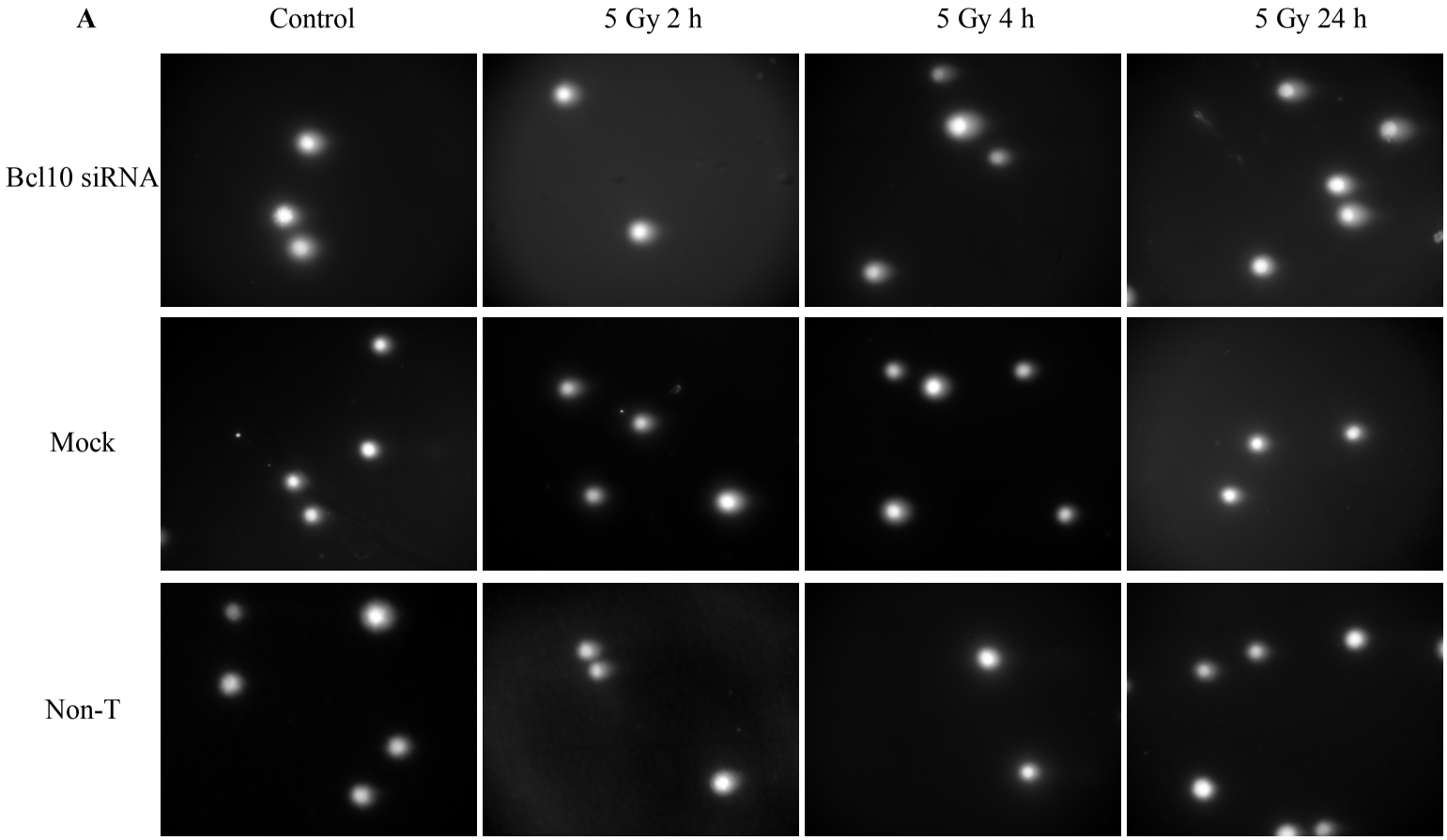
A
Control
5 Gy 2 h
5 Gy 4 h
5 Gy 24 h
Bcl10 siRNA
Mock
Non-T

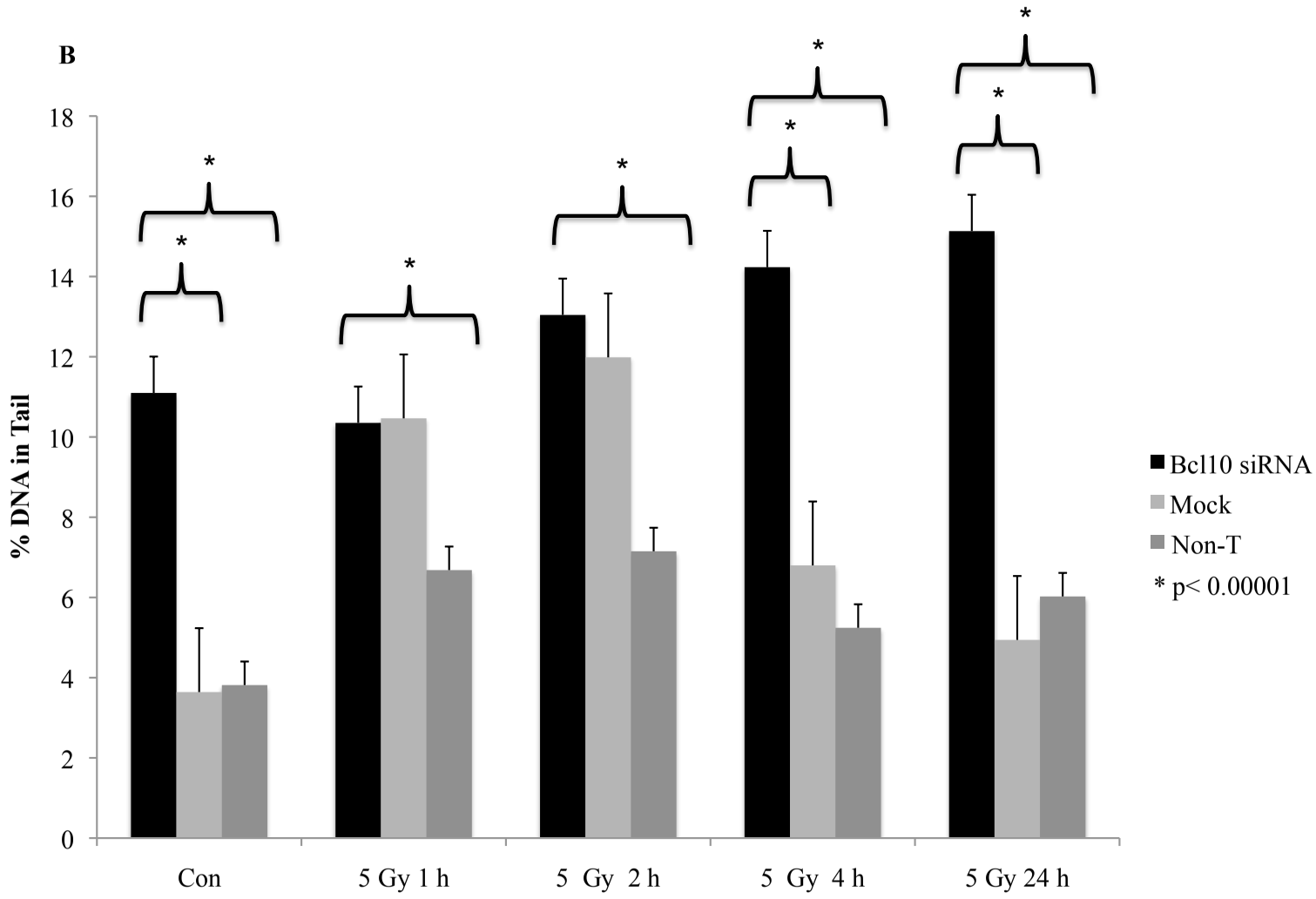
B
% DNA in Tail
18
16
14
12
10
8
6
4
2
0
Con
5 Gy 1 h
5 Gy 2 h
5 Gy 4 h
5 Gy 24 h
Bcl10 siRNA
Mock
Non-T
* p< 0.00001

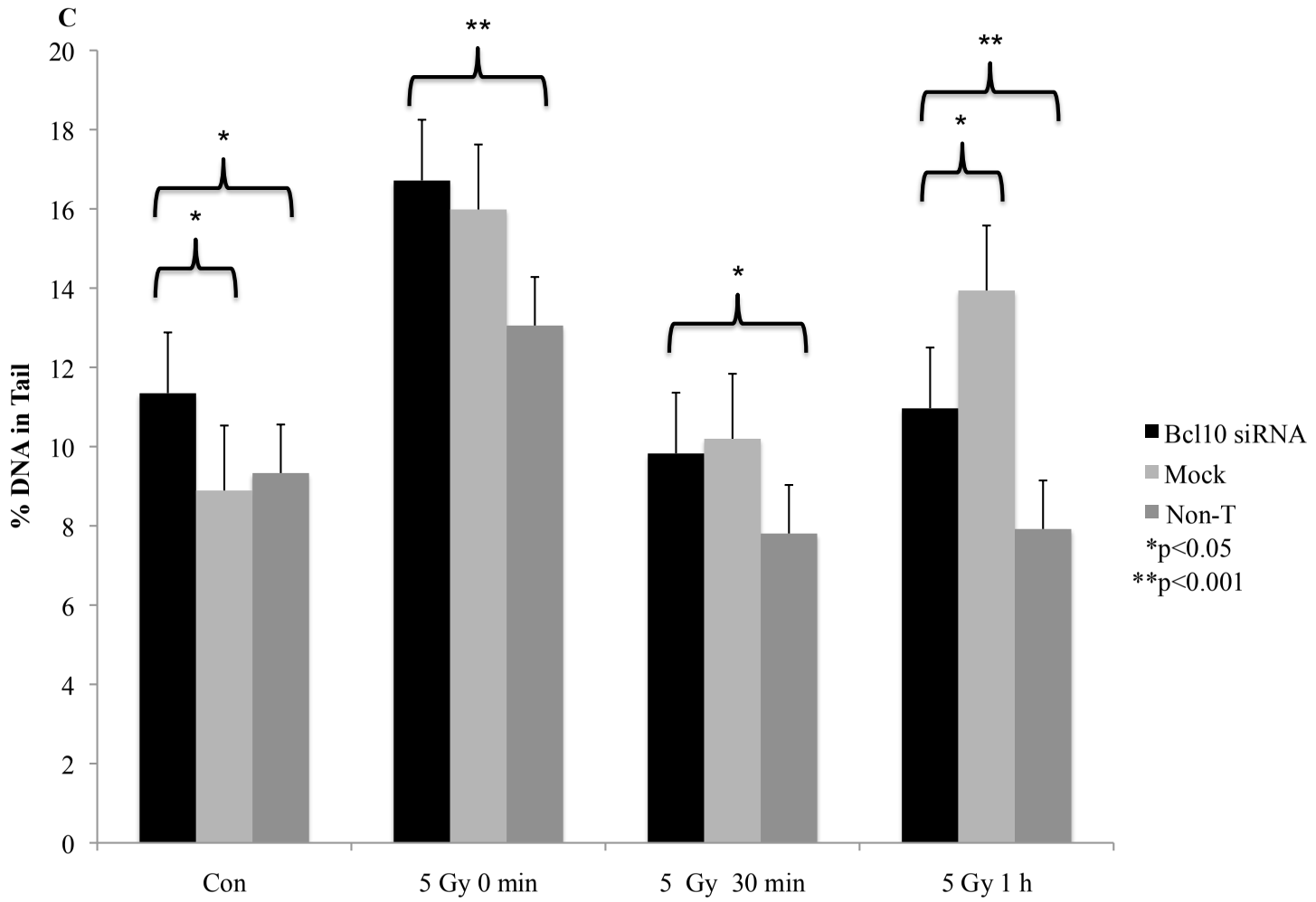
C
% DNA in Tail
20
18
16
14
12
10
8
6
4
2
0
*
*
**
*
*
**
Con
5 Gy 0 min
5 Gy 30 min
5 Gy 1 h
Bcl10 siRNA
Mock
Non-T
*p<0.05
**p<0.001

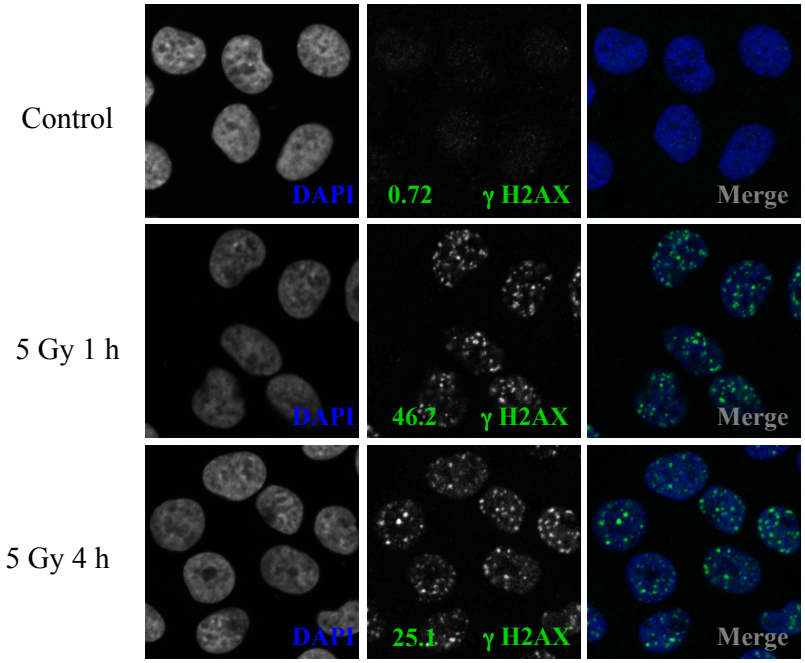

A. hTERT- HME1 Bcl10 siRNA

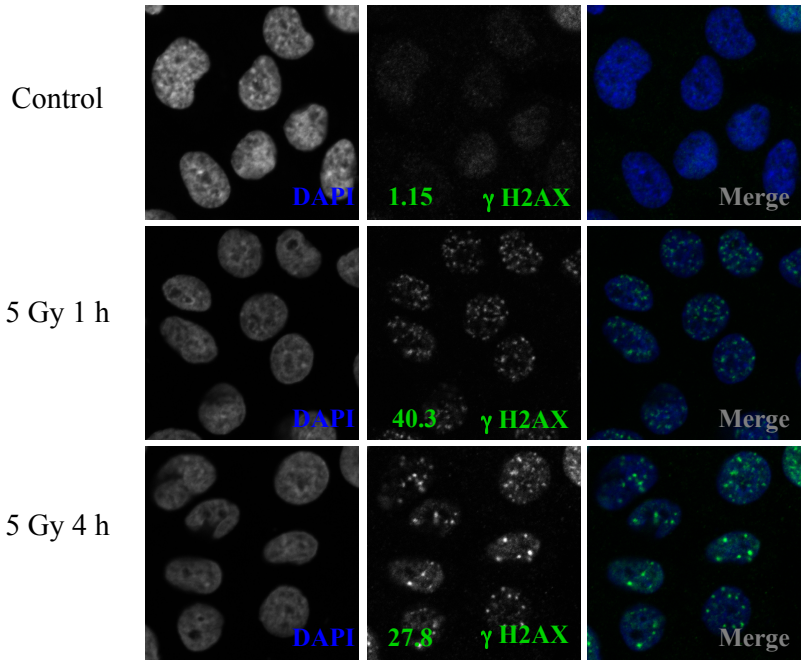

B. hTERT- HME1 Mock

Figure 3.18 Bcl10 knockdown does not alter γH2AX foci formation in hTERT-HME1 cells. hTERT-HME1 cells were transfected with Bcl10 siRNA (A) scrambled siRNA (B) or non-transfected (C). 48 h post-transfection cells were exposed to 5 Gy ionizing radiation and fixed after 1 h and 4 h. Unirradiated cells were fixed as a control. Fixed cells were stained with mouse anti-γH2AX and counterstained with DAPI. Numbers represent average γH2AX foci per nuclei. (D) Foci were quantified using Imaris. Error bars represent SEM.

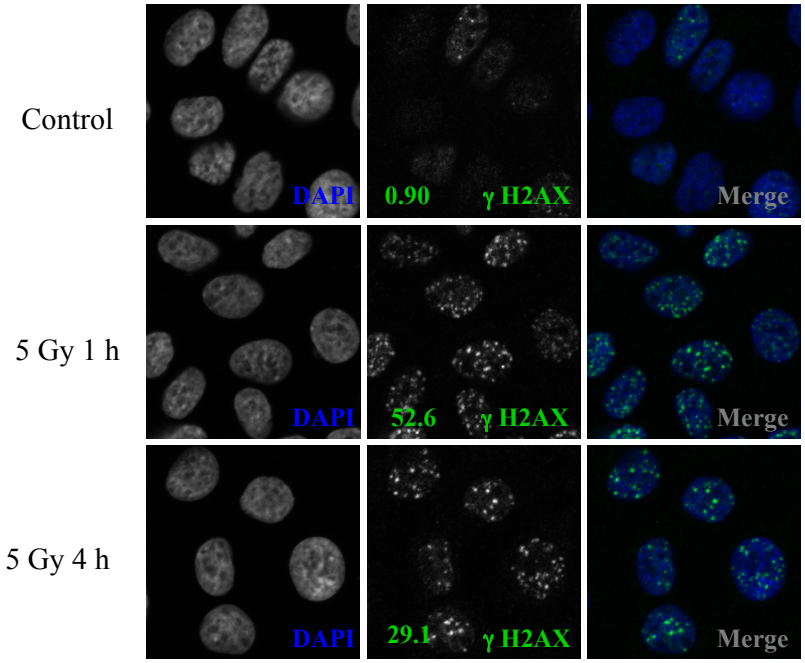

C. hTERT- HME1 Non-Transfected

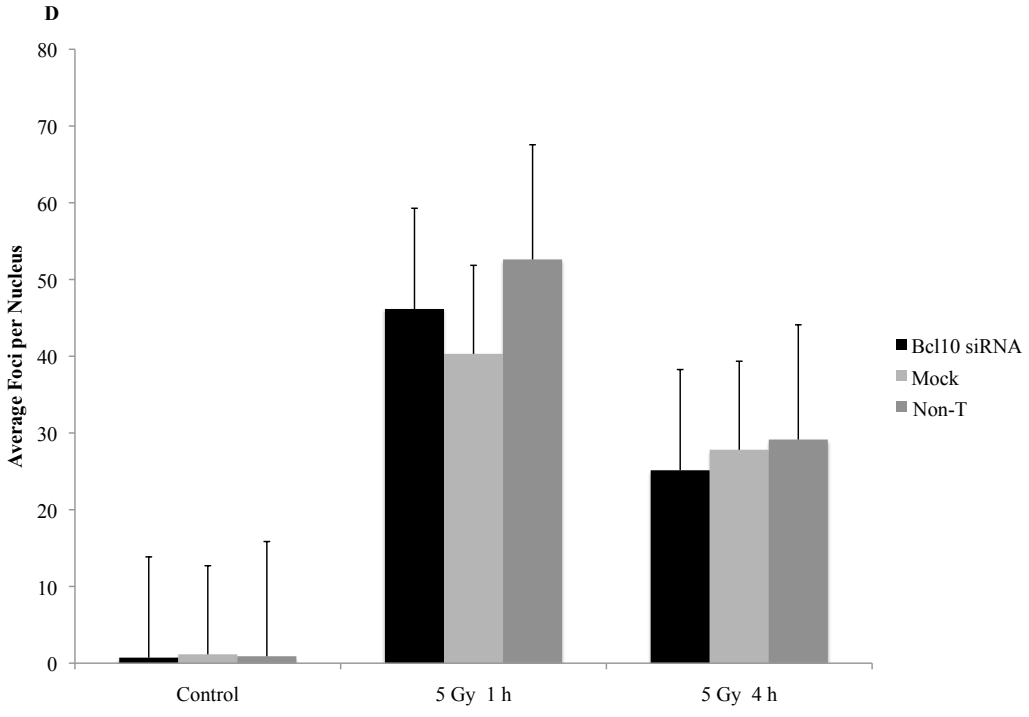

the foci themselves grow in size and reduce in number (Figure 3.19A). This is also what we observe in DMSO-treated hTERT-HME1 cells (Figure 3.19B). We also observed that unirradiated hTERT-HME1 cells contain almost no cryptogenic foci (Figure 3.19 A and B). Like we previously observed in T47D cells, Bcl10 has a very strong association with P-ATM following 2 Gy irradiation, such that Bcl10 co-localizes with 100% of the P-ATM foci by 5 min post-IR and remains strongly associated at 30 mins, 1 h, 4 h, and 8 h, in both Bay-11 (C) and DMSO (D) treated cells (Figure 3.19 C and D). Figure 3.19 E shows that Bay-11 treatment effectively inhibits p65 nuclear translocation, p65 is largely absent from the nucleus at 1 h and 4 h post-IR, as well as in the unirradiated control, whereas with DMSO treatment we see an increase in nuclear p65 staining from the unirradiated control to 1 h post-IR and then a further increase by 4 h post-IR (Figure 3.19F). This indicates that Bay-11 is able to inhibit NF-κB activation induced by 2 Gy.

To determine if there are any dose-dependent responses, we repeated the same experiments at 5 Gy. Bcl10 recruitment to γH2AX foci is slower at 5 Gy; by 5 mins post-IR we see some Bcl10 recruitment to γH2AX foci, not until 1 h post-IR do we see ~ 100% co-localization, with the association between Bcl10 and γH2AX getting stronger at later time points, this is true for both Bay-11 (A) and DMSO (B) treated hTERT-HME1 cells (Figure 3.20 A and B). As shown in figure 3.20 C and D Bcl10 has a very robust relationship with P-ATM; in Bay-11 (C) and DMSO (D) treated cells, we see that Bcl10 is rapidly recruited to P-ATM

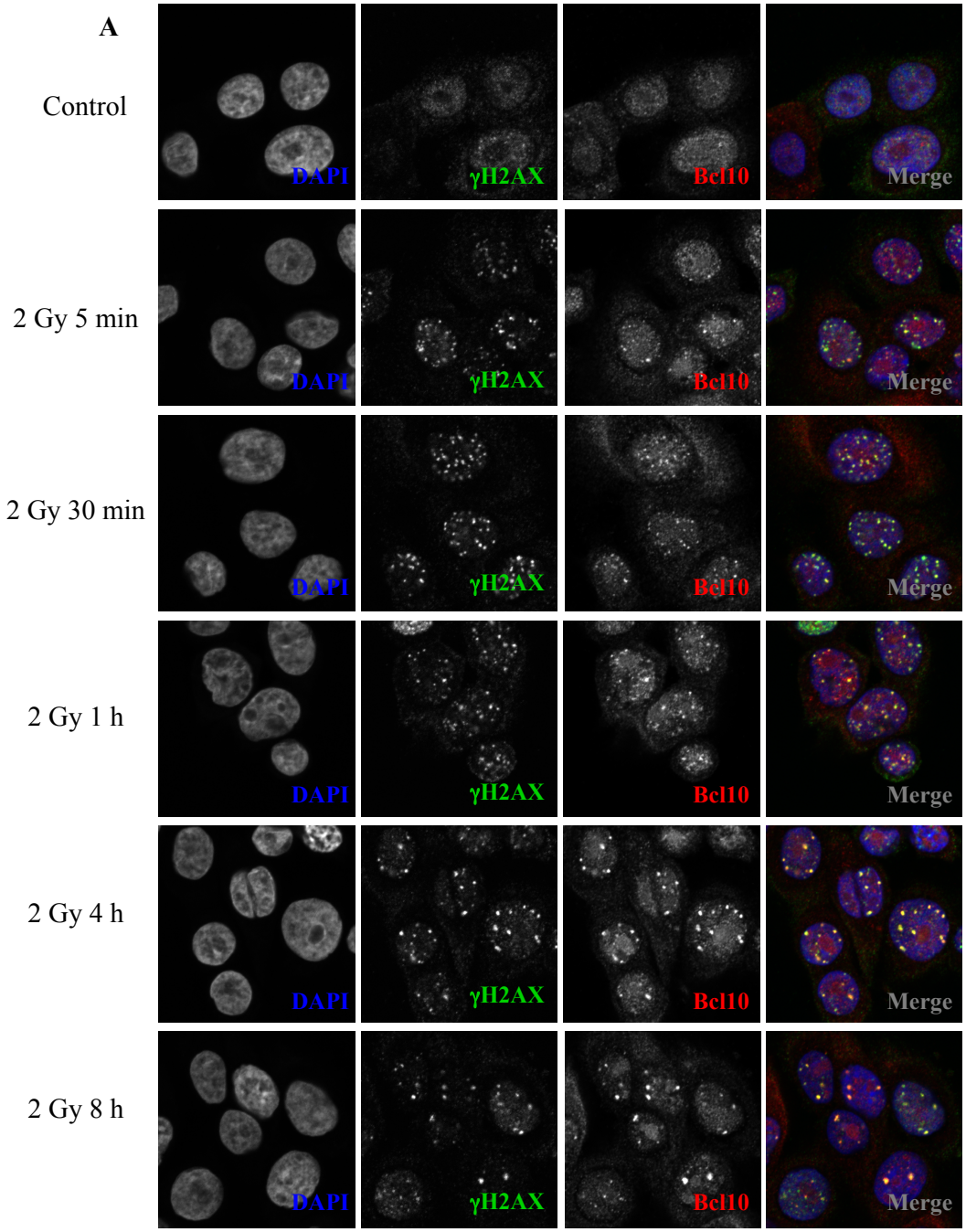

Figure 3.19 Bcl10 is recruited to ionizing radiation-induced foci in hTERT-HME1 cells treated with Bay-11 (2 Gy). hTERT-HME1 cells were treated with 3.5 μM Bay-11 (A, C, E) or DMSO (B, D, F) 2 h prior to ionizing radiation with 2 Gy, cells were fixed after 5 mins, 30 mins, 1 h, 4 h, and 8 h, unirradiated cells were fixed as a control. DAPI was used as a counterstain. (A+B) Fixed cells were stained with mouse anti-γH2AX (FITC, green), rabbit anti-Bcl10 (Cy3, red). (C+D) Fixed cells were stained with mouse anti-P-ATM (FITC, green), rabbit anti-Bcl10 (Cy3, red). (E+F) Fixed cells were stained with mouse anti-p65 (FITC, green).

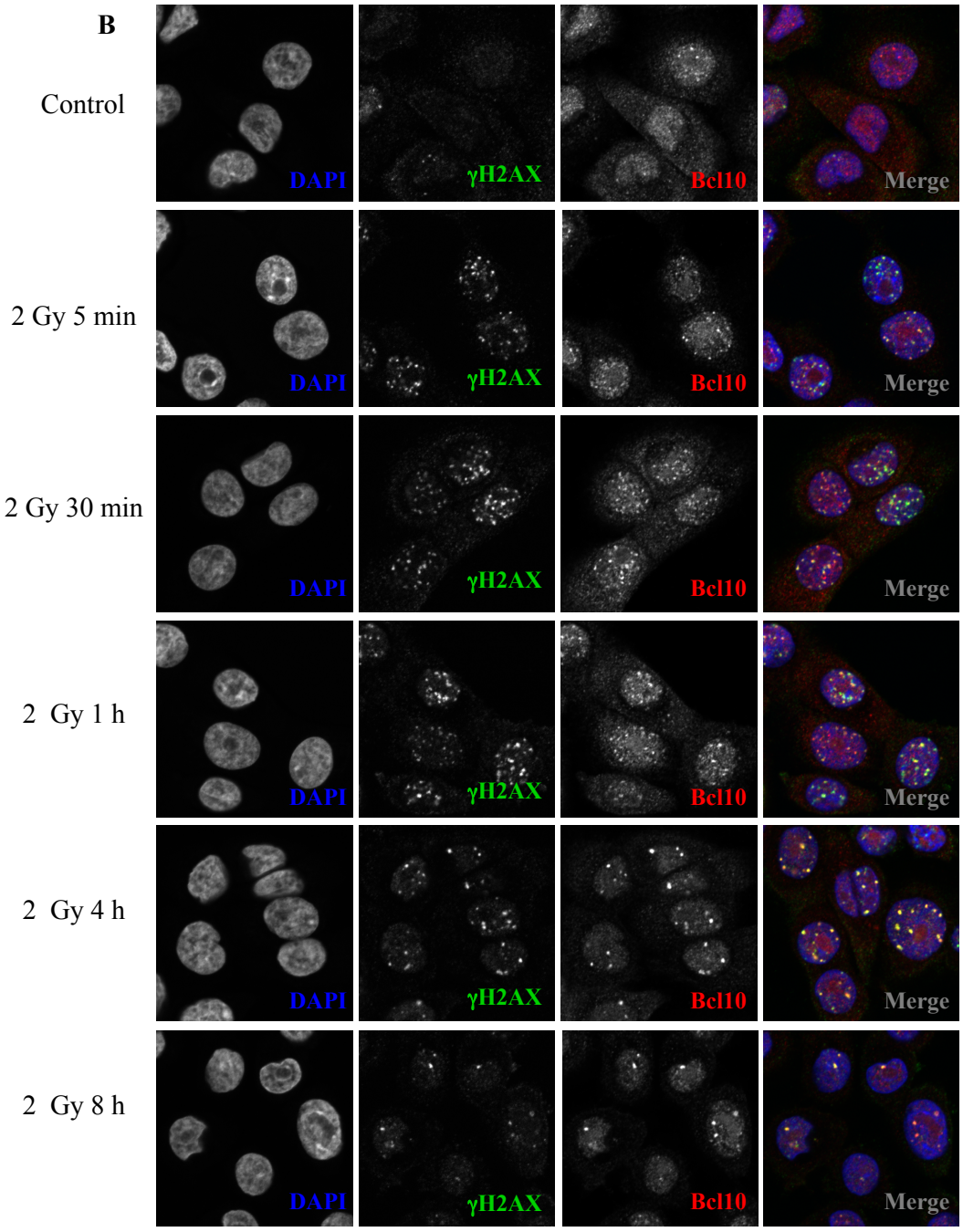
B
Control
2 Gy 5 min
2 Gy 30 min
2 Gy 1 h
2 Gy 4 h
2 Gy 8 h
DAPI
γH2AX
Bcl10
Merge

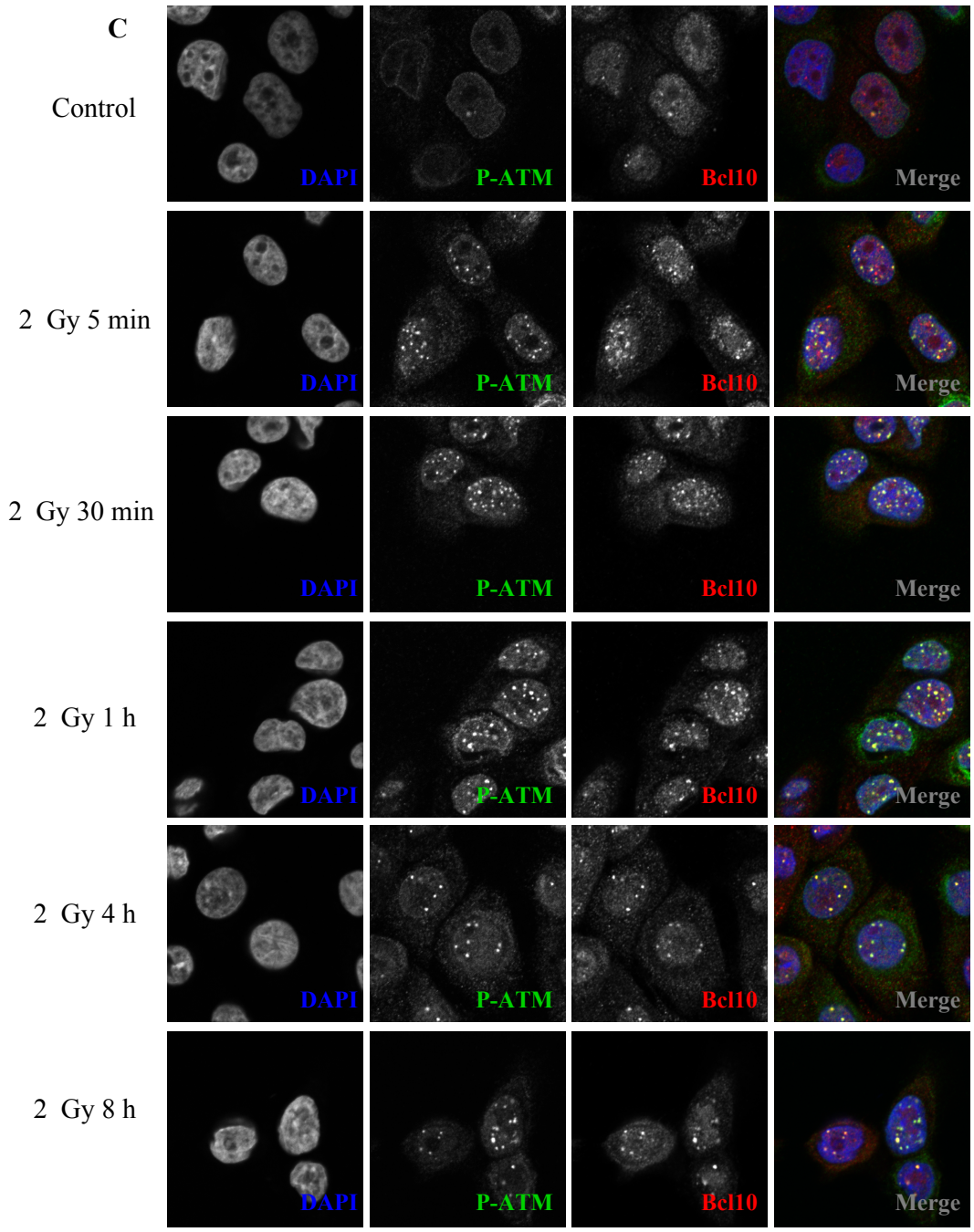
C
Control
DAPI
P-ATM
Bcl10
Merge
2 Gy 5 min
DAPI
P-ATM
Bcl10
Merge
2 Gy 30 min
DAPI
P-ATM
Bcl10
Merge
2 Gy 1 h
DAPI
P-ATM
Bcl10
Merge
2 Gy 4 h
DAPI
P-ATM
Bcl10
Merge
2 Gy 8 h
DAPI
P-ATM
Bcl10
Merge

D

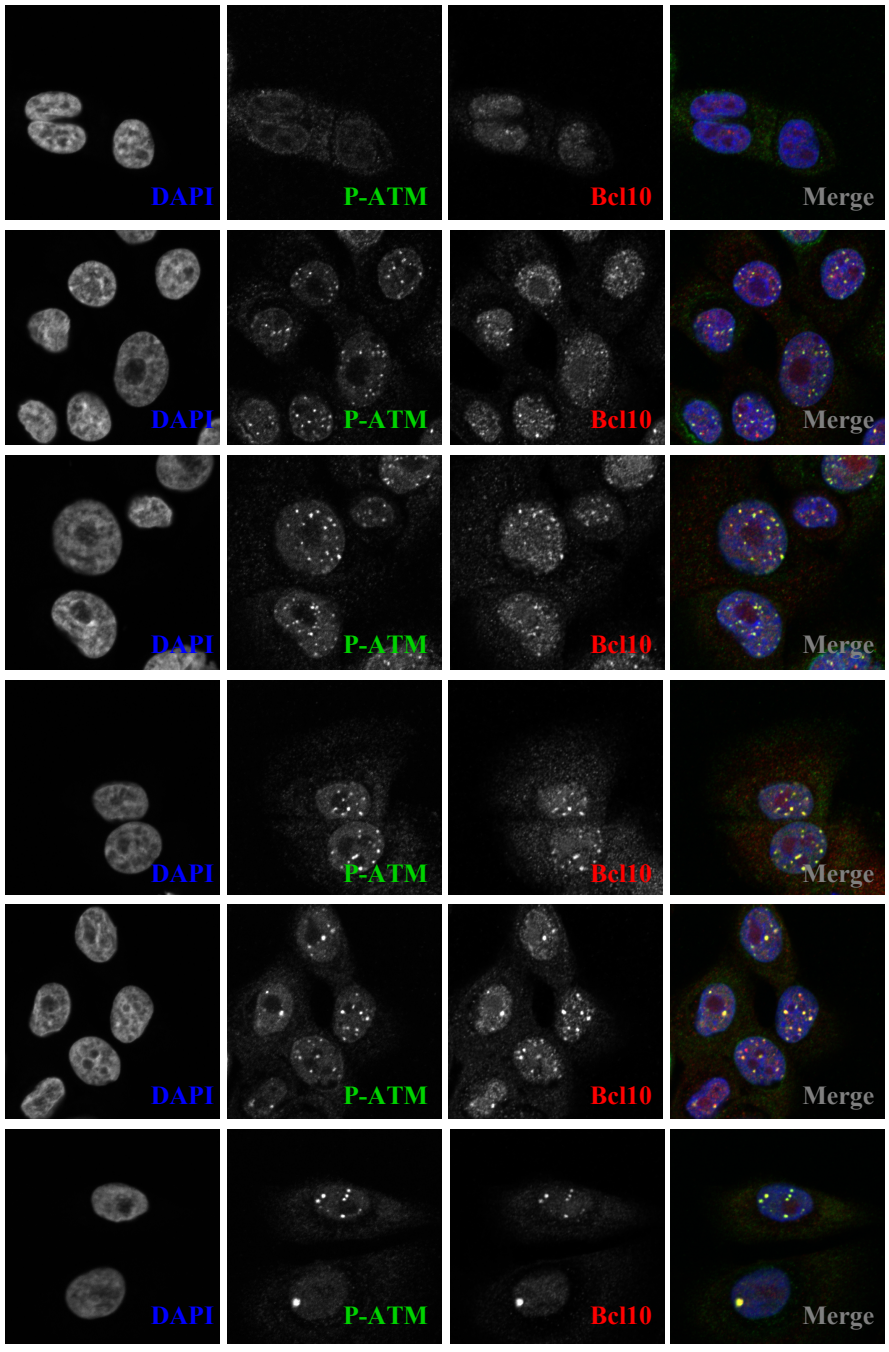
Control
DAPI
P-ATM
Bcl10
Merge
2 Gy 5 min
DAPI
P-ATM
Bcl10
Merge
2 Gy 30 min
DAPI
P-ATM
Bcl10
Merge
2 Gy 1 h
DAPI
P-ATM
Bcl10
Merge
2 Gy 4 h
DAPI
P-ATM
Bcl10
Merge
2 Gy 8 h
DAPI
P-ATM
Bcl10
Merge

E

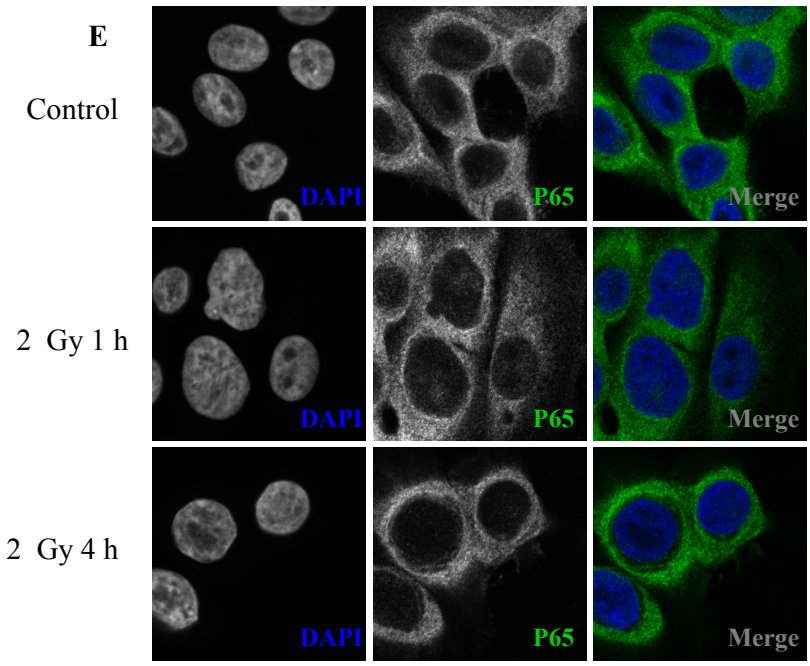

hTERT-HME1 Bay11 Treatment

F

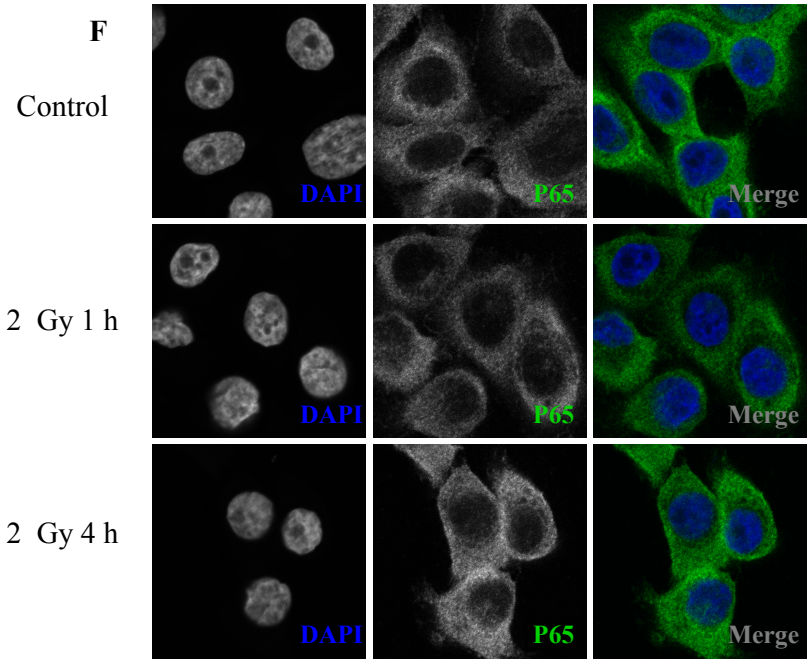

hTERT-HME1 DMSO Treatment

foci at 5 and 30 mins post-IR, co-localizing with the majority of P-ATM foci by 30 mins and 100% of the foci by 1 h post-IR and building up in the foci at 4 and 8 h post-IR. To ensure that Bay-11 is successfully blocking NF-κB activation, we monitored p65 nuclear translocation. In Bay-11-treated cells, we see almost no nuclear p65 in the unirradiated control and at 1 h and 4 h post-IR (Figure 3.20E). In DMSO-treated cells however, we see a similar amount of nuclear p65 in the unirradiated control and at 1 h post-IR and then an increase in nuclear p65 at 4 h post-IR (Figure 3.20F). Indicating that Bay-11 is effectively blocking NF-κB activation.

3.3.6 NF-κB inhibition has no effect on the repair of radiation-induced DNA damage in hTERT-HME1 cells

Comet assays were performed to assess DNA repair in Bay-11 and DMSO-treated hTERT-HME1 cells. Figure 3.21A shows that Bay-11 and DMSO-treated cells have similar tail lengths in the unirradiated control and at 2, 4, and 24 h post-IR with 5 Gy. Quantification of the percent of DNA in the tail revealed that there is no significant difference between Bay-11-treated cells and DMSO-treated cells at all time points (Figure 3.21B). Similarly, there is no significant difference in the number of γH2AX foci in Bay-11 and DMSO-treated cells in the unirradiated control, and at 1 h and 4 h post-IR (Figure 3.22). Bay-11-treated cells contain 0.56, 57.9 and 27.0 γH2AX foci per nucleus in the unirradiated control, at 1 h post-IR and 4 h post-IR, respectively. While DMSO-treated cells contain 0.18,

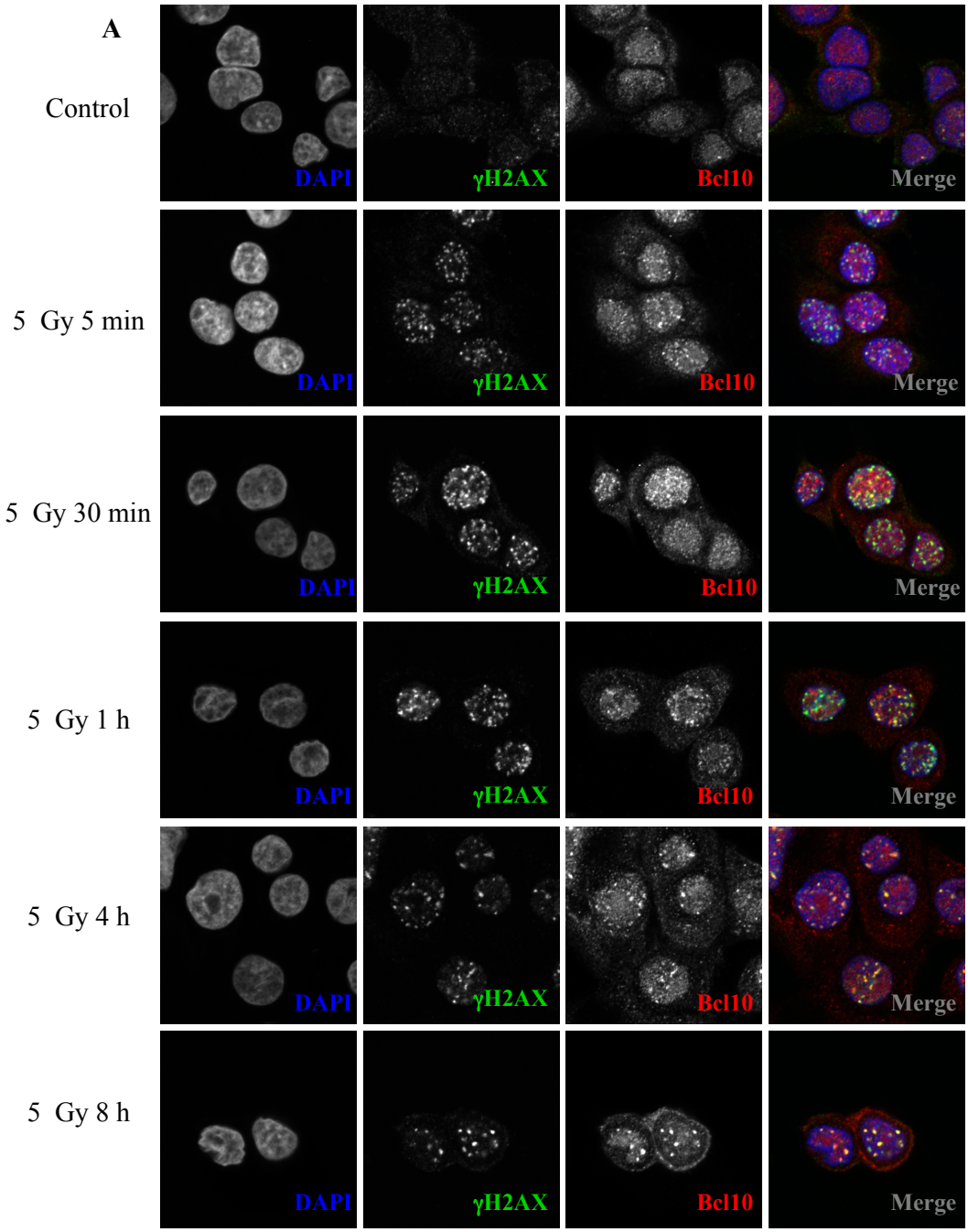

Figure 3.20 Bcl10 is recruited to ionizing radiation-induced foci in hTERT-HME1 cells treated with Bay-11 (5 Gy). hTERT-HME1 cells were treated with 3.5 μM Bay-11 (A, C, E) or DMSO (B, D, F) 2 h prior to irradiation with 5 Gy, cells were fixed after 5 mins, 30 mins, 1 h, 4 h, and 8 h, unirradiated cells were fixed as a control. DAPI was used as a counterstain. (A+B) Fixed cells were stained with mouse anti-γH2AX (FITC, green), rabbit anti-Bcl10 (Cy3, red). (C+D) Fixed cells were stained with mouse anti-P-ATM (FITC, green), rabbit anti-Bcl10 (Cy3, red). (E+F) Fixed cells were stained with mouse anti-p65 (FITC, green).

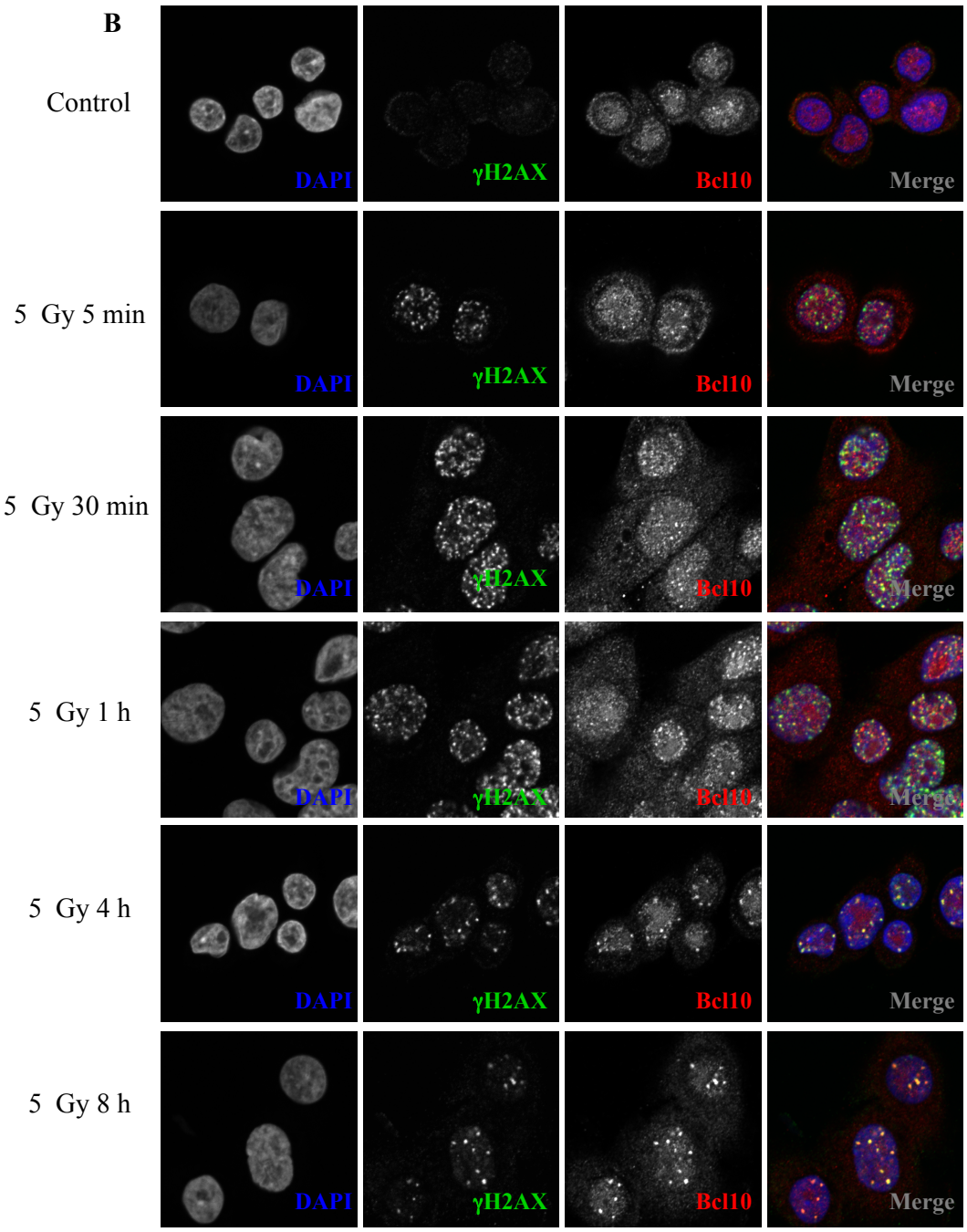
B
Control
5 Gy 5 min
5 Gy 30 min
5 Gy 1 h
5 Gy 4 h
5 Gy 8 h
DAPI
γH2AX
Bcl10
Merge

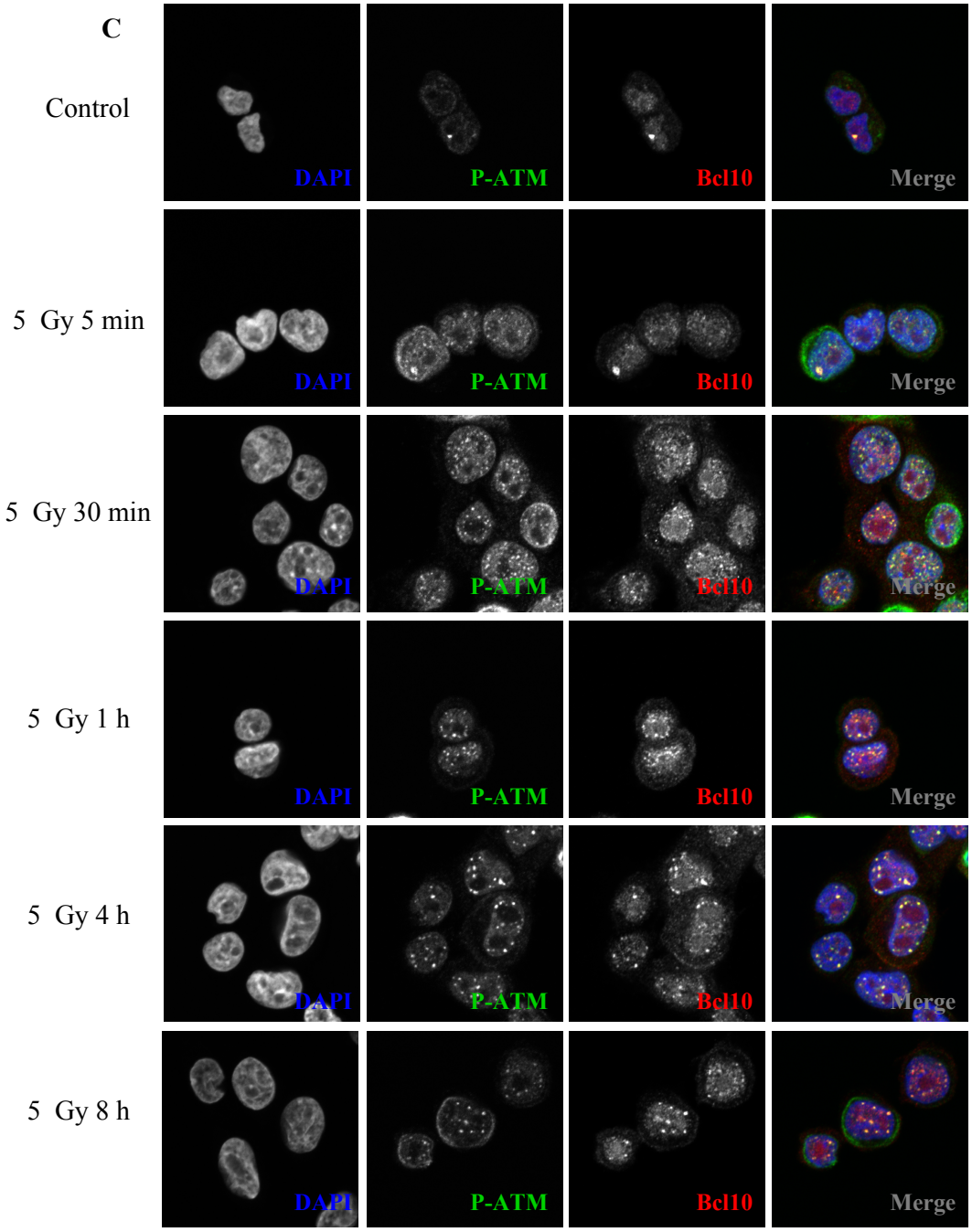
C
Control
DAPI
P-ATM
Bcl10
Merge
5 Gy 5 min
DAPI
P-ATM
Bcl10
Merge
5 Gy 30 min
DAPI
P-ATM
Bcl10
Merge
5 Gy 1 h
DAPI
P-ATM
Bcl10
Merge
5 Gy 4 h
DAPI
P-ATM
Bcl10
Merge
5 Gy 8 h
DAPI
P-ATM
Bcl10
Merge

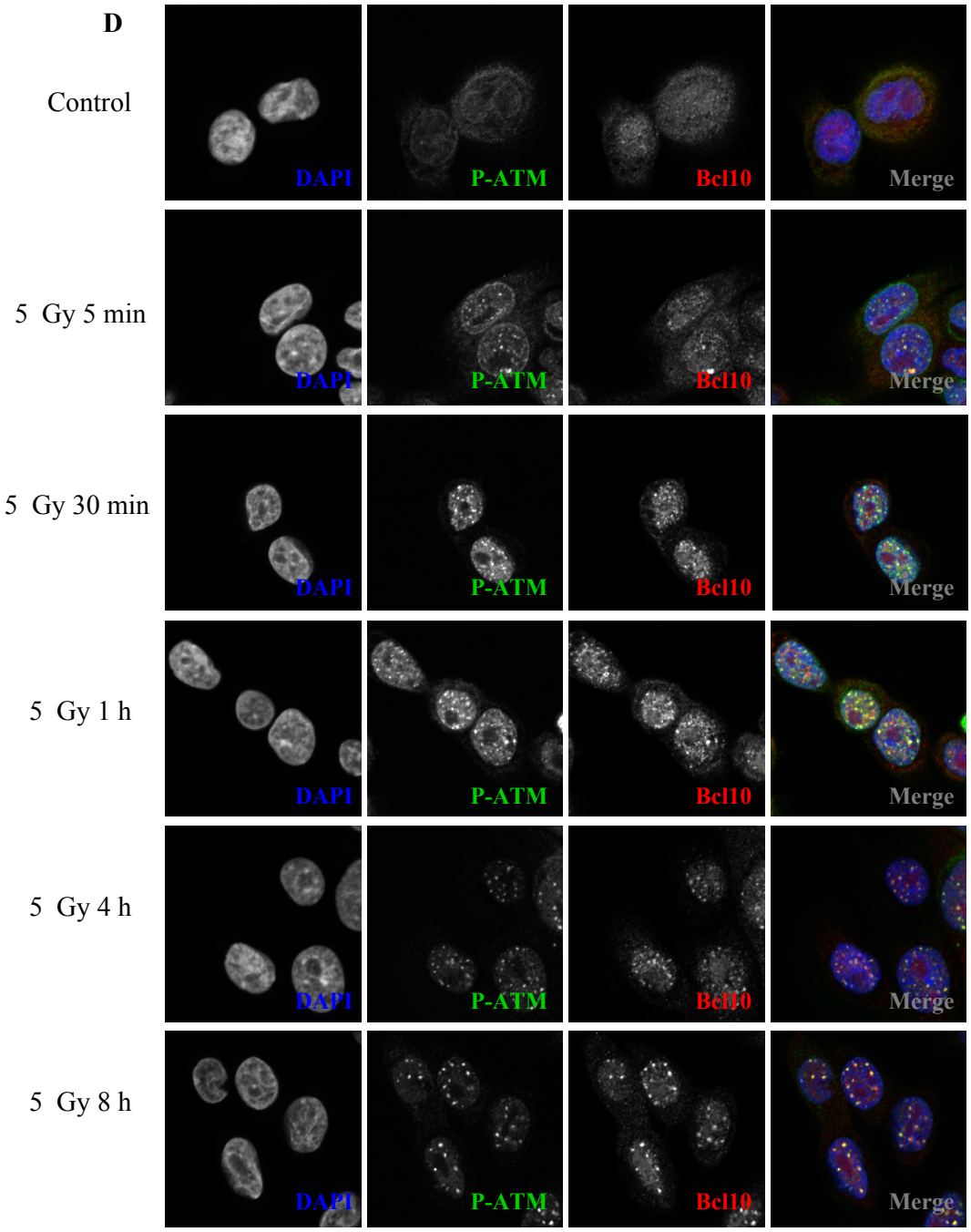
D
Control
DAPI
P-ATM
Bcl10
Merge
5 Gy 5 min
DAPI
P-ATM
Bcl10
Merge
5 Gy 30 min
DAPI
P-ATM
Bcl10
Merge
5 Gy 1 h
DAPI
P-ATM
Bcl10
Merge
5 Gy 4 h
DAPI
P-ATM
Bcl10
Merge
5 Gy 8 h
DAPI
P-ATM
Bcl10
Merge

E

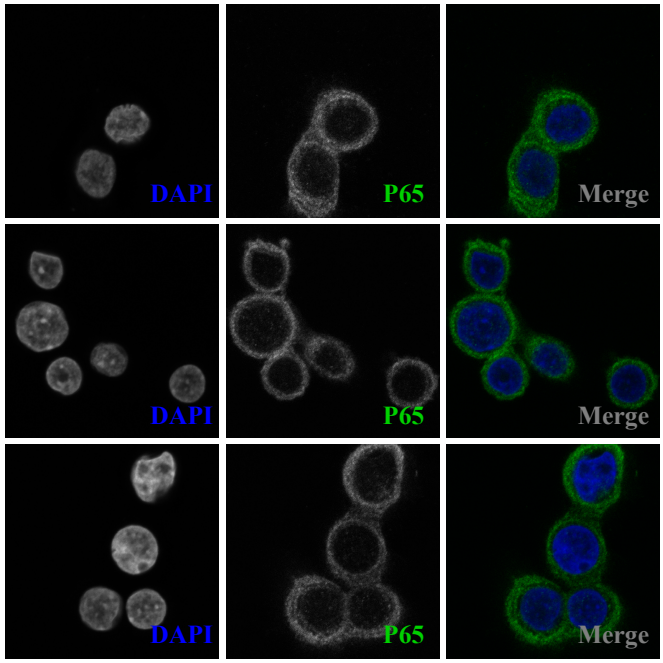

hTERT-HME1 Bay11 Treatment

F

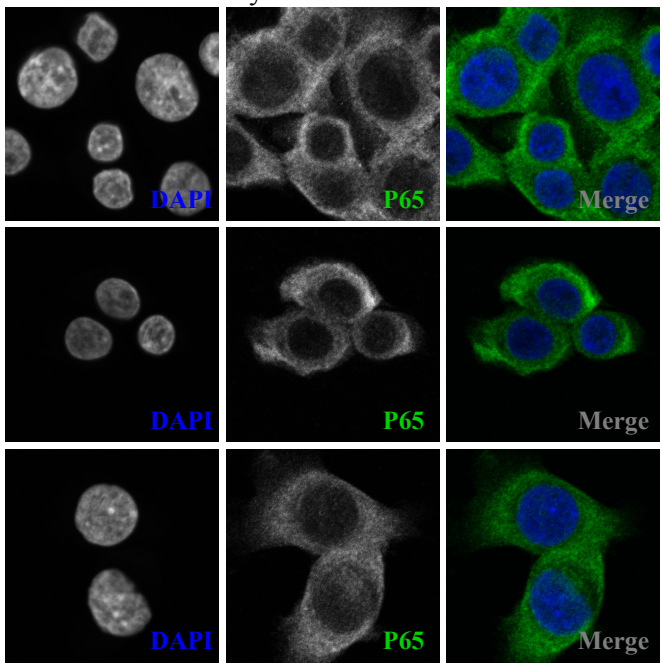

hTERT-HME1 DMSO Treatment

Figure 3.21 Bay-11 treatment does not alter the repair of radiation-induced DNA damage in hTERT-HME1 cells. hTERT-HME1 cells were treated with Bay-11 or DMSO. Two hours after treatment, cells were exposed to 5 Gy ionizing radiation and introduced into the comet assay 1 h, 2 h, 4 h and 24 h post-IR. Unirradiated cells served as a control. (A) Images were taken using a Zeiss Image.Z.1 upright microscope with a Cooke SensiCam High performance camera and a 20X/0.8 NA Zeiss Plan-ApoChromat dry lens. (B) Comet tails were measured using CometScore. Error bars represent SEM.

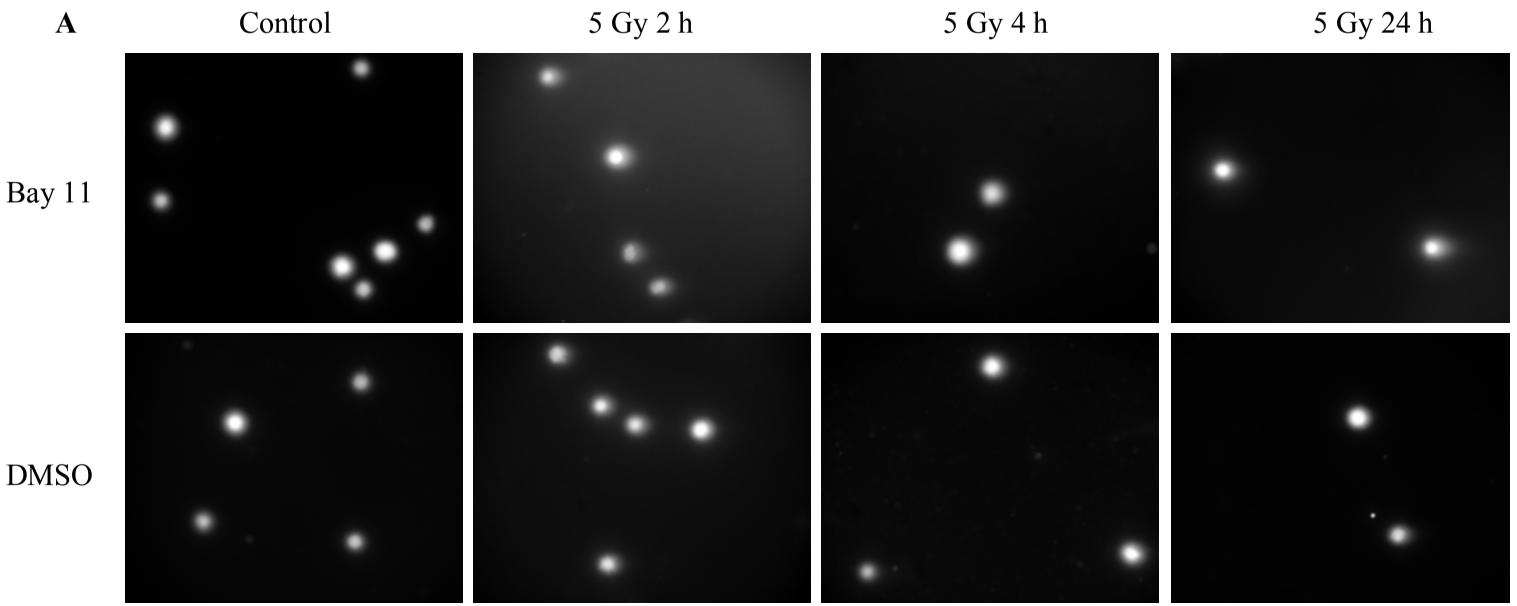
A
Control
5 Gy 2 h
5 Gy 4 h
5 Gy 24 h
Bay 11
DMSO

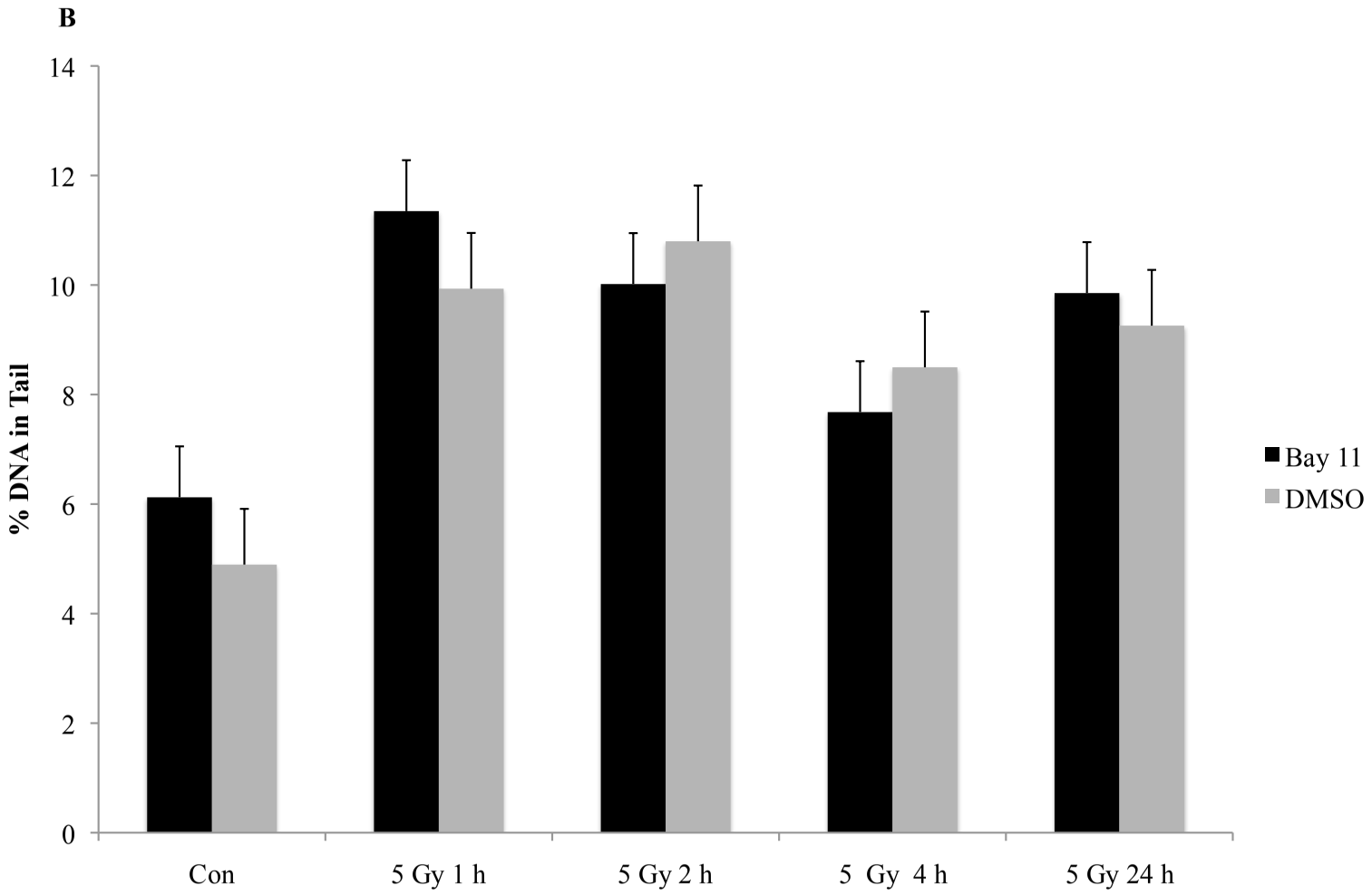
B
% DNA in Tail
14
12
10
8
6
4
2
0
Con
5 Gy 1 h
5 Gy 2 h
5 Gy 4 h
5 Gy 24 h
Bay 11
DMSO

Figure 3.22 Bay-11 treatment does not alter γH2AX foci formation in hTERT-HME1 cells. hTERT-HME1 cells were treated with 3.5 μM Bay-11 or DMSO. After 2 h, cells were exposed to 5 Gy ionizing radiation and fixed in 3.7% formaldehyde 1 h and 4 h post-IR. Unirradiated cells were fixed as a control. Fixed cells were stained with mouse anti-γH2AX and counterstained with DAPI. Foci were quantified using Imaris. Error bars represent SEM.

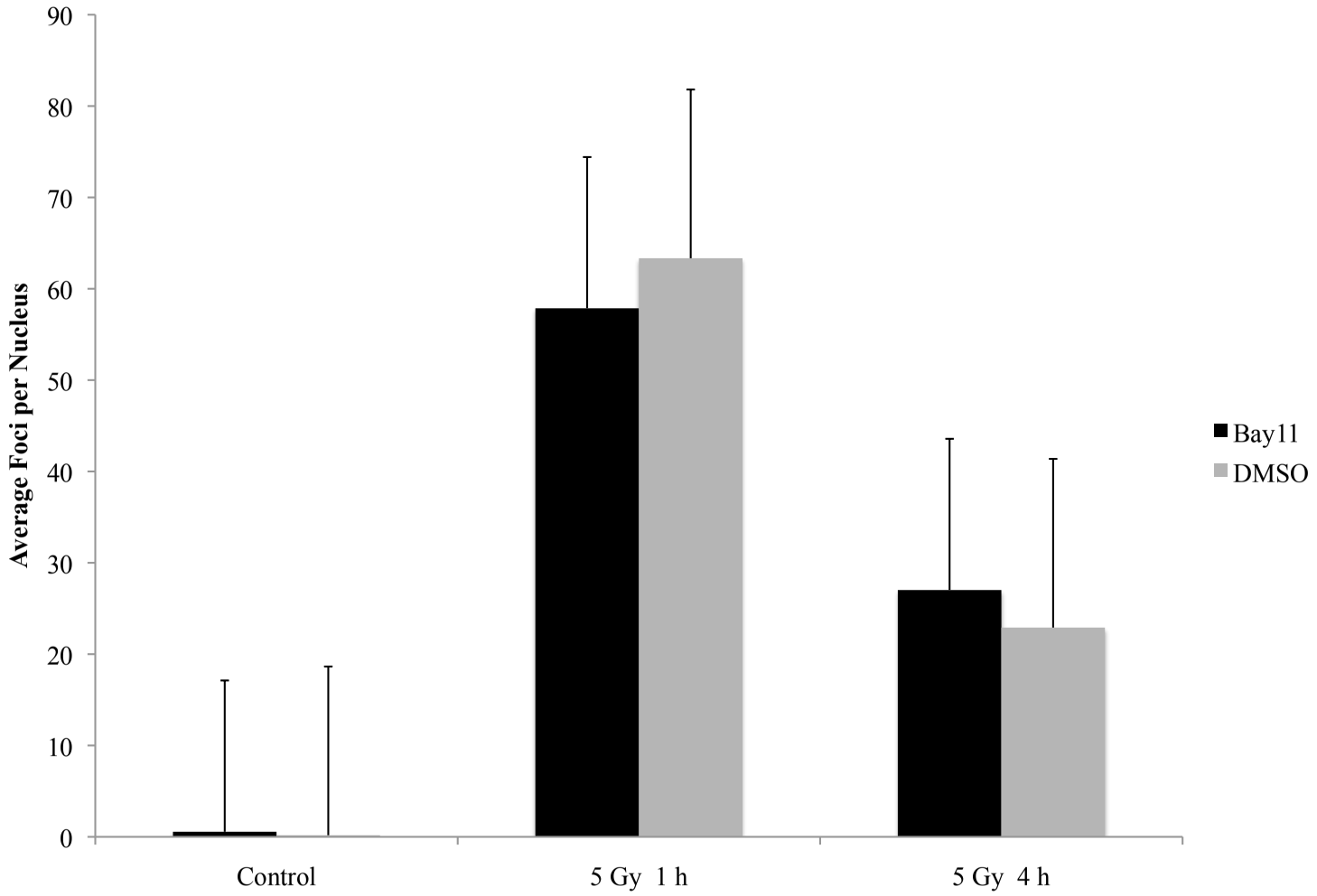
Average Foci per Nucleus
90
80
70
60
50
40
30
20
10
0
Control
5 Gy 1 h
5 Gy 4 h
Bay11
DMSO

63.3 and 22.9 foci per nucleus in the unirradiated control, at 1 h post-IR and 4 h post-IR, respectively.

3.4 Bcl10 protects breast cancer cells from cellular senescence

There is a lot of controversy over the function and origins of cryptogenic foci. Recently, it has been published that a proportion of cryptogenic foci in cancer cells associate with dysfunctional telomeres [39]. Dysfunctional telomeres and severe DNA damage, in particular DSB, have been linked to the induction of cellular senescence [89, 102]. Since we have observed that Bcl10 co-localizes to cryptogenic foci and has an important role in the repair of radiation-induced DNA damage, we wanted to investigate whether Bcl10 also plays a role in cellular senescence.

3.4.1 Bcl10 knockdown results in the collapse of cryptogenic foci while MALT1 has no effect

Using transient transfection in combination with indirect immunofluorescent staining, we examined whether Bcl10 knockdown has any effect on cryptogenic foci. When we looked at T47D cells 48 h post-transfection, we noticed that cells treated with Bcl10 siRNA have almost no cryptogenic foci, while foci are still present in mock-transfected cells (Figure 3.23A). Figure 3.23B shows that Bcl10 siRNA transfected cells contain significantly fewer γH2AX foci than mock-transfected cells ($p < 0.001$). The western blot in figure 3.23C shows that Bcl10 levels are efficiently reduced. To investigate how Bcl10 knockdown effects cell

survival and radio-sensitivity, we performed cell survival experiments. We observe that Bcl10 knockdown prior to irradiation causes ~2.4-fold decrease in survival, this decrease is maintained until 4 Gy where it increases to ~3-fold and continues to further increase out to 10 Gy where we see a ~5.9-fold decrease in survival compared to mock-transfected cells (Figure 3.24). This suggests that Bcl10 knockdown drastically reduces breast cancer cell survival and radio-sensitivity.

Apart from Bcl10, we also observed that MALT1, a Bcl10 interacting protein, co-localizes to cryptogenic foci, so we wanted to determine if MALT1 knockdown would have a similar effect. MALT1 knockdown, unlike Bcl10 knockdown, appears to have no effect on cryptogenic foci; when we look at cells 48 h post-transfection, we see that MALT1 siRNA-treated cells still have Bcl10/γH2AX foci like mock-transfected cells however, MALT1 is absent from these foci (Figure 3.25A). Quantification of the γH2AX foci revealed that there is no significant difference in the number of foci present in MALT1 siRNA transfected cells compared to mock-transfected cells (Figure 3.25B). Figure 3.25C shows that MALT1 siRNA sufficiently reduces MALT1 protein levels. Cell survival experiments reveal that MALT1 knockdown increases T47D cell radio-sensitivity, starting at 2 Gy, where we see a ~2 fold decrease in survival, out to 10 Gy where we see a ~3.7 fold decrease in survival compared to mock-transfected cells (Figure 3.26).

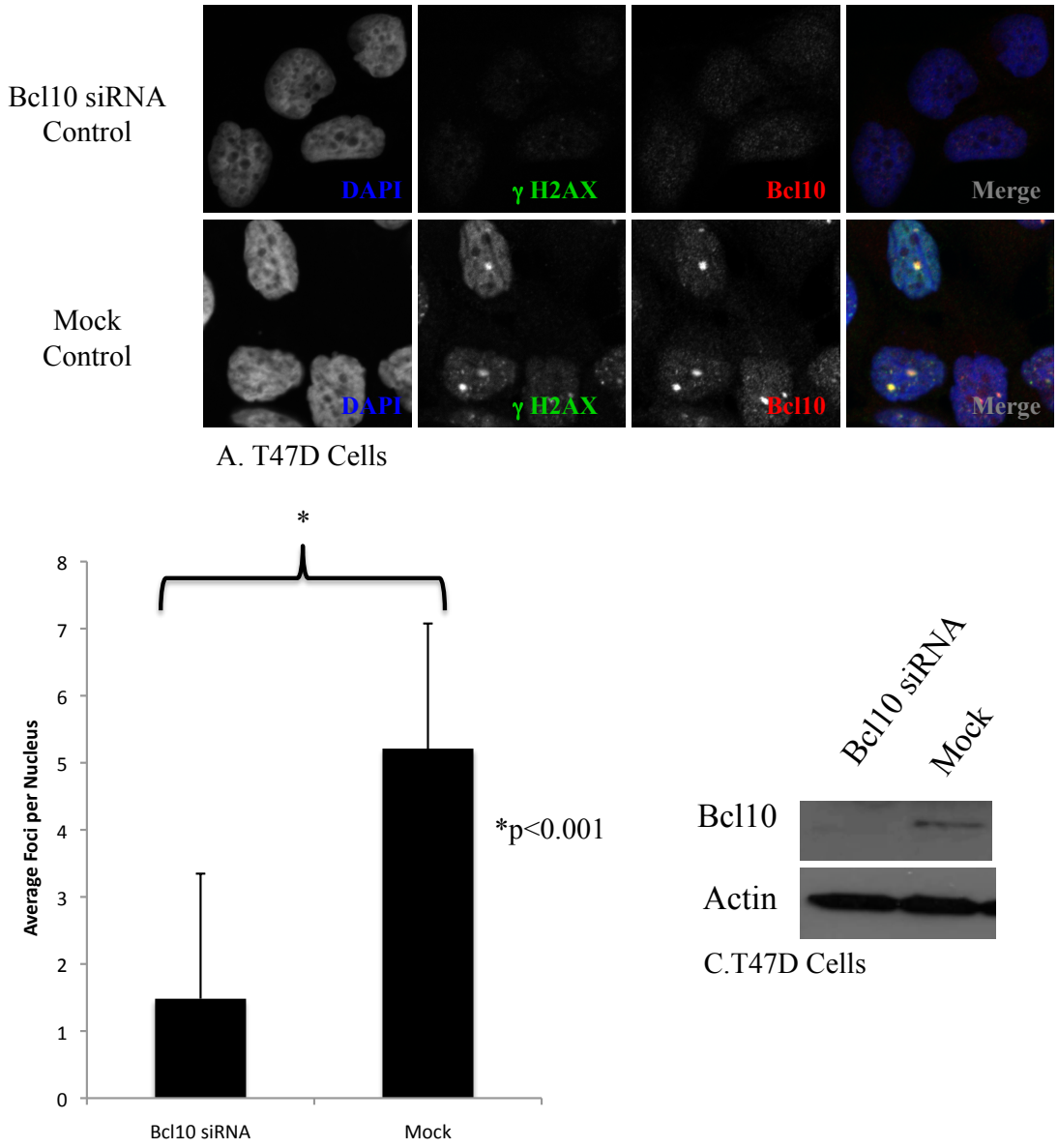

Figure 3.23 Bcl10 knockdown disrupts cryptogenic foci. T47D cells were transfected with Bcl10 siRNA or scrambled siRNA (mock). 48 h after transfection cells were: (A) Fixed and stained with mouse anti-γH2AX (FITC, green) and rabbit anti-Bcl10 (Cy3, red), and counterstained with DAPI. (B) Foci were quantified using Imaris. Error bar represent SEM. (C) Whole cell lysates were isolated and separated on a 12% SDS-polyacrylamide gel. The samples were transferred to a nitrocellulose membrane and immunostained with mouse anti-actin, and rabbit anti-Bcl10. Primary antibodies were detected with goat anti-mouse IgG-peroxidase or goat anti-rabbit IgG-peroxidase and developed with Amersham ECL Western Blotting Detection Reagent.

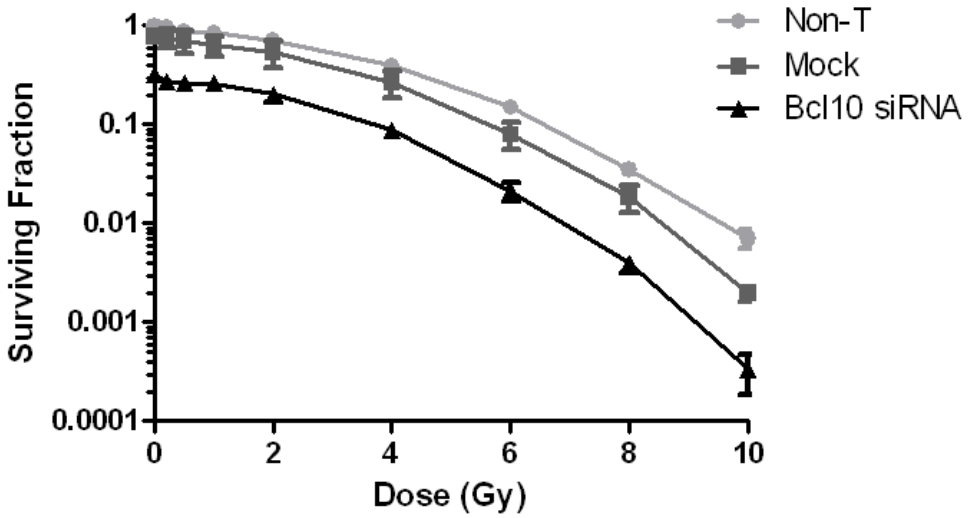

Figure 3.24 Bcl10 knockdown impairs T47D cell survival. T47D cells were transfected with Bcl10 siRNA or a scrambled siRNA, non-transfected cells were included as a control. 48 h post-transfection cells were counted, diluted to the desired cell numbers and re-plated, six replicates were plated for each treatment condition. The following day plates were irradiated at 0.2, 0.5, 1, 2, 4, 6, 8, or 10 Gy and incubated at 37°C and 5% CO_2 for 14 days, unirradiated cells were included as a control. Plates were then stained with crystal violet and the colonies were manually counted. Error bars represent SEM.

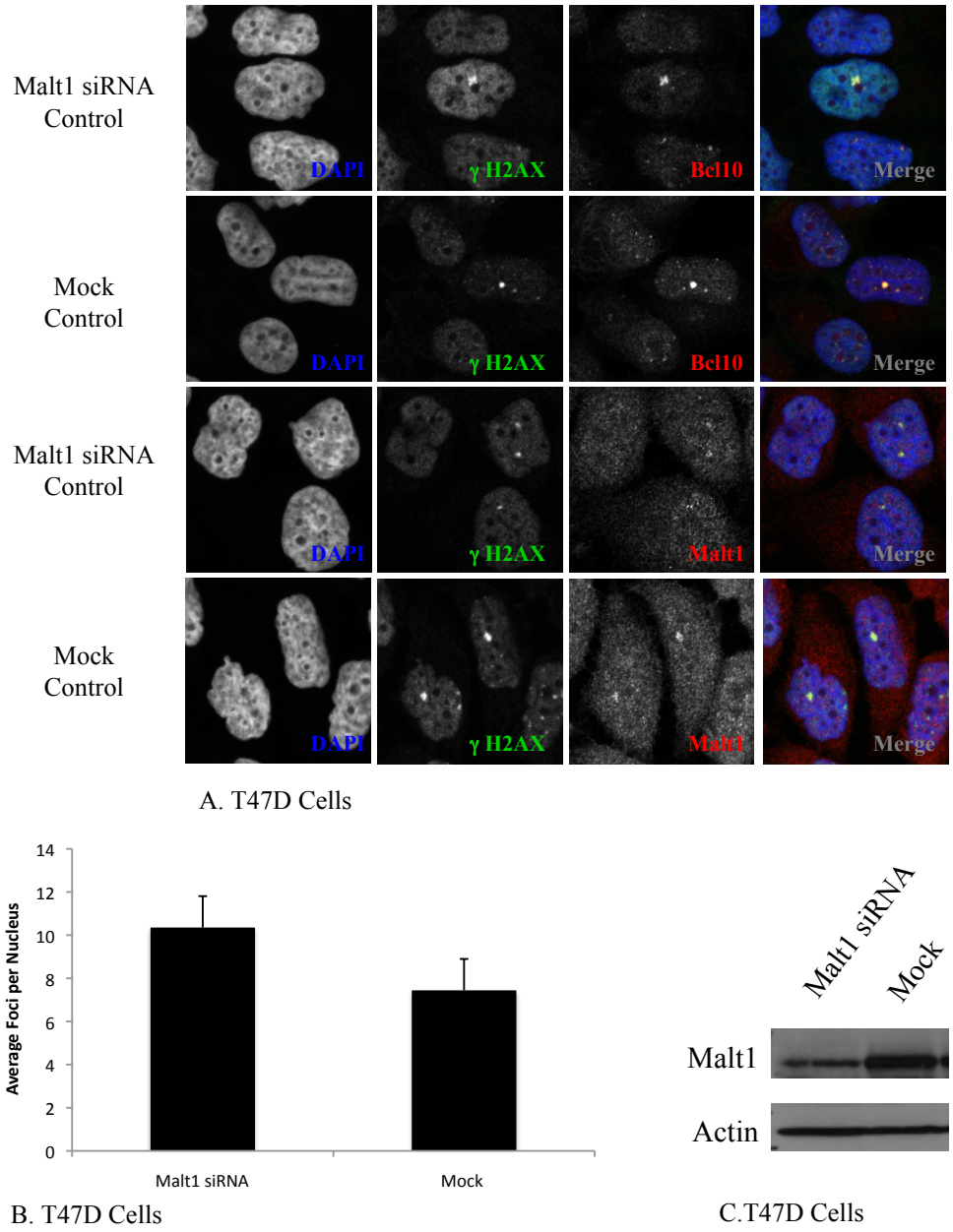

Figure 3.25 MALT1 knockdown does not disrupt cryptogenic foci. T47D cells were transfected with MALT1 siRNA or scrambled siRNA (mock). 48 h after transfection cells were: (A) Fixed and stained with mouse anti-γH2AX (FITC, green) and rabbit anti-Bcl10 (Cy3, red), or rabbit anti-MALT1 (Cy3, red) and counterstained with DAPI. (B) Foci were quantified using Imaris. Error bars represent SEM. (C) Whole cell lysates were isolated and separated on a 10% SDS-polyacrylamide gel. The samples were transferred to a nitrocellulose membrane and immunostained with mouse anti-actin, and rabbit anti-MALT1. Primary antibodies were detected with goat anti-mouse IgG-peroxidase or goat anti-rabbit IgG-peroxidase and developed with Amersham ECL Western Blotting Detection Reagent.

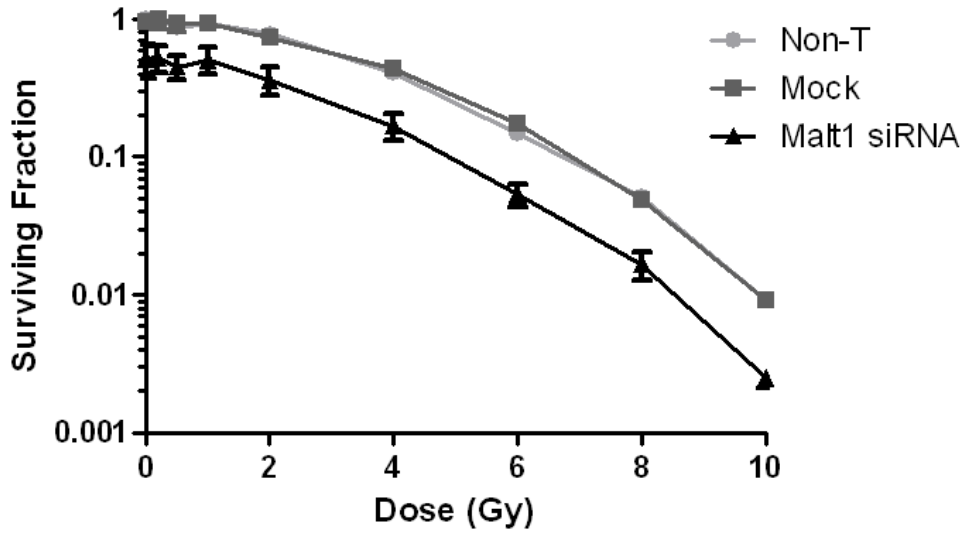

Figure 3.26 MALT1 knockdown increases radio-sensitivity in T47D cells. T47D cells were transfected with MALT1 siRNA or a scrambled siRNA, non-transfected cells were included as a control. 48 h post-transfection cells were counted, diluted to the desired cell numbers and re-plated. Six replicates were plated for each treatment condition. The following day plates were irradiated at 0.2, 0.5, 1, 2, 4, 6, 8, or 10 Gy and incubated at 37°C and 5% CO_2 for 14 days, unirradiated cells were included as a control. Plates were then stained with crystal violet and the colonies were manually counted. Error bars represent SEM.

We also compared the number of cryptogenic foci present in breast cancer cells, T47D, to the number present in normal breast epithelial cells that have been immortalized with telomerase, hTERT-HME1. We found that hTERT-HME1 cells contain very few cryptogenic foci compared to T47D cells (Figure 3.27A). Quantification of these results revealed that this difference is statistically significant (Figure 3.27B).

3.4.2 Bcl10 knockdown induces cellular senescence in T47D cells

Since we observed that Bcl10 knockdown drastically decreases T47D cell survival, we wanted to determine if this was attributed to cellular senescence. To achieve this, we used transient transfection in combination with a senescence-associated β-galactosidase (SA-β-gal) assay. With this assay, senescent cells are identified by the appearance of a blue color in the cytoplasm. We first looked at senescence in T47D cells 48 h after transfection and found that more Bcl10 siRNA transfected cells were senescent (SA-β-gal positive), compared to mock and non-transfected cells (Figure 3.28A). Figure 3.28B shows that significantly more Bcl10 siRNA transfected cells stain positive for SA-β-gal compared to mock and non-transfect cells ($p < 0.05$). To verify this phenotype, we passaged cells 48 h after transfection and allowed them to grow for another 72 h before performing the SA-β-gal staining (5 days post-transfection). We observed that, at 5 days post-transfection, the majority of Bcl10 siRNA transfected cells stain positive, while only a minor proportion of mock and non-transfected cells appear

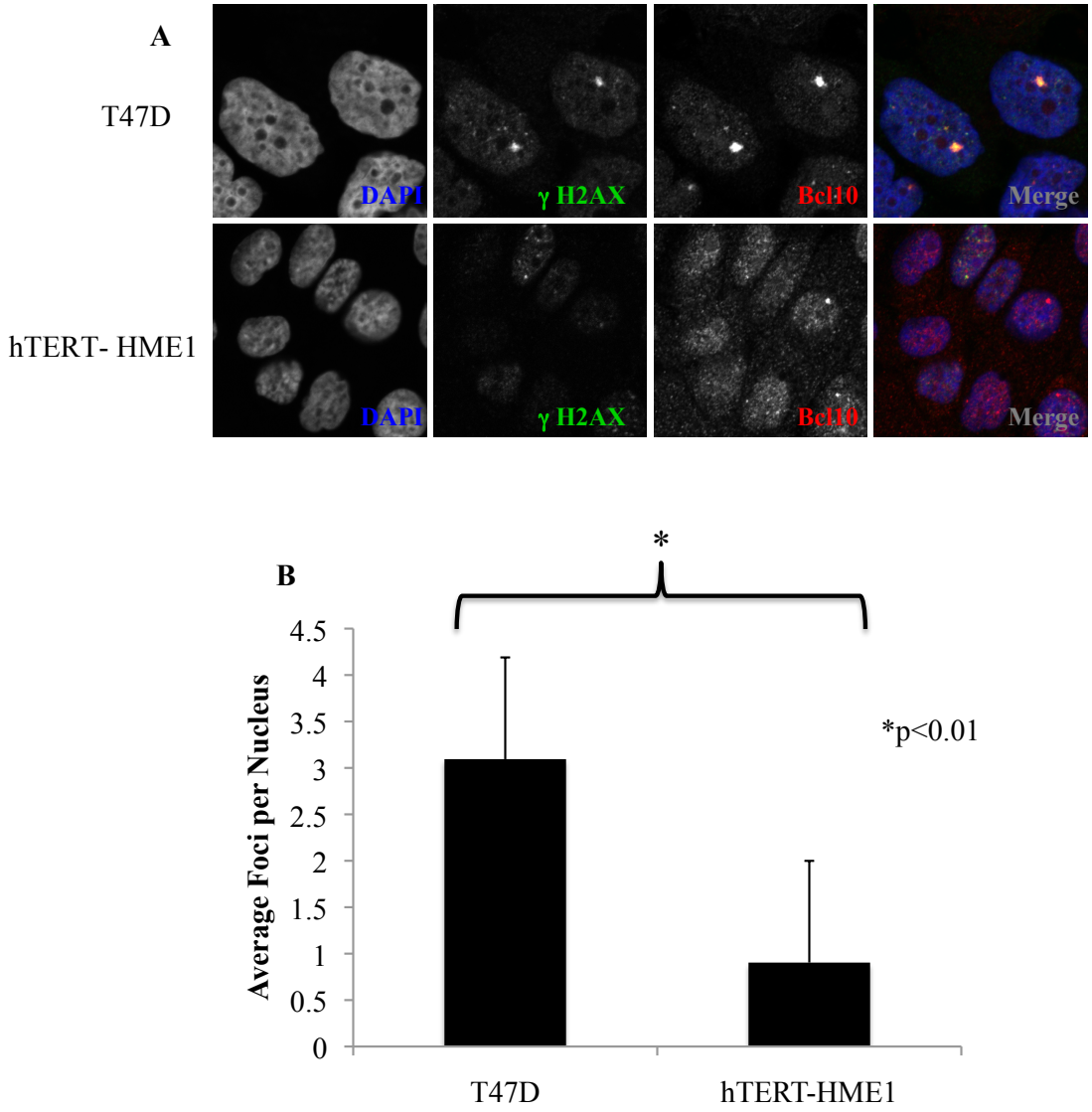

Figure 3.27 hTERT-HME1 cells contain very few cryptogenic foci compared to T47D cells. hTERT-HME1 and T47D cells were: (A) Fixed and stained with mouse anti-γH2AX (FITC, green) and rabbit anti-Bcl10 (Cy3, red) and counterstained with DAPI. (B) Foci were quantified using Imaris. Error bar represent SEM.

Figure 3.28 Bcl10 knockdown induces cellular senescence in T47D cells (48 h). T47D cells were transfected with Bcl10 siRNA, scrambled siRNA (mock), or non-transfected. 48 h after transfection, cells were fixed and stained for SA-β-galactosidase. (A) Cells were imaged using an Olympus microscope equipped with a Zeiss axiocam MRC and an Olympus UPlanFL 20X/0.50 N.A dry lens. (B) Images were analyzed using Metamorph. Error bars represent SEM.

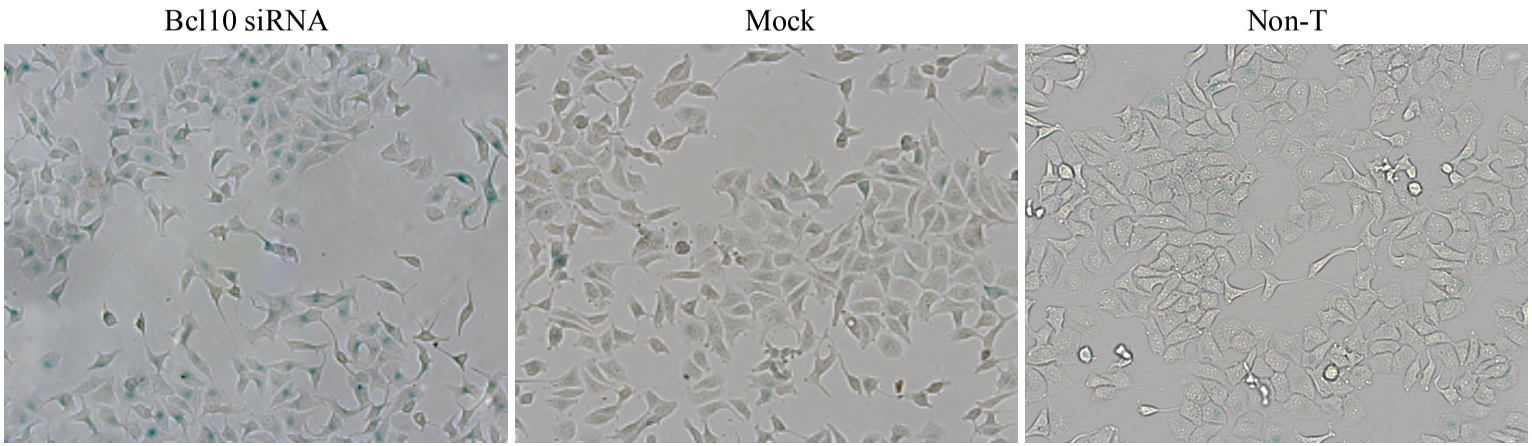

A. T47D 48 h

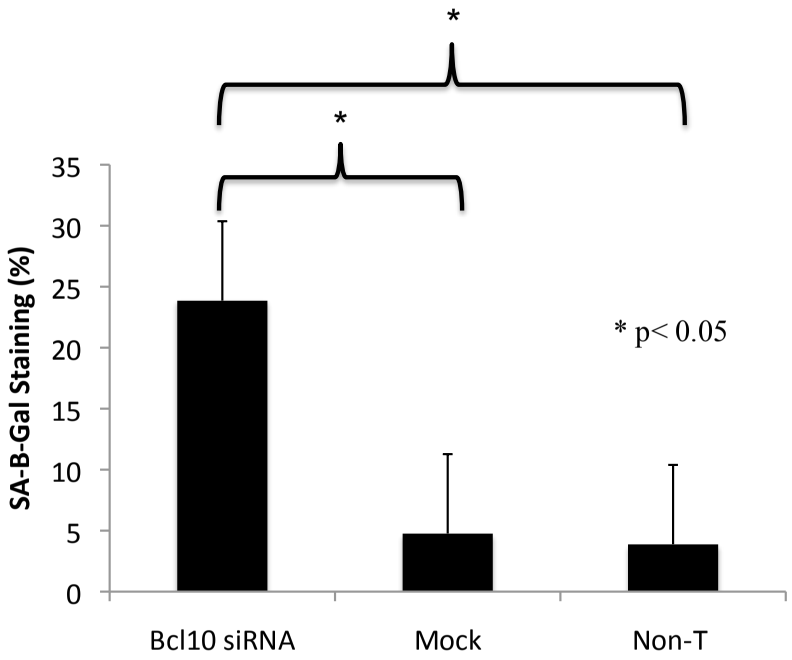

B. T47D 48 h

positive, we also noted that mock and non-transfected cells are more confluent than Bcl10 siRNA cells (Figure 3.29A). Significantly more Bcl10 siRNA transfected cells stain positive for SA-β-gal than mock and non-transfected cells (Figure 3.29B). When we combine the 48 h and the 5 day data we find that there is a significant increase, 23% to 55%, in the number of senescent cells in the Bcl10 siRNA transfected population, while there is only a slight increase, 5% to 10%, in mock-transfected cells, and no change, 3.9% to 4.0%, in non-transfected cells (Figure 3.29C).

3.4.3 Bcl10 knockdown enhances DNA damage-induced cellular senescence in hTERT-HME1 cells

Since hTERT-HME1 cells are a normal cell line that is immortalized with telomerase, we made the assumption that they have functional telomeres. Therefore we decided to use this cell line to assess the role of Bcl10 in DNA-damage induced cellular senescence. hTERT-HME1 cells were transfected and at 48 h post-transfection, cells were irradiated at 5 Gy and allowed to recover for another 72 h before SA-β-gal staining; unirradiated cells plated and transfected at the same time serve as a control. Figure 3.30A shows that Bcl10 knockdown alone slightly increases the number of positive SA-β-gal cells compared to the mock and non-transfected cells. Irradiation at 5 Gy further increases the number of positive SA-β-gal cells in the Bcl10 siRNA population but appears to have a minimal effect on the mock and non-transfected cells (Figure 3.30B). Quantification revealed that significantly more Bcl10 siRNA transfected control

cells stain positive than mock and non-transfected control cells, this is also true for cells irradiated at 5 Gy ($p<0.01$) (Figure 3.30C). Furthermore, there is a significant increase in SA-β-gal staining from Bcl10 siRNA control cells to Bcl10 siRNA cells irradiated at 5 Gy ($p<0.01$).

Figure 3.29 Bcl10 knockdown induces cellular senescence in T47D cells (5 day). T47D cells were transfected with Bcl10 siRNA, scrambled siRNA (mock), or non-transfected. 48 h after transfection cells were passaged into a p100 cell culture dish and allowed to grow for another 72 h. Cells were then fixed and stained for SA-β-galactosidase. (A) Cells were imaged using an Olympus microscope equipped with a Zeiss axiocam MRC and an Olympus UPlanFL 20X/0.50 N.A dry lens. (B) Images were analyzed using Metamorph. Error bars represent SEM. (C) Graph of 48 h and 5 day data. Error bars represent SEM.

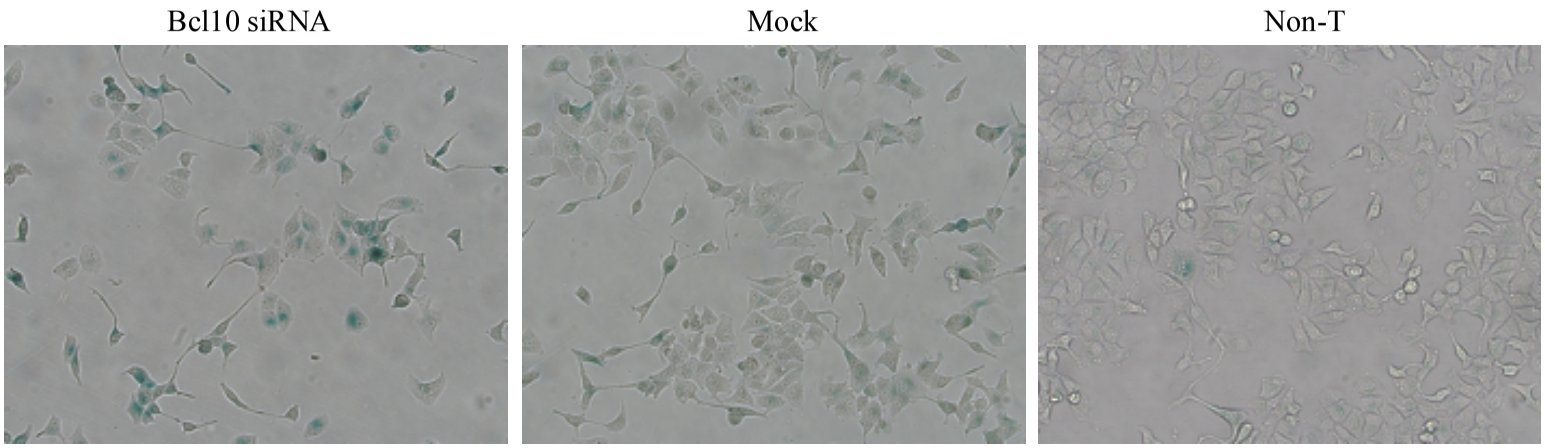

A. T47D 5 day (48 h re-plate)

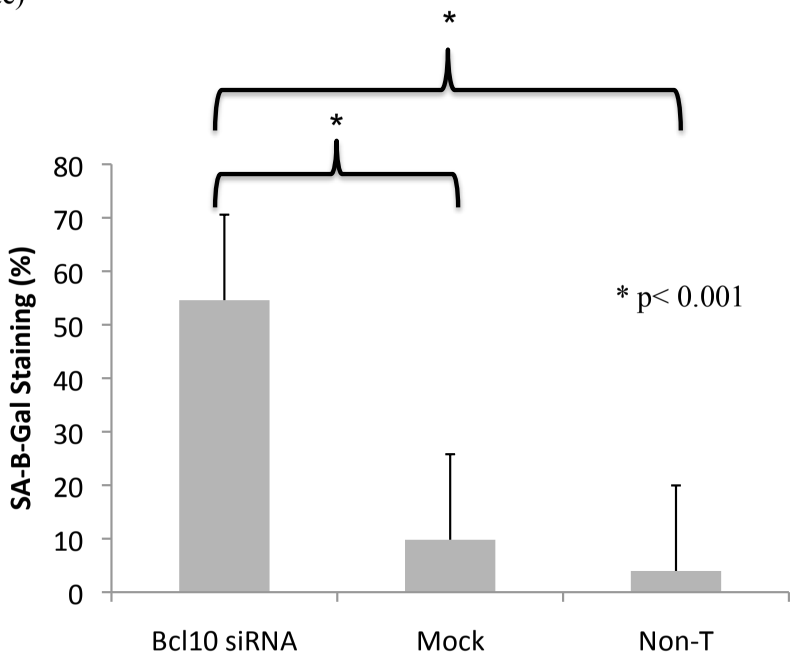

B. T47D 5day (48 h re-plate)

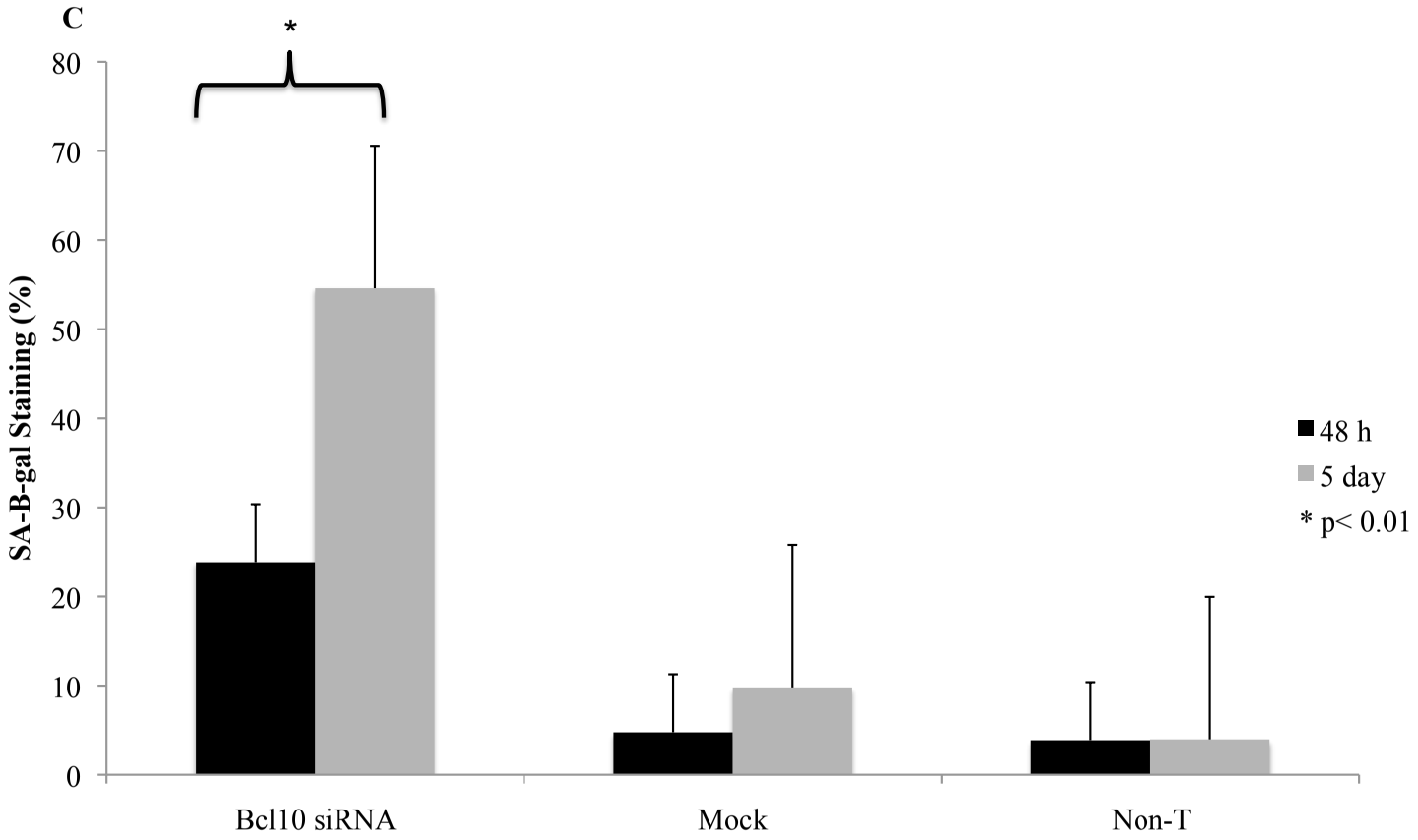
C
*
80
70
60
50
40
30
20
10
0
SA-B-gal Staining (%)
48 h
5 day
* p< 0.01
Bcl10 siRNA
Mock
Non-T

Figure 3.30 Bcl10 knockdown induces cellular senescence in hTERT-HME1 cells following 5 Gy irradiation. hTERT-HME1 cells were transfected with Bcl10 siRNA, scrambled siRNA (mock), or non-transfected. 48 h after transfection cells were irradiated at 5 Gy and allowed to recover for another 72 h. Cells plated and transfected at the same time served as a control (A). Cells were then fixed and stained for SA-β-galactosidase. (A+B) Cells were imaged using an Olympus microscope equipped with a Zeiss axiocam MRC and an Olympus UPlanFL 20X/0.50 N.A dry lens. (C) Images were analyzed using Metamorph. Error bars represent SEM.

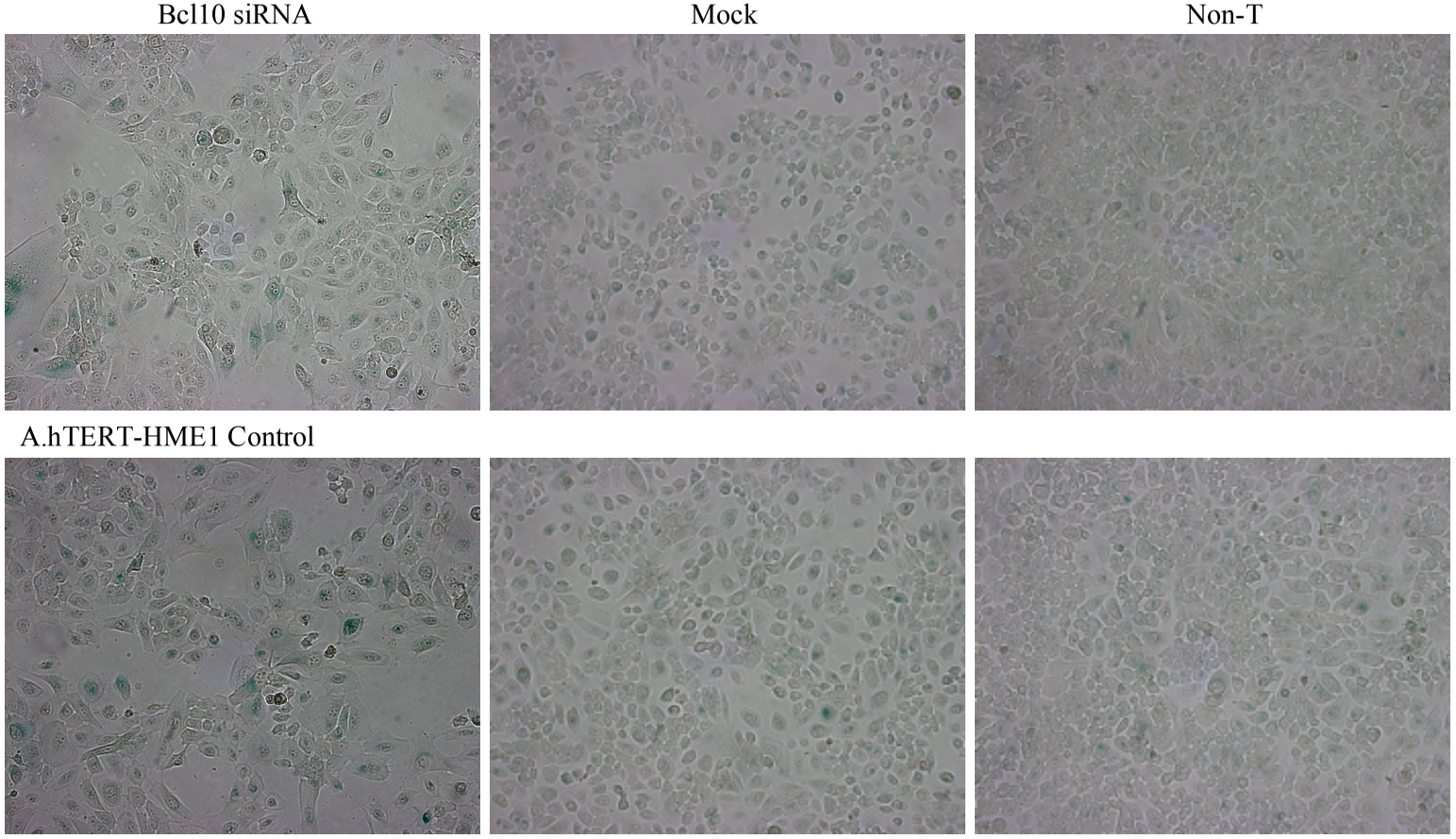
Bcl10 siRNA
Mock
Non-T
A.hTERT-HME1 Control
B.hTERT-HME1 5 Gy

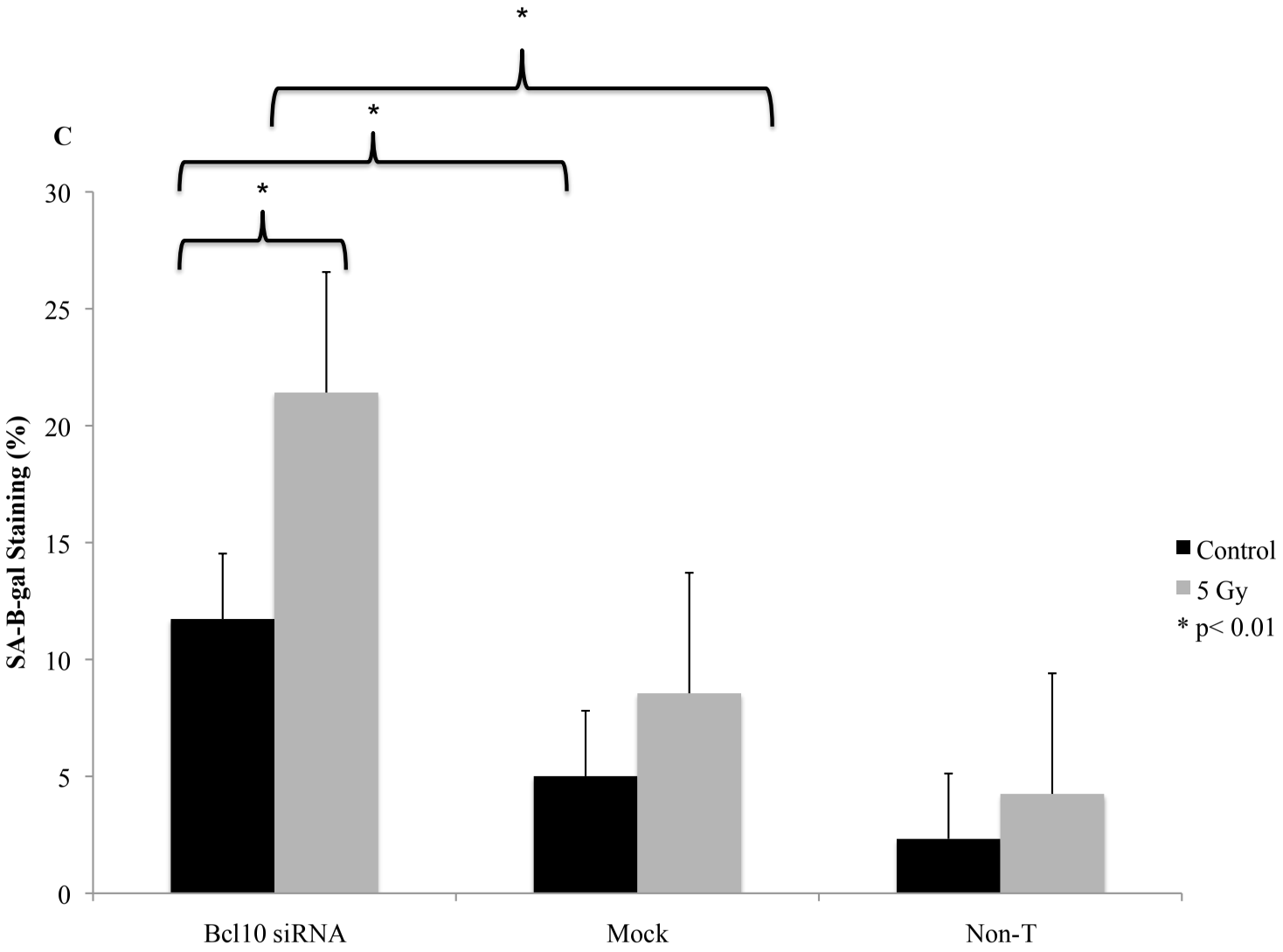
C
SA-B-gal Staining (%)
30
25
20
15
10
5
0
*
*
*
Bcl10 siRNA
Mock
Non-T
Control
5 Gy
* p< 0.01

Chapter 4. Discussion

Bcl10 has been largely investigated for its role in NF-κB activation, a process that occurs in the cytoplasm of lymphoid cells. However, nuclear localization of Bcl10 has been linked with more aggressive lymphoid tumors and poor patient outcome suggesting that Bcl10 performs additional functions in the nucleus that are linked to cancer progression [25, 26]. In our study, we investigated the role of Bcl10 in the nucleus of breast cancer cells with the hope of better understanding functions performed by Bcl10 outside the lymphatic system. We first identified Bcl10 in the nucleus of breast cancer cells where it localized to a small number of large nuclear foci enriched in γH2AX and DNA repair proteins known as "cryptogenic foci". Since Bcl10 had not previously been associated with γH2AX in the nucleus, this finding raised an intriguing question: "Could Bcl10 contribute to DNA repair?", a question that established the framework for the rest of the project. From here we investigated Bcl10 sub-cellular localization in response to treatment with two different doses of γ-radiation, 2 Gy and 5 Gy, and found that Bcl10 is rapidly recruited to IRIF in a dose-dependent manner. To help determine the role of Bcl10 in IRIF, we first asked whether Bcl10 was required for radiation-induced NF-κB activation and found that Bcl10 plays only a minimal role. Next, we looked at DNA repair and found that Bcl10 has a profound and unexpected role in the repair of radiation-induced DNA damage, which was largely independent of NF-κB. To determine if this function of Bcl10 was specific for breast cancer cells, we performed similar experiments in immortalized normal breast epithelial cells and observed that Bcl10 also localized to IRIF and was required for efficient

DNA repair. Since DNA damage is usually lethal to normal cells but not to cancer cells, we asked whether Bcl10 had any influence on cell survival. To our surprise, we found that Bcl10 knockdown alone was sufficient to induce cellular senescence in breast cancer cells yet had a minimal effect on normal breast epithelial cells. The work in this thesis therefore identifies several novel roles for Bcl10 in the nucleus and provides evidence that Bcl10 maybe an important anti-cancer target. The nuclear roles of Bcl10 are summarized in Figure 4.0

4.1 Bcl10 plays a minor role in radiation-induced NF-κB activation, while MALT1 is absolutely required

DNA damage-induced NF-κB activation is an important pro-survival response allowing cells time to repair their DNA by inducing genes associated with cell survival [11, 103]. If the DNA is not repaired the cells die. In normal cells, this is an advantageous response. However, cancer cells have evolved mechanisms that manipulate this response to ensure their continued survival even in the presence of unrepaired DNA damage. This poses a significant clinical problem since cancer patients treated with genotoxic agents that induce DSB often evolve chemo and radio-resistance to treatment. Chemo and radio-resistance of tumors has been linked to the specific pro-survival pathways induced by activation of NF-κB signaling in response to DSB [104]. Yet, the mechanisms linking DSB to NF-κB activation and to the pro-survival phenotype are poorly understood. Since Bcl10 is recognized to play an important role in the activation of NF-κB in the cytoplasm, we initially hypothesized that Bcl10 might be acting as a signal transducer linking

Figure 4.0 Novel roles of Bcl10 in the nucleus. In the nucleus of resting breast cancer cells, Bcl10 is present in discrete foci containing γH2AX, P-ATM, Mre11 and MALT1. The accumulation of proteins at these sites blocks telomere and DNA-damage induced senescence. Following treatment with γ-radiation, two things occur **1)** Bcl10 and MALT1 complexes exit the nucleus and are recruited to and activate the IKK complex. Active IKK complex dissociates from Bcl10/MALT1 complexes, and phosphorylates the IκB complex targeting it for degradation. Degradation of the IκB complex releases NF-κB dimers, which translocate into the nucleus and promote transcription.[10, 19, 23, 24] **2)** ATM dissociates from PP2A and autophosphorylates itself at a serine-1981 residue, producing activated monomers. At the same time the MRN complex, composed of a dimer of Mre11, a dimer of Rad50 and a monomer of NBS-1, is recruited to the break site. At the break sites, Mre11 binds the free DNA end, Rad50 links the Mre11 proteins and NBS-1 directly binds Mre11 and recruits P-ATM. The interaction between the MRN complex and P-ATM promotes an optimal ATM signaling cascade. P-ATM phosphorylates H2AX, producing γH2AX foci, and various other proteins which lead to repair via NHEJ or HR and the activation of cellular checkpoints, cell cycle arrest and apoptotic pathways [27, 42, 49-61]. Bcl10 is rapidly recruited to these γH2AX foci, where it plays an important role in the repair process.

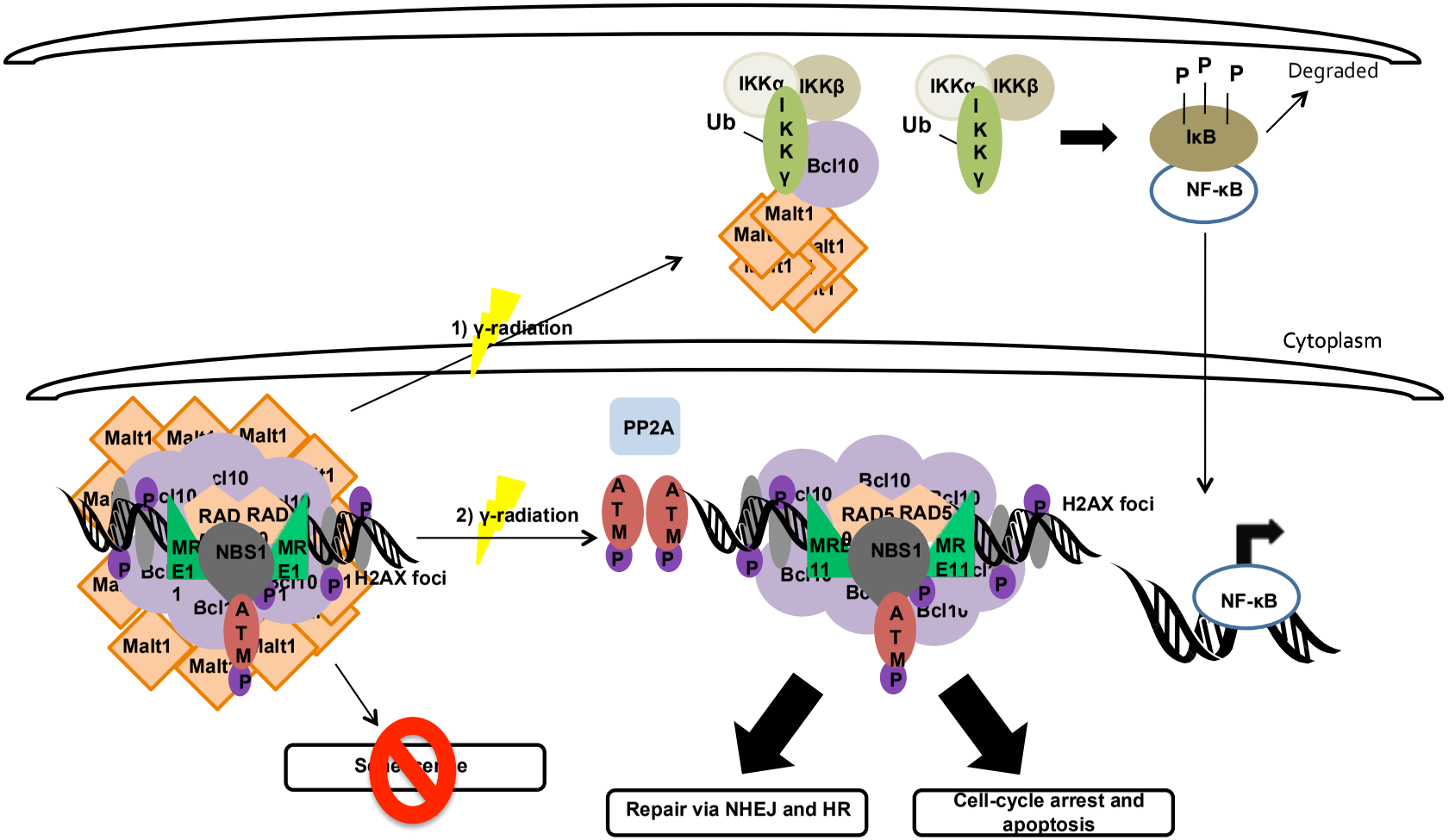
IKKα
IKKβ
Ub
IKKγ
Bcl10
Malt1
P P P
Degraded
IκB
NF-κB
Cytoplasm
1) γ-radiation
PP2A
ATM
P
2) γ-radiation
RAD
NBS1
MRE11
H2AX foci
NF-κB
Repair via NHEJ and HR
Cell-cycle arrest and apoptosis

DNA damage in the nucleus to cytoplasmic activation of NF-κB. Here we provide evidence that although Bcl10 and MALT1 contribute to such a function, the major role of Bcl10 appears to be in DNA repair.

MALT1 is a paracaspase protein containing an amino-terminal death domain, two Ig-like domains, and a carboxy terminal caspase-like domain [10]. In the cytoplasm, association of MALT1 with Bcl10 is required for NF-κB activation [105]. Here we found that in contrast to Bcl10, knockdown of MALT1 severely impairs the activation of NF-κB in response to irradiation. The association of Bcl10 with MALT1 has been extensively investigated. It was originally thought that only a small 13 amino acid motif (MALT1 motif) in Bcl10 was important for Bcl10 interaction with the MALT1 Ig-like domain [106]. However, a study by Langel *et al.* determined that the area required for interaction is much larger than this 13 amino acid region [105]. They found that in addition to the MALT1 motif interacting with the Ig-like domain, the C-terminal portion of the CARD domain interacts with the MALT1 death domain to stabilize the interaction [105]. This is of particular interest because it is only the second reported case of a CARD/death domain interaction [105]. Apart from these structural interaction domains, MALT1 also contains a C-terminal nuclear export signal (NES) that mediates nuclear cytoplasmic shuttling [107]. Not only can MALT1 mediate its' own subcellular localization, it has also been shown to mediate Bcl10 nuclear export [107]. This suggests a possible mechanism for Bcl10/MALT1 mediated NF-κB activation in response to DNA damage. We hypothesized that following treatment

with γ-radiation, Bcl10 could be recruited to DSB sites or in resting cells "cryptogenic foci", where it acts as a damage sensor. At these sites, MALT1 might bind Bcl10 to form complexes that are exported to cytoplasm, where they interact with the IKK complex resulting in degradation of the IκB complex and the release of NF-κB dimers, which are then free to translocate into the nucleus and activate transcription. Here we provide strong evidence that MALT1 plays a major role in linking radiation-induced DSB in the nucleus to NF-κB activation in the cytoplasm.

Numerous studies provide evidence that in lymphoid cells MALT1 acts downstream of Bcl10, and cannot induce NF-κB activation on its own [10]. In fact mutations that disrupt the interaction between MALT1 and Bcl10 abolish NF-κB activation [105]. How can we reconcile our observation that MALT1 knockdown impairs NF-κB activation following irradiation while Bcl10 knockdown has only a negligible effect? In the cytoplasm, the interaction between Bcl10 and MALT1 promotes MALT1 oligomerization resulting in IKK activation [19, 23, 24]. Our results indicate that the availability of MALT1 maybe the limiting factor. If the amount of Bcl10 exceeds that of MALT1 then when we reduce Bcl10 protein levels there would still be sufficient Bcl10 to interact with MALT1, promote its oligomerization and activate NF-κB (Figure 4.1). Conversely, if we reduce MALT1 protein levels we might expect to severely impair NF-κB activation (Figure 4.1).

Figure 4.1 MALT1 protein levels are the limiting factor in Bcl10/MALT1 mediated NF-κB activation. In order to active NF-κB Bcl10 and MALT1 must form these activating complexes, which have a stoichiometric ratio of 3:1 MALT1 molecules:Bcl10 molecules. Under normal conditions (first panel) there is plenty of Bcl10 and MALT1 present to form these complexes, therefore NF-κB activation occurs normally. When we reduce Bcl10 protein levels (second panel) we slightly decrease the number of active complexes causing a slight decrease in NF-κB activation. Finally, when we reduce MALT1 protein levels (third panel) we drastically decrease, by half, the number of active complexes formed and consequently drastically decrease NF-κB activation.

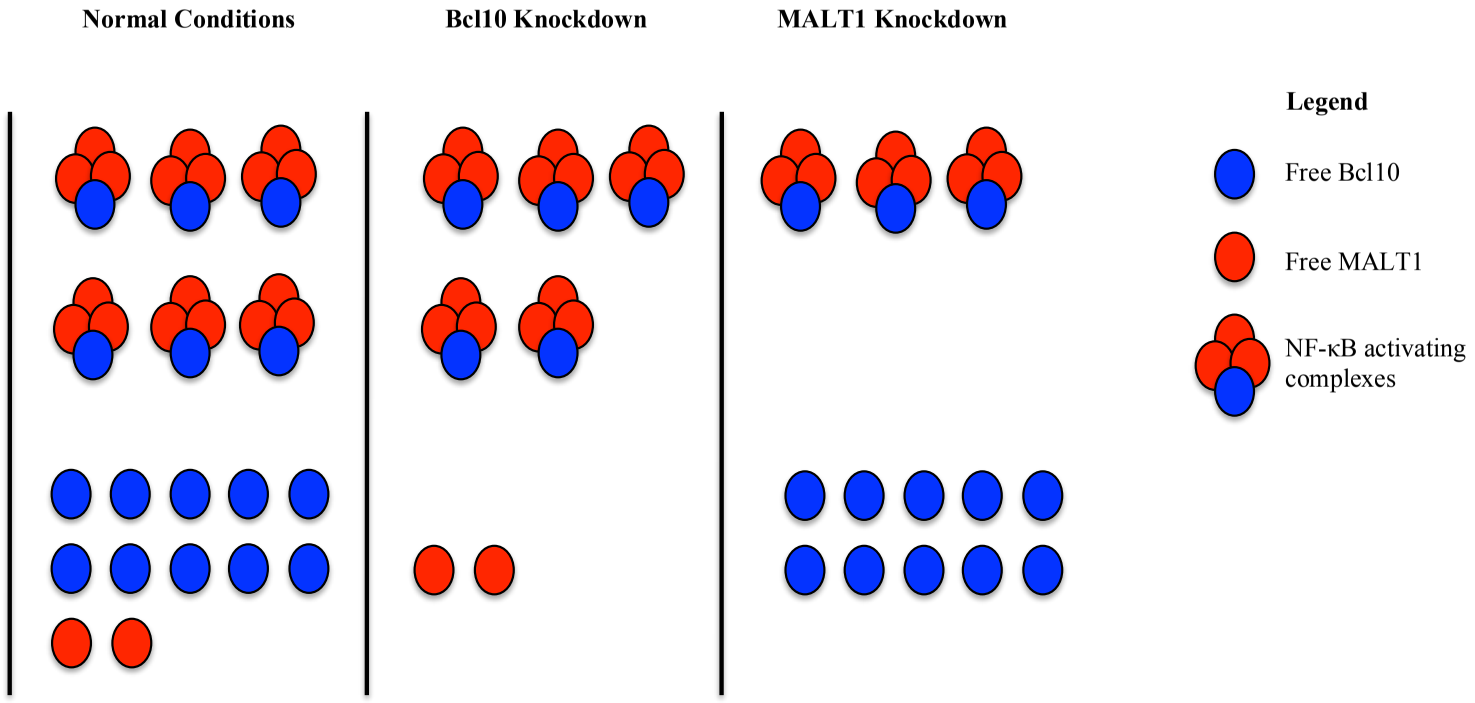
Normal Conditions
Bcl10 Knockdown
MALT1 Knockdown
Legend
Free Bcl10
Free MALT1
NF-κB activating complexes

NF-κB activation in response to DSB has been linked to chemo and radio-resistance [104]. Our results are interesting because they suggest for the first time that MALT1 would be an effective target for the treatment of chemo- and radio-resistant tumors. Small molecule inhibitors of MALT1 might therefore be used in combination with radiation to significantly reduce the development of radio-resistance.

4.2 Nuclear Bcl10 accumulates at endogenous γH2AX foci and nascent sites of DNA-damage

4.2.1 Bcl10 is recruited to ionizing radiation-induced foci, nascent sites of DNA damage, in a dose-dependent manner

A number of proteins are recruited to IRIF, including DNA repair, cell cycle checkpoint and pro- and anti-survival proteins [60, 61]. Every protein that is recruited to IRIF has a distinct role, determining the kinetics of protein recruitment to these foci can provide clues as to their function. We observed that Bcl10 co-localizes with the DNA repair proteins, P-ATM and Mre11, and the NF-κB adaptor protein MALT1, in preformed foci in the nuclei of resting breast cancer cells. This prompted us to examine whether Bcl10 would be recruited to *de novo* radiation-induced DSB. To investigate this, we performed radiation time course experiments and monitored Bcl10 recruitment using indirect immunofluorescent staining. When breast cancer cells were irradiated at 2 Gy, we observed that Bcl10 was rapidly recruited to IRIF and strongly co-localized with γH2AX and P-ATM early in the time course (5 mins, 30 mins post-IR). In

contrast, we were unable to detect MALT1 recruitment to IRIF (supplementary figure 1 and 2) suggesting that Bcl10 may perform a function at the foci that is independent of its role in NF-κB activation. However, it must be borne in mind that MALT1 levels appear limiting and that it may therefore be difficult to visualize MALT1 when it is dispersed among multiple foci. When we increased the ionizing radiation dose to 5 Gy, we observed that Bcl10 was still recruited to IRIF, however the response appeared to be delayed and we did not observe strong co-localization of Bcl10 with γH2AX and P-ATM until later time points, when the foci were reduced in number (1 h, 4 h post-IR). Since Bcl10 protein levels are unlikely to change significantly over this time period, it seems probable that the detection of Bcl10 at sites of DNA damage reflect the overall number and size of these foci.

Since the visualization of proteins by indirect immunofluorescent staining is restricted by sensitivity, it is probable that staining must cross a threshold before we can observe it. Consequently, it is likely that Bcl10 must reach a critical concentration at break sites in order for us to see it. Our results could be explained by assuming that there is sufficient Bcl10 in the nucleus to associate with the number of DSB induced by 2 Gy but not by 5 Gy. Thus, Bcl10 build up would be most evident at later time-points when most of the easily repaired DSB have been repaired. These findings propose that the stoichiometric composition of Bcl10 foci varies at different doses and times after irradiation. By exploring the role of Bcl10

at these IRIF, we can gain some insight into why we see these recruitment kinetics.

4.2.2 Bcl10 recruitment to ionizing radiation-induced foci is a wide spread phenomenon that is not restricted to breast cancer cells

In order to fully understand the role of Bcl10 in the nucleus, it was important for us to determine if this descriptive phenomenon was an aberrant function of cancer cells or if it also occurred in normal human cells. To approach this question, we performed parallel radiation time course experiments on normal breast epithelial cells and on normal human foreskin fibroblasts. These revealed that Bcl10 is recruited to IRIF in normal cells with similar kinetics to those we observed in breast cancer cells suggesting that the phenomenon is widespread and not restricted to cancer cells.

4.2.3 Concluding Remarks

It is possible that Bcl10 builds up at later time points because it is especially important for late repair processes. Additionally, there may be something structurally and functionally different about the later foci that requires more Bcl10. Finally, its likely that DNA damage that is not easily repaired will accumulate more Bcl10 simply because there are fewer foci. Either way, the recruitment of Bcl10 to IRIF implies that it has an important function at these sites; we had already determined that Bcl10 plays only a minimal role in radiation-induced NF-κB activation, therefore we wanted to investigate whether

localization to IRIF pointed to a role in the repair of radiation-induced DNA damage.

4.3 Bcl10 is required for efficient repair of radiation-induced DNA Damage

4.3.1 Bcl10 knockdown significantly diminishes the repair of radiation-induced DNA damage in T47D and hTERT-HME1 cells

Using a neutral comet assay to measure DNA repair, we found that both T47D and hTERT-HME1 cells require Bcl10 to efficiently repair radiation-induced DNA damage. In both cell lines, we observed that Bcl10 knockdown results in a significant increase in DNA damage at 4 h and 24 h post-IR. We also observed an increase in DNA damage in Bcl10 knockdown unirradiated controls. This was unexpected but likely indicates that Bcl10 contributes to the repair of endogenous DNA damage. The increase in DNA damage attributable to Bcl10 knockdown was most evident at later time points following irradiation indicating that Bcl10 plays a critical role in the repair of radiation-induced DNA damage. To confirm these results, we quantified the effect of Bcl10 knockdown on the number of γH2AX foci induced by irradiation in T47D cells and found that cells deficient in Bcl10 have more γH2AX foci remaining at 4 h post-IR than the controls.. In contrast, we found that although Bcl10 knockdown in hTERT-HME1 cells reduced DNA repair it did not appear to influence the number of γH2AX foci. This could reflect a difference in the types of lesions in transformed and non-transformed cells.

Radiation treatment causes an array of different types of DNA damage including sugar damage, apurinic/apyrimidinic sites, single strand breaks (SSB), base lesions, double strand breaks (DSB), and clustered DNA damage [41]. Clustered DNA damage is defined as "two or more lesions formed within 1-2 helical turns of DNA by a single radiation track" [41]. These lesions can be any combination of DNA damage. Consequently the repair of these clustered DNA lesions is difficult and complex [47]. Repair of clustered DNA lesion can give rise to DSB as a consequence of the repair process, for example if base excision repair was to occur on two opposing lesions three or more nucleotides apart a DSB would be formed [47, 108, 109]. One could deduce that this would give rise to DSB at later time points post-IR such as 2 or 4 h. A large proportion, 50-80%, of the DNA damage induced by ionizing radiation is attributed to clustered DNA lesions [47, 110, 111]. If Bcl10 is important for the repair of these later formed complex DSB, it would explain why we see a significant repair defect at 4 and 24 h post-IR. In normal cells the repair of these lesions would be complete by this time. This also explains why in the mock and non-transfected cells we see an increase in DNA damage from 1 h to 2 h post-IR, as this is presumably when these complex DSB would be arising. Not only does this explain the repair defect that we see it also justifies the recruitment kinetics that we observe, with Bcl10 showing a stronger association with foci at later time-points, these later foci representing complex DSB. The exact role Bcl10 plays in DNA repair is not understood but there are at least two major possibilities:

1) The DNA within a cell is extensively packaged; DNA packaged along with histone proteins forms what is known as chromatin [112, 113]. Chromatin undergoes further packaging to give rise to chromosomes. When DSB occur, the chromatin in and around break sites is remodeled in order to allow for efficient repair. This remodeling often occurs through the post-translational modification of core histones, such as phosphorylation of H2AX [27, 112]. Besides phosphorylation, histones are also modified by ubiquitylation. Following the development of DSB, H2AX is rapidly phosphorylated by ATM, giving rise to γH2AX foci [27, 55]. These γH2AX foci are recognized by a protein, MDC1, this interaction not only protects γH2AX from phosphatases it also promotes a positive ATM feedback loop [114-122]. More notably, this interaction has been found to be important for the recruitment of 53BP1 and BRCA1, a protein important for signaling cell cycle checkpoints and repair via HR and NHEJ [122-133]. Recruitment of these proteins to MDC1 is thought to occur through a ubiquitin dependent pathway, the specifics of which are not well understood [122]. The E3 ubiquitin ligase RNF8 has an FHA domain that recognizes and binds proteins phosphorylated within a "TQXF" motif, such as MDC1, which is phosphorylated by ATM [122, 134-136]. RNF8 along with UBC13, a ubiquitin conjugating protein, are recruited to γH2AX-MDC1 sites where they mediate the ubiquitylation of histones H2A and H2AX [122, 134, 136, 137].These ubiquitinated histones then recruit RNF168, another E3 ubiquitin ligase, which results in further ubiquitylation and the recruitment of BRCA1 and other proteins [122, 134, 136, 137]. This pathway represents a very important regulatory

pathway for monitoring DNA lesions in which ubiquitylation has a prominent role [122].

Cytoplasmic Bcl10 is important for the activation of the NF-κB pathway in response to various types of stimuli. In this pathway, Bcl10 plays a critical role in the ubiquitylation of IKKγ [19]. Furthermore, Bcl10 must interact with a paracaspase, such as MALT1, and form a complex with UBC13-MMS2 in order for ubiquitylation to occur [19]. It is entirely possible that Bcl10 plays a similar role in the nucleus where it is involved in the ubiquitylation of histones. This would explain the DNA repair defect that we observe when we knockdown Bcl10 in breast cancer and normal breast epithelial cells.

When we treat cells with 5 Gy, we observe that throughout the entire time course Bcl10 has a stronger association with P-ATM than with γH2AX. The fact that Bcl10 recruitment to IRIF is very similar to P-ATM suggests that Bcl10 interacts directly with P-ATM and might even be a target of ATM phosphorylation. Interestingly, ATM phosphorylates proteins within a minimum consensus "S/TQ" amino acid motif and upon examination of the Bcl10 amino acid sequence we identified a "TQ" amino acid motif at residue 91, that is a potential target for ATM phosphorylation [138] . We have preliminary evidence to support such a phosphorylation event. When we treated T47D cells with the PP2A inhibitor, okadaic acid, we observed an upward shift in the molecular weight of Bcl10 indicative of a post-translational modification (supplementary figure 3). However,

a large-scale proteomics screen failed to identify Bcl10 as an ATM/ATR target protein [139]. The "TQ" motif that we identified is part of a larger "TQXF" motif, which is a target for interaction with the RNF8 FHA domain [122, 134-136]. This suggests a model for the involvement of Bcl10 in DNA repair. We speculate that Bcl10 is rapidly recruited to IRIF where ATM is localized. ATM may phosphorylate Bcl10 in its "TQXF" motif, which then recruits RNF8-UBC13 promoting the ubiquitylation of H2A and H2AX, and the subsequent recruitment of repair proteins like BRCA1. An interesting possibility is that complex breaks that are more difficult to repair have an increased requirement for Bcl10.

2) It is accepted that actin is present in the nucleus of eukaryotic cells, even though F-actin is extremely difficult to visualize [140]. In order for DNA repair proteins to gain access to break sites, chromatin has to be opened up or otherwise remodeled [51]. To ensure the integrity of the chromatin and proper repair some type of support structure needs to be in place [141, 142]. Recent work has shown that nuclear actin plays a critical role in DNA DSB repair, by providing such a framework [141, 142]. Interestingly, Bcl10 has been implicated in TCR and FcγR-induced actin polymerization in lymphocytes [20]. Furthermore, Bcl10 can oligomerize through its CARD domain to form large molecular complexes. It is possible therefore that Bcl10 is recruited to IRIF where it oligomerizes and promotes actin polymerization. One might predict that this would create a strong scaffolding network, like a spiderweb, that would stabilize break sites and serve as a platform for the recruitment of repair proteins. Break sites that are more

difficult to repair such as those present at later time points, in transformed cells, would likely require more stabilization and the accumulation of Bcl10. Bcl10 may therefore play a basic role in DNA repair, from the earliest to the most persistent lesions. However, Bcl10 may also play an additional role by helping cancer cells with irreparable DNA lesions avoid cell cycle arrest. These two theories about the role of Bcl10 in DNA repair are not mutually exclusive and if verified would indicate Bcl10 plays a fundamental role in tumorigenesis.

4.3.2 NF-κB inhibition has a minimal effect on the repair of radiation-induced DNA damage in T47D cells and no effect on repair in hTERT-HME1 cells

Our observations indicate the role of Bcl10 in DNA repair is largely independent of NF-κB. However, we did find that Bcl10 recruitment to IRIF following higher doses of γ-radiation is reduced in cells treated with NF-κB inhibitors, suggesting that NF-κB could exert a positive feedback role. Alternatively, this could be due to off target effects of the NF-κB inhibitor. A lot of cancer cells constitutively express NF-κB in order to gain survival advantages [143]. This explains the DNA damage we observe in Bay11-treated T47D cells. At 24 h post-IR, we see significantly more DNA damage in the Bay11-treated cells than the DMSO control cells, which can be attributed to DNA fragmentation induced by apoptosis. These cells become apoptotic because they are highly dependent on NF-κB to promote their survival. This also explains why we see a recruitment delay in the T47D cells but not in the hTERT-HME1 cells, the T47D cells simply have a higher NF-κB requirement and therefore a higher Bcl10 requirement.

4.3.3 Concluding Remarks

Understanding how cells recognize and repair DNA damage is extremely important for the future development of cancer therapies. We have evidence to suggest that Bcl10 plays an important role in the repair of radiation-induced DNA damage, in particular complex DNA lesions, independent of NF-κB. This identifies Bcl10 as an intriguing anti-cancer target, especially if used in combination with other genotoxic therapies. In order to fully understand the anti-cancer effects of inhibiting Bcl10 function, we investigated the effect of Bcl10 knockdown on cell fate.

4.4 Bcl10 protects breast cancer cells from cellular senescence

4.4.1.Bcl10 knockdown results in the collapse of cryptogenic foci and induced cellular senescence in T47D cells

Senescence is a general response to DNA damage, whether it is DSB and/or dysfunctional telomeres, therefore genetic and epigenetic events that avert senescence are necessary for malignant transformation [89, 144]. The exact mechanisms that induce or trigger cellular senescence are poorly understood. We originally identified Bcl10 in cryptogenic foci, which are thought to be sites of failed DSB repair and/or sites of telomere dysfunction. Normal breast epithelial cells are largely devoid of these foci, while breast cancer cells contain numerous large foci. We found that Bcl10 knockdown resulted in the disappearance of cryptogenic foci and induced significant levels of cellular senescence in breast cancer cells. This not only indicates that Bcl10 is important for protecting these

cells from senescence, but that it is important for stabilizing these foci. Furthermore, we observed that senescence induced by Bcl10 knockdown is maintained through cell passage indicating that it is a permanent state and not just temporary cell cycle arrest, this is also reflected in the cell survival curve. An intriguing possibility is that the ability of Bcl10 to stabilize cryptogenic foci may be linked to its ability to protect breast cancer cells from senescence.

4.4.2 Bcl10 knockdown enhances DNA damage-induced cellular senescence in hTERT-HME1 cells

Since hTERT-HME1 cells are normal breast epithelial cells immortalized with telomerase, they have functional telomeres. We therefore used this cell line to determine whether Bcl10 is important for DSB-induced senescence. We observed that Bcl10 knockdown in these cells significantly increases DNA damage-induced cellular senescence. However, the amount of cellular senescence induced by Bcl10 knockdown in hTERT-HME1 cells treated with 5 Gy (~21%) is considerably lower than senescence induced in T47D cells treated with Bcl10 siRNA alone (~60%). This suggests that Bcl10 may play a greater role in protecting cells from telomere-induced senescence than DNA damage-induced senescence.

4.4.3 Concluding Remarks

In normal cells, signaling from unrepaired DSB foci and γH2AX foci associated with dysfunctional telomeres induces cellular senescence through a p53-

dependent pathway [91, 92, 145, 146]. Specifically, p53 is activated by ATM and signals cellular senescence through the upregulation of p21, a cell cycle regulator protein that mediates the activity of cyclin-dependent kinases [90, 147]. Our findings are contradictory to this mechanism; instead of a build up of DNA repair proteins (γH2AX, P-ATM) at these sites signaling senescence, we find it is the removal of these proteins, via Bcl10 knockdown, that signals senescence. It is difficult to envision how cancer cells utilize this pathway to prevent cellular senescence, yet there is one possible explanation. A recent study has identified that p21 can be upregulated through a p53-independent mechanism in response to the destabilization of the nuclear actin cytoskeleton [147]. As was previously discussed, Bcl10 is know to regulate actin polymerization in the cytoplasm, if a similar pathway exists in the nucleus you could infer that Bcl10 knockdown would destabilize actin resulting in the upregulation of p21 and the induction of cellular senescence [20, 90, 147].

4.5 Conclusions

In conclusion, our evidence identifies novel roles for Bcl10 in the nucleus. We show for the first time that Bcl10 is a major constituent of γH2AX foci and provide evidence linking Bcl10 to the repair of radiation-induced DNA damage and in particular complex DSB. Although, we provide evidence that Bcl10 plays a minimal role in the activation of NF-κB in response to DNA damage, we conclude that its role in DNA repair is independent of NF-κB. We observed that MALT1 knockdown severely impairs radiation-induced NF-κB activation and

consequently makes cells more radiosensitive. This suggests that MALT1 would be an effective therapeutic target for the treatment of radio-resistant tumors. We show that Bcl10 protects breast cancer cells from telomere and DNA damage-induced senescence and have evidence suggesting Bcl10 may play a greater role in telomere-induced senescence than in DNA damage-induced senescence. Bcl10 may therefore function differently at IRIF and at cryptogenic foci, congruent with our observation that MALT1 is present in cryptogenic foci and not IRIF.

The majority of current cancer therapies, including radiation and chemotherapeutics, aim to overwhelm cancer cells with genotoxic lesions and induce apoptosis. The problem with these types of therapies is two-fold, 1) these therapies do not selectively target cancer cells and 2) cancer cells often have dysfunctional apoptotic pathways. If we could improve these therapies by selectively targeting cancer cells and inducing other cell death pathways such as senescence, we could overcome some of the obstacles. In this thesis project, we provided evidence to identify Bcl10 as a very promising therapeutic target for the treatment of breast cancer.

4.6 Future Directions

In order to better understand the role of Bcl10 in the nucleus, it would be beneficial to perform a mutagenesis screen. I suggest performing two different mutagenesis screens, a random screen and a site directed screen. With the random screen, we would hope to gain information about what parts of the protein are

important for recruitment to IRIF and DNA repair. Furthermore, if we can identify which amino acids are critical for DNA repair, we can use this mutant to determine if Bcl10 is important for histone ubiquitylation. With a site directed mutagenesis screen, the plan would be to mutate the "TQXF" motif in Bcl10 in order to determine if Bcl10 is phosphorylated by P-ATM. To investigate whether nuclear Bcl10 is important for polymerizing actin, we would mutate the serine-138 residue, which has been shown to be critical for Bcl10-mediated actin polymerization [20]. To further understand how post-translational modifications play a role, it would be valuable to perform an in vitro phosphorylation assay, initially with ATM as the kinase and then ATR and DNA-PK. To help unravel more about the role of Bcl10 in cellular senescence, a protein-DNA telomere FISH assay should be performed. This will tell us what proportion of Bcl10 cryptogenic foci co-localize with telomeres. This along with the mutagenesis data will hopefully give us a better idea how Bcl10 mediates cellular senescence. These are the key experiments that would further the preliminary evidence presented in this thesis.

Chapter 5. Bibliography

1. Willis, T.G., D.M. Jadayel*, et al.*, Bcl10 is involved in t(1;14)(p22;q32) of MALT B cell lymphoma and mutated in multiple tumor types. Cell, 1999. 96. p. 35-45.

2. Thome, M. and R. Weil, Post-translational modifications regulate distinct functions of CARMA1 and BCL10. Trends Immunol, 2007. 28. p. 281-288.

3. Liang, H. and S.W. Fesik, Three-dimensional structures of proteins involved in programmed cell death. J Mol Biol, 1997. 274(3): p. 291-302.

4. Weber, C.H. and C. Vincenz, The death domain superfamily: a tale of two interfaces? Trends Biochem Sci, 2001. 26(8): p. 475-481.

5. Solt, L.A. and M.J. May, The IkappaB kinase complex: master regulator of NF-kappaB signaling. Immunol Res, 2008. 42. p. 3-18.

6. Thome, M. and J. Tschopp, TCR-induced NF-kappaB activation: a crucial role for Carma1, Bcl10 and MALT1. Trends Immunol, 2003. 24(8): p. 419-424.

7. Jun, J.E. and C.C. Goodnow, Scaffolding of antigen receptors for immunogenic versus tolerogenic signaling. Nat Immunol, 2003. 4(11): p. 1057-1064.

8. Xue, L., S.W. Morris*, et al.*, Defective development and function of Bcl10-deficient follicular, marginal zone and B1 B cells. Nat Immunol, 2003. 4(9): p. 857-865.

9. Ruland, J. and T.W. Mak, Transducing signals from antigen receptors to nuclear factor kappaB. Immunol Rev, 2003. 193: p. 93-100.

10. Thome, M., CARMA1, BCL-10 and MALT1 in lymphocyte development and activation. Nat Rev Immunol, 2004. 4. p. 348-359.

11. Wang, D., Y. You*, et al.*, Bcl10 plays a critical role in NF-kappaB activation induced by G protein-coupled receptors. Proc Natl Acad Sci USA, 2007. 104. p. 145-150.

12. McAllister-Lucas, L.M., J. Ruland*, et al.*, CARMA3/Bcl10/MALT1-dependent NF-kappaB activation mediates angiotensin II-responsive inflammatory signaling in nonimmune cells. Proc Natl Acad Sci USA, 2007. 104. p. 139-144.

13. Klemm, S., S. Zimmermann, *et al.*, Bcl10 and Malt1 control lysophosphatidic acid-induced NF-kappaB activation and cytokine production. Proc Natl Acad Sci USA, 2007. 104. p. 134-138.

14. Gilmore, T.D., Introduction to NF-kappaB: players, pathways, perspectives. Oncogene, 2006. 25(51): p. 6680-6684.

15. Gaide, O., F. Martinon, *et al.*, Carma1, a CARD-containing binding partner of Bcl10, induces Bcl10 phosphorylation and NF-kappaB activation. FEBS Lett, 2001. 496(2-3): p. 121-127.

16. Bertin, J., L. Wang, *et al.*, CARD11 and CARD14 are novel caspase recruitment domain (CARD)/membrane-associated guanylate kinase (MAGUK) family members that interact with BCL10 and activate NF-kappa B. J Biol Chem, 2001. 276(15): p. 11877-11882.

17. McAllister-Lucas, L.M., N. Inohara, *et al.*, Bimp1, a MAGUK family member linking protein kinase C activation to Bcl10-mediated NF-kappaB induction. J Biol Chem, 2001. 276(33): p. 30589-30597.

18. Hofmann, K., P. Bucher, and J. Tschopp, The CARD domain: a new apoptotic signalling motif. Trends Biochem Sci, 1997. 22(5): p. 155-156.

19. Zhou, H., I. Wertz, *et al.*, Bcl10 activates the NF-kappaB pathway through ubiquitination of NEMO. Nature, 2004. 427(6970): p. 167-171.

20. Rueda, D., O. Gaide, *et al.*, Bcl10 controls TCR- and FcgammaR-induced actin polymerization. J Immunol, 2007. 178. p. 4373-4384.

21. Liu, Y., W. Dong, *et al.*, Characterization of Bcl10 as a potential transcriptional activator that interacts with general transcription factor TFIIB. Biochem Biophys Res Commun, 2004. 320. p. 1-6.

22. Chen, M., L.Y. Li, and Y.P. Qi, Bcl10 protein can act as a transcription activator in yeast. Mol Cell Biochem, 2003. 246(1-2): p. 97-103.

23. Rebeaud, F., S. Hailfinger, *et al.*, The proteolytic activity of the paracaspase MALT1 is key in T cell activation. Nat Immunol, 2008. 9. p. 272-281.

24. Sun, L., L. Deng, *et al.*, The TRAF6 ubiquitin ligase and TAK1 kinase mediate IKK activation by BCL10 and MALT1 in T lymphocytes. Mol Cell, 2004. 14(3): p. 289-301.

25. Gallardo, F., B. Bellosillo, *et al.*, Aberrant nuclear BCL10 expression and lack of t(11;18)(q21;q21) in primary cutaneous marginal zone B-cell lymphoma. Hum Pathol, 2006. 37(7): p. 867-873.

26. Chang, H.H., M.Y. Kuo*, et al.*, Expression of BCL10 is significantly associated with the progression and prognosis of oral squamous cell carcinomas in Taiwan. Oral Oncol, 2009. 45(7): p. 589-593.

27. Rogakou, E.P., D.R. Pilch*, et al.*, DNA double-stranded breaks induce histone H2AX phosphorylation on serine 139. J Biol Chem, 1998. 273(10): p. 5858-5868.

28. Downs, J.A., S. Allard*, et al.*, Binding of chromatin-modifying activities to phosphorylated histone H2A at DNA damage sites. Mol Cell, 2004. 16(6): p. 979-990.

29. Nakamura, T.M., L.L. Du*, et al.*, Histone H2A phosphorylation controls Crb2 recruitment at DNA breaks, maintains checkpoint arrest, and influences DNA repair in fission yeast. Mol Cell Biol, 2004. 24(14): p. 6215-6230.

30. Unal, E., A. Arbel-Eden*, et al.*, DNA damage response pathway uses histone modification to assemble a double-strand break-specific cohesin domain. Mol Cell, 2004. 16(6): p. 991-1002.

31. van Attikum, H., O. Fritsch*, et al.*, Recruitment of the INO80 complex by H2A phosphorylation links ATP-dependent chromatin remodeling with DNA double-strand break repair. Cell, 2004. 119(6): p. 777-788.

32. Botuyan, M.V., J. Lee*, et al.*, Structural basis for the methylation state-specific recognition of histone H4-K20 by 53BP1 and Crb2 in DNA repair. Cell, 2006. 127(7): p. 1361-1373.

33. Du, L.L., T.M. Nakamura, and P. Russell, Histone modification-dependent and -independent pathways for recruitment of checkpoint protein Crb2 to double-strand breaks. Genes Dev, 2006. 20(12): p. 1583-1596.

34. Wyman, C. and R. Kanaar, DNA double-strand break repair: all's well that ends well. Annu Rev Genet, 2006. 40: p. 363-383.

35. Strom, L., H.B. Lindroos*, et al.*, Postreplicative recruitment of cohesin to double-strand breaks is required for DNA repair. Mol Cell, 2004. 16(6): p. 1003-1015.

36. Xie, A., N. Puget*, et al.*, Control of sister chromatid recombination by histone H2AX. Mol Cell, 2004. 16(6): p. 1017-1025.

37. Morrison, A.J., J. Highland*, et al.*, INO80 and gamma-H2AX interaction links ATP-dependent chromatin remodeling to DNA damage repair. Cell, 2004. 119(6): p. 767-775.

38. Srivastava, N., S. Gochhait, *et al.*, Role of H2AX in DNA damage response and human cancers. Mutat Res, 2009. 681. p. 180-188.

39. Nakamura, A.J., C.E. Redon, *et al.*, Telomere-dependent and telomere-independent origins of endogenous DNA damage in tumor cells. Aging (Albany NY), 2009. 1. p. 212-218.

40. Yu, T., S.H. MacPhail, *et al.*, Endogenous expression of phosphorylated histone H2AX in tumors in relation to DNA double-strand breaks and genomic instability. DNA Repair (Amst), 2006. 5(8): p. 935-946.

41. Shikazono, N., M. Noguchi, *et al.*, The yield, processing, and biological consequences of clustered DNA damage induced by ionizing radiation. J Radiat Res (Tokyo), 2009. 50(1): p. 27-36.

42. Riches, L.C., A.M. Lynch, and N.J. Gooderham, Early events in the mammalian response to DNA double-strand breaks. Mutagenesis, 2008. 23. p. 331-339.

43. Saleh-Gohari, N., H.E. Bryant, *et al.*, Spontaneous homologous recombination is induced by collapsed replication forks that are caused by endogenous DNA single-strand breaks. Mol Cell Biol, 2005. 25(16): p. 7158-7169.

44. Mirabelli, C.K., C.H. Huang, *et al.*, Quantitative measurement of single- and double-strand breakage of DNA in Escherichia coli by the antitumor antibiotics bleomycin and talisomycin. Antimicrob Agents Chemother, 1985. 27(4): p. 460-467.

45. Povirk, L.F., T. Zhou, *et al.*, Processing of 3'-phosphoglycolate-terminated DNA double strand breaks by Artemis nuclease. J Biol Chem, 2007. 282(6): p. 3547-3558.

46. vanAnkeren, S.C., D. Murray, and R.E. Meyn, Induction and rejoining of gamma-ray-induced DNA single- and double-strand breaks in Chinese hamster AA8 cells and in two radiosensitive clones. Radiat Res, 1988. 116(3): p. 511-525.

47. Georgakilas, A.G., Processing of DNA damage clusters in human cells: current status of knowledge. Mol Biosyst, 2008. 4(1): p. 30-35.

48. Hartlerode, A.J. and R. Scully, Mechanisms of double-strand break repair in somatic mammalian cells. Biochem J, 2009. 423(2): p. 157-168.

49. Modesti, M. and R. Kanaar, DNA repair: spot(light)s on chromatin. Curr Biol, 2001. 11(6): p. R229-232.

50. Rogakou, E.P., C. Boon*, et al.*, Megabase chromatin domains involved in DNA double-strand breaks in vivo. J Cell Biol, 1999. 146(5): p. 905-916.

51. Iijima, K., M. Ohara*, et al.*, Dancing on damaged chromatin: functions of ATM and the RAD50/MRE11/NBS1 complex in cellular responses to DNA damage. J Radiat Res, 2008. 49. p. 451-464.

52. Goodarzi, A.A., J.C. Jonnalagadda*, et al.*, Autophosphorylation of ataxia-telangiectasia mutated is regulated by protein phosphatase 2A. EMBO J, 2004. 23(22): p. 4451-4461.

53. Bakkenist, C.J. and M.B. Kastan, DNA damage activates ATM through intermolecular autophosphorylation and dimer dissociation. Nature, 2003. 421(6922): p. 499-506.

54. Guo, C.Y., D.L. Brautigan, and J.M. Larner, ATM-dependent dissociation of B55 regulatory subunit from nuclear PP2A in response to ionizing radiation. J Biol Chem, 2002. 277(7): p. 4839-4844.

55. Burma, S., B.P. Chen*, et al.*, ATM phosphorylates histone H2AX in response to DNA double-strand breaks. J Biol Chem, 2001. 276. p. 42462-42467.

56. Costanzo, V., T. Paull*, et al.*, Mre11 assembles linear DNA fragments into DNA damage signaling complexes. PLoS Biol, 2004. 2(5): p. E110.

57. Horejsi, Z., J. Falck*, et al.*, Distinct functional domains of Nbs1 modulate the timing and magnitude of ATM activation after low doses of ionizing radiation. Oncogene, 2004. 23(17): p. 3122-3127.

58. Hopfner, K.P., L. Craig*, et al.*, The Rad50 zinc-hook is a structure joining Mre11 complexes in DNA recombination and repair. Nature, 2002. 418(6897): p. 562-566.

59. Moreno-Herrero, F., M. de Jager*, et al.*, Mesoscale conformational changes in the DNA-repair complex Rad50/Mre11/Nbs1 upon binding DNA. Nature, 2005. 437(7057): p. 440-443.

60. Kobayashi, J., K. Iwabuchi*, et al.*, Current topics in DNA double-strand break repair. J Radiat Res, 2008. 49. p. 93-103.

61. Lee, J.-H. and T.T. Paull, Activation and regulation of ATM kinase activity in response to DNA double-strand breaks. Oncogene, 2007. 26. p. 7741-7748.

62. Cary, R.B., S.R. Peterson*, et al.*, DNA looping by Ku and the DNA-dependent protein kinase. Proc Natl Acad Sci U S A, 1997. 94(9): p. 4267-4272.

63. Walker, J.R., R.A. Corpina, and J. Goldberg, Structure of the Ku heterodimer bound to DNA and its implications for double-strand break repair. Nature, 2001. 412(6847): p. 607-614.

64. Yaneva, M., T. Kowalewski, and M.R. Lieber, Interaction of DNA-dependent protein kinase with DNA and with Ku: biochemical and atomic-force microscopy studies. EMBO J, 1997. 16(16): p. 5098-5112.

65. Ma, Y., U. Pannicke*, et al.*, Hairpin opening and overhang processing by an Artemis/DNA-dependent protein kinase complex in nonhomologous end joining and V(D)J recombination. Cell, 2002. 108(6): p. 781-794.

66. Grawunder, U., M. Wilm*, et al.*, Activity of DNA ligase IV stimulated by complex formation with XRCC4 protein in mammalian cells. Nature, 1997. 388(6641): p. 492-495.

67. Kass, E.M. and M. Jasin, Collaboration and competition between DNA double-strand break repair pathways. FEBS Lett, 2010. 584(17): p. 3703-3708.

68. Ivanov, E.L., N. Sugawara*, et al.*, Mutations in XRS2 and RAD50 delay but do not prevent mating-type switching in Saccharomyces cerevisiae. Mol Cell Biol, 1994. 14(5): p. 3414-3425.

69. Lee, S.E., J.K. Moore*, et al.*, Saccharomyces Ku70, mre11/rad50 and RPA proteins regulate adaptation to G2/M arrest after DNA damage. Cell, 1998. 94(3): p. 399-409.

70. Sugawara, N. and J.E. Haber, Characterization of double-strand break-induced recombination: homology requirements and single-stranded DNA formation. Mol Cell Biol, 1992. 12(2): p. 563-575.

71. Sung, P. and H. Klein, Mechanism of homologous recombination: mediators and helicases take on regulatory functions. Nat Rev Mol Cell Biol, 2006. 7(10): p. 739-750.

72. Hemel, D. and S.M. Domchek, Breast cancer predisposition syndromes. Hematol Oncol Clin North Am, 2010. 24(5): p. 799-814.

73. Chen, S. and G. Parmigiani, Meta-analysis of BRCA1 and BRCA2 penetrance. J Clin Oncol, 2007. 25(11): p. 1329-1333.

74. Antoniou, A., P.D. Pharoah*, et al.*, Average risks of breast and ovarian cancer associated with BRCA1 or BRCA2 mutations detected in case Series unselected for family history: a combined analysis of 22 studies. Am J Hum Genet, 2003. 72(5): p. 1117-1130.

75. Zhou, B.-B.S., H. Zhang*, et al.*, Tumour-initiating cells: challenges and opportunities for anticancer drug discovery. Nat Rev Drug Discov, 2009. 8. p. 806-823.

76. Diehn, M., R.W. Cho*, et al.*, Association of reactive oxygen species levels and radioresistance in cancer stem cells. Nature, 2009. 458(7239): p. 780-783.

77. Tribius, S., A. Pidel, and D. Casper, ATM protein expression correlates with radioresistance in primary glioblastoma cells in culture. Int J Radiat Oncol Biol Phys, 2001. 50(2): p. 511-523.

78. Masuda, K., R. Aramaki*, et al.*, Possible explanation of radioresistance of glioblastoma in situ. Int J Radiat Oncol Biol Phys, 1983. 9(2): p. 255-258.

79. Kauffmann, A., F. Rosselli*, et al.*, High expression of DNA repair pathways is associated with metastasis in melanoma patients. Oncogene, 2008. 27(5): p. 565-573.

80. Munshi, A., J.F. Kurland*, et al.*, Histone deacetylase inhibitors radiosensitize human melanoma cells by suppressing DNA repair activity. Clin Cancer Res, 2005. 11(13): p. 4912-4922.

81. Plummer, E.R., M.R. Middleton*, et al.*, Temozolomide pharmacodynamics in patients with metastatic melanoma: dna damage and activity of repair enzymes O6-alkylguanine alkyltransferase and poly(ADP-ribose) polymerase-1. Clin Cancer Res, 2005. 11(9): p. 3402-3409.

82. Rass, K. and J. Reichrath, UV damage and DNA repair in malignant melanoma and nonmelanoma skin cancer. Adv Exp Med Biol, 2008. 624: p. 162-178.

83. Fischer, U. and E. Meese, Glioblastoma multiforme: the role of DSB repair between genotype and phenotype. Oncogene, 2007. 26(56): p. 7809-7815.

84. Inoue, R., M. Isono*, et al.*, A genotype of the polymorphic DNA repair gene MGMT is associated with de novo glioblastoma. Neurol Res, 2003. 25(8): p. 875-879.

85. Chen, G.G., F.L. Sin*, et al.*, Glioblastoma cells deficient in DNA-dependent protein kinase are resistant to cell death. J Cell Physiol, 2005. 203(1): p. 127-132.

86. Ruan, S., M.F. Okcu*, et al.*, Overexpressed WAF1/Cip1 renders glioblastoma cells resistant to chemotherapy agents 1,3-bis(2-chloroethyl)-1-nitrosourea and cisplatin. Cancer Res, 1998. 58(7): p. 1538-1543.

87. Dutreix, M., J.M. Cosset, and J.S. Sun, Molecular therapy in support to radiotherapy. Mutat Res, 2010. 704(1-3): p. 182-189.

88. Campisi, J., S.H. Kim*, et al.*, Cellular senescence, cancer and aging: the telomere connection. Exp Gerontol, 2001. 36(10): p. 1619-1637.

89. Campisi, J. and F. d'Adda di Fagagna, Cellular senescence: when bad things happen to good cells. Nat Rev Mol Cell Biol, 2007. 8. p. 729-740.

90. Herbig, U., W.A. Jobling*, et al.*, Telomere shortening triggers senescence of human cells through a pathway involving ATM, p53, and p21(CIP1), but not p16(INK4a). Mol Cell, 2004. 14(4): p. 501-513.

91. d'Adda di Fagagna, F., P.M. Reaper*, et al.*, A DNA damage checkpoint response in telomere-initiated senescence. Nature, 2003. 426(6963): p. 194-198.

92. Takai, H., A. Smogorzewska, and T. de Lange, DNA damage foci at dysfunctional telomeres. Curr Biol, 2003. 13(17): p. 1549-1556.

93. Gire, V., P. Roux*, et al.*, DNA damage checkpoint kinase Chk2 triggers replicative senescence. EMBO J, 2004. 23(13): p. 2554-2563.

94. Gatz, S.A. and L. Wiesmuller, p53 in recombination and repair. Cell Death Differ, 2006. 13(6): p. 1003-1016.

95. Saito, S., H. Yamaguchi*, et al.*, Phosphorylation site interdependence of human p53 post-translational modifications in response to stress. J Biol Chem, 2003. 278(39): p. 37536-37544.

96. Vaziri, H., M.D. West*, et al.*, ATM-dependent telomere loss in aging human diploid fibroblasts and DNA damage lead to the post-translational activation of p53 protein involving poly(ADP-ribose) polymerase. EMBO J, 1997. 16(19): p. 6018-6033.

97. Wang, X., K. Ohnishi*, et al.*, Poly(ADP-ribosyl)ation is required for p53-dependent signal transduction induced by radiation. Oncogene, 1998. 17(22): p. 2819-2825.

98. Brown, J.P., W. Wei, and J.M. Sedivy, Bypass of senescence after disruption of p21CIP1/WAF1 gene in normal diploid human fibroblasts. Science, 1997. 277(5327): p. 831-834.

99. Artandi, S.E. and R.A. Depinho, Telomeres and telomerase in cancer. Carcinogenesis, 2010. 31. p. 9-18.

100. Chang, S., C.M. Khoo*, et al.*, Telomere-based crisis: functional differences between telomerase activation and ALT in tumor progression. Genes Dev, 2003. 17(1): p. 88-100.

101. Sedelnikova, O.A., I. Horikawa*, et al.*, Senescing human cells and ageing mice accumulate DNA lesions with unrepairable double-strand breaks. Nat Cell Biol, 2004. 6. p. 168-170.

102. Nakamura, A.J., Y.J. Chiang*, et al.*, Both telomeric and non-telomeric DNA damage are determinants of mammalian cellular senescence. Epigenetics & chromatin, 2008. 1. p. 6.

103. Ghosh, S., M.J. May, and E.B. Kopp, NF-kappa B and Rel proteins: evolutionarily conserved mediators of immune responses. Annu Rev Immunol, 1998. 16: p. 225-260.

104. Baldwin, A.S., Control of oncogenesis and cancer therapy resistance by the transcription factor NF-kappaB. J Clin Invest, 2001. 107(3): p. 241-246.

105. Langel, F.D., N.A. Jain*, et al.*, Multiple protein domains mediate interaction between Bcl10 and MALT1. J Biol Chem, 2008. 283. p. 32419-32431.

106. Lucas, P.C., M. Yonezumi*, et al.*, Bcl10 and MALT1, independent targets of chromosomal translocation in malt lymphoma, cooperate in a novel NF-kappa B signaling pathway. J Biol Chem, 2001. 276(22): p. 19012-19019.

107. Nakagawa, M., Y. Hosokawa*, et al.*, MALT1 contains nuclear export signals and regulates cytoplasmic localization of BCL10. Blood, 2005. 106. p. 4210-4216.

108. Wallace, S.S., Enzymatic processing of radiation-induced free radical damage in DNA. Radiat Res, 1998. 150(5 Suppl): p. S60-79.

109. Semenenko, V.A. and R.D. Stewart, Monte carlo simulation of base and nucleotide excision repair of clustered DNA damage sites. II. Comparisons of model predictions to measured data. Radiat Res, 2005. 164(2): p. 194-201.

110. Sutherland, B.M., P.V. Bennett*, et al.*, Clustered DNA damages induced by x rays in human cells. Radiat Res, 2002. 157(6): p. 611-616.

111. Gulston, M., C. de Lara*, et al.*, Processing of clustered DNA damage generates additional double-strand breaks in mammalian cells post-irradiation. Nucleic Acids Res, 2004. 32(4): p. 1602-1609.

112. Dellaire, G. and D.P. Bazett-Jones, Beyond repair foci: subnuclear domains and the cellular response to DNA damage. Cell Cycle, 2007. 6. p. 1864-1872.

113. Kornberg, R.D., Chromatin structure: a repeating unit of histones and DNA. Science, 1974. 184(139): p. 868-871.

114. Stucki, M., J.A. Clapperton, *et al.*, MDC1 directly binds phosphorylated histone H2AX to regulate cellular responses to DNA double-strand breaks. Cell, 2005. 123(7): p. 1213-1226.

115. Chowdhury, D., M.C. Keogh, *et al.*, gamma-H2AX dephosphorylation by protein phosphatase 2A facilitates DNA double-strand break repair. Mol Cell, 2005. 20(5): p. 801-809.

116. Nakada, S., G.I. Chen, *et al.*, PP4 is a gamma H2AX phosphatase required for recovery from the DNA damage checkpoint. EMBO Rep, 2008. 9(10): p. 1019-1026.

117. Chowdhury, D., X. Xu, *et al.*, A PP4-phosphatase complex dephosphorylates gamma-H2AX generated during DNA replication. Mol Cell, 2008. 31(1): p. 33-46.

118. Spycher, C., E.S. Miller, *et al.*, Constitutive phosphorylation of MDC1 physically links the MRE11-RAD50-NBS1 complex to damaged chromatin. J Cell Biol, 2008. 181(2): p. 227-240.

119. Melander, F., S. Bekker-Jensen, *et al.*, Phosphorylation of SDT repeats in the MDC1 N terminus triggers retention of NBS1 at the DNA damage-modified chromatin. J Cell Biol, 2008. 181(2): p. 213-226.

120. Chapman, J.R. and S.P. Jackson, Phospho-dependent interactions between NBS1 and MDC1 mediate chromatin retention of the MRN complex at sites of DNA damage. EMBO Rep, 2008. 9(8): p. 795-801.

121. Lou, Z., K. Minter-Dykhouse, *et al.*, MDC1 maintains genomic stability by participating in the amplification of ATM-dependent DNA damage signals. Mol Cell, 2006. 21(2): p. 187-200.

122. Panier, S. and D. Durocher, Regulatory ubiquitylation in response to DNA double-strand breaks. DNA Repair (Amst), 2009. 8(4): p. 436-443.

123. Goldberg, M., M. Stucki, *et al.*, MDC1 is required for the intra-S-phase DNA damage checkpoint. Nature, 2003. 421(6926): p. 952-956.

124. Stewart, G.S., B. Wang, *et al.*, MDC1 is a mediator of the mammalian DNA damage checkpoint. Nature, 2003. 421(6926): p. 961-966.

125. Bekker-Jensen, S., C. Lukas*, et al.*, Spatial organization of the mammalian genome surveillance machinery in response to DNA strand breaks. J Cell Biol, 2006. 173(2): p. 195-206.

126. Bekker-Jensen, S., C. Lukas*, et al.*, Dynamic assembly and sustained retention of 53BP1 at the sites of DNA damage are controlled by Mdc1/NFBD1. J Cell Biol, 2005. 170(2): p. 201-211.

127. Lou, Z., C.C. Chini*, et al.*, Mediator of DNA damage checkpoint protein 1 regulates BRCA1 localization and phosphorylation in DNA damage checkpoint control. J Biol Chem, 2003. 278(16): p. 13599-13602.

128. Xu, B., S. Kim, and M.B. Kastan, Involvement of Brca1 in S-phase and G(2)-phase checkpoints after ionizing irradiation. Mol Cell Biol, 2001. 21(10): p. 3445-3450.

129. Yarden, R.I., S. Pardo-Reoyo*, et al.*, BRCA1 regulates the G2/M checkpoint by activating Chk1 kinase upon DNA damage. Nat Genet, 2002. 30(3): p. 285-289.

130. Moynahan, M.E., J.W. Chiu*, et al.*, Brca1 controls homology-directed DNA repair. Mol Cell, 1999. 4(4): p. 511-518.

131. Stark, J.M., A.J. Pierce*, et al.*, Genetic steps of mammalian homologous repair with distinct mutagenic consequences. Mol Cell Biol, 2004. 24(21): p. 9305-9316.

132. Wang, H.C., W.C. Chou*, et al.*, Ataxia telangiectasia mutated and checkpoint kinase 2 regulate BRCA1 to promote the fidelity of DNA end-joining. Cancer Res, 2006. 66(3): p. 1391-1400.

133. Zhuang, J., J. Zhang*, et al.*, Checkpoint kinase 2-mediated phosphorylation of BRCA1 regulates the fidelity of nonhomologous end-joining. Cancer Res, 2006. 66(3): p. 1401-1408.

134. Huen, M.S., R. Grant*, et al.*, RNF8 transduces the DNA-damage signal via histone ubiquitylation and checkpoint protein assembly. Cell, 2007. 131(5): p. 901-914.

135. Kolas, N.K., J.R. Chapman*, et al.*, Orchestration of the DNA-damage response by the RNF8 ubiquitin ligase. Science, 2007. 318(5856): p. 1637-1640.

136. Mailand, N., S. Bekker-Jensen*, et al.*, RNF8 ubiquitylates histones at DNA double-strand breaks and promotes assembly of repair proteins. Cell, 2007. 131(5): p. 887-900.

137. Stewart, G.S., S. Panier, *et al.*, The RIDDLE syndrome protein mediates a ubiquitin-dependent signaling cascade at sites of DNA damage. Cell, 2009. 136(3): p. 420-434.

138. Kim, S.T., D.S. Lim, *et al.*, Substrate specificities and identification of putative substrates of ATM kinase family members. J Biol Chem, 1999. 274(53): p. 37538-37543.

139. Matsuoka, S., B.A. Ballif, *et al.*, ATM and ATR substrate analysis reveals extensive protein networks responsive to DNA damage. Science, 2007. 316(5828): p. 1160-1166.

140. Skarp, K.P. and M.K. Vartiainen, Actin on DNA-an ancient and dynamic relationship. Cytoskeleton (Hoboken), 2010. 67(8): p. 487-495.

141. Andrin, C.A., McDonald, D., Horlich, L., Missiaen, K., Rodrigue, A., Ghosh, S., Mizayans, R., Masson, J.Y., and M.J. Hendzel, In preparation. 2009.

142. Gieni, R.S. and M.J. Hendzel, Actin dynamics and functions in the interphase nucleus: moving toward an understanding of nuclear polymeric actin. Biochem Cell Biol, 2009. 87(1): p. 283-306.

143. Biswas, D.K., Q. Shi, *et al.*, NF-kappa B activation in human breast cancer specimens and its role in cell proliferation and apoptosis. Proc Natl Acad Sci USA, 2004. 101. p. 10137-10142.

144. Mallette, F.A. and G. Ferbeyre, The DNA damage signaling pathway connects oncogenic stress to cellular senescence. Cell Cycle, 2007. 6. p. 1831-1836.

145. Artandi, S.E. and R.A. DePinho, Telomeres and telomerase in cancer. Carcinogenesis, 2010. 31(1): p. 9-18.

146. Di Leonardo, A., S.P. Linke, *et al.*, DNA damage triggers a prolonged p53-dependent G1 arrest and long-term induction of Cip1 in normal human fibroblasts. Genes Dev, 1994. 8(21): p. 2540-2551.

147. Lee, Y.J., C.H. Tsai, *et al.*, Involvement of a p53-independent and post-transcriptional up-regulation for p21WAF/CIP1 following destabilization of the actin cytoskeleton. Int J Oncol, 2009. 34(2): p. 581-589.

Chapter 6. Appendix/Supplementary Figures

6.1 Malt1 is not recruited to IRIF

6.1.1 Materials and Methods

T47D cells were grown as described in materials and methods section 2.1. Cells were immunostained as described in materials and methods section 2.4. Cells were stained with 1:1000 mouse anti-phospho-Histone H2A.X (JBW301, Millipore, Billerica, MA), and 1:50 rabbit anti-MALT1 (28246, Santa Cruz, Santa Cruz, CA).

6.1.2 Results

We used radiation time course experiments in combination with immunofluorescence to study the localization of MALT1 to DSB/IRIF. Following treatment with 2 Gy, in T47D cells, we observe that MALT1 is not recruited to IRIF until 8 h post-IR when we observe a small amount of co-localization (supplementary figure 1A). Supplementary figure 1B shows that MALT1 is not recruited to IRIF at any time point following treatment with 5 Gy. However, at some time points, we do observe intense MALT1 staining that is adjacent to the γH2AX foci. To verify these results similar experiments were carried out in the human mammary epithelial cell line, hTERT-HME1 cells. Supplementary figure 2A and B reveal that MALT1 is not recruited to IRIF following treatment with 2 Gy (A) or 5 Gy (B) except for a small amount of co-localization with γH2AX at 8 h post-IR.

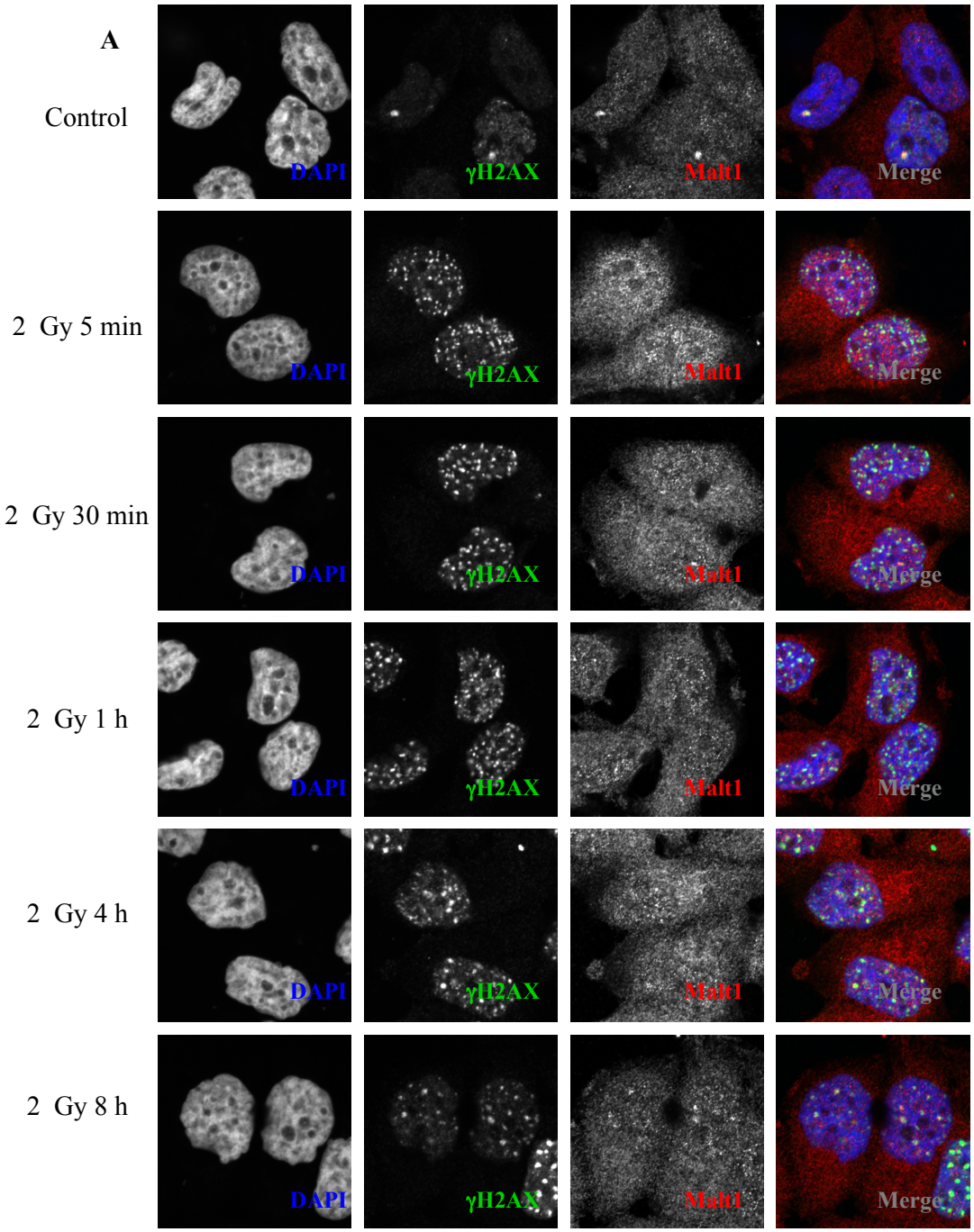

Supplementary Figure 1. MALT1 is not recruited to ionizing radiation-induced foci in T47D cells. T47D cells were irradiated at 2 Gy (A) or 5 Gy (B) and fixed in 3.7% formaldehyde after 5 mins, 30 mins, 1 h, 4 h, and 8 h, unirradiated cells were fixed and stained as a control. (A) Fixed cells were stained with mouse anti-γH2AX (FITC, green), rabbit anti-MALT1 (Cy3, red), and counterstained with DAPI. Images are representative of at least two separate experiments.

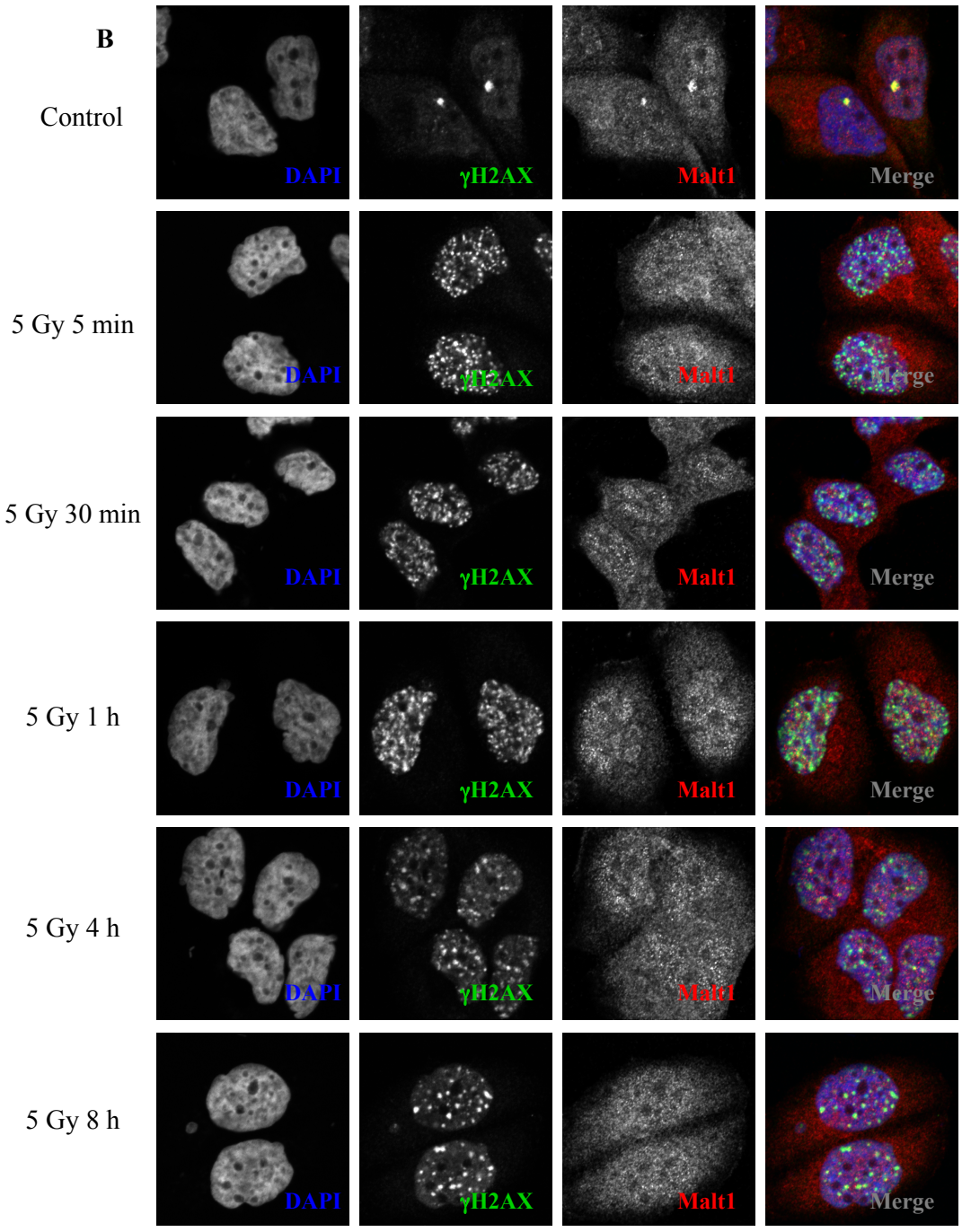
B
Control
5 Gy 5 min
5 Gy 30 min
5 Gy 1 h
5 Gy 4 h
5 Gy 8 h
DAPI
γH2AX
Malt1
Merge

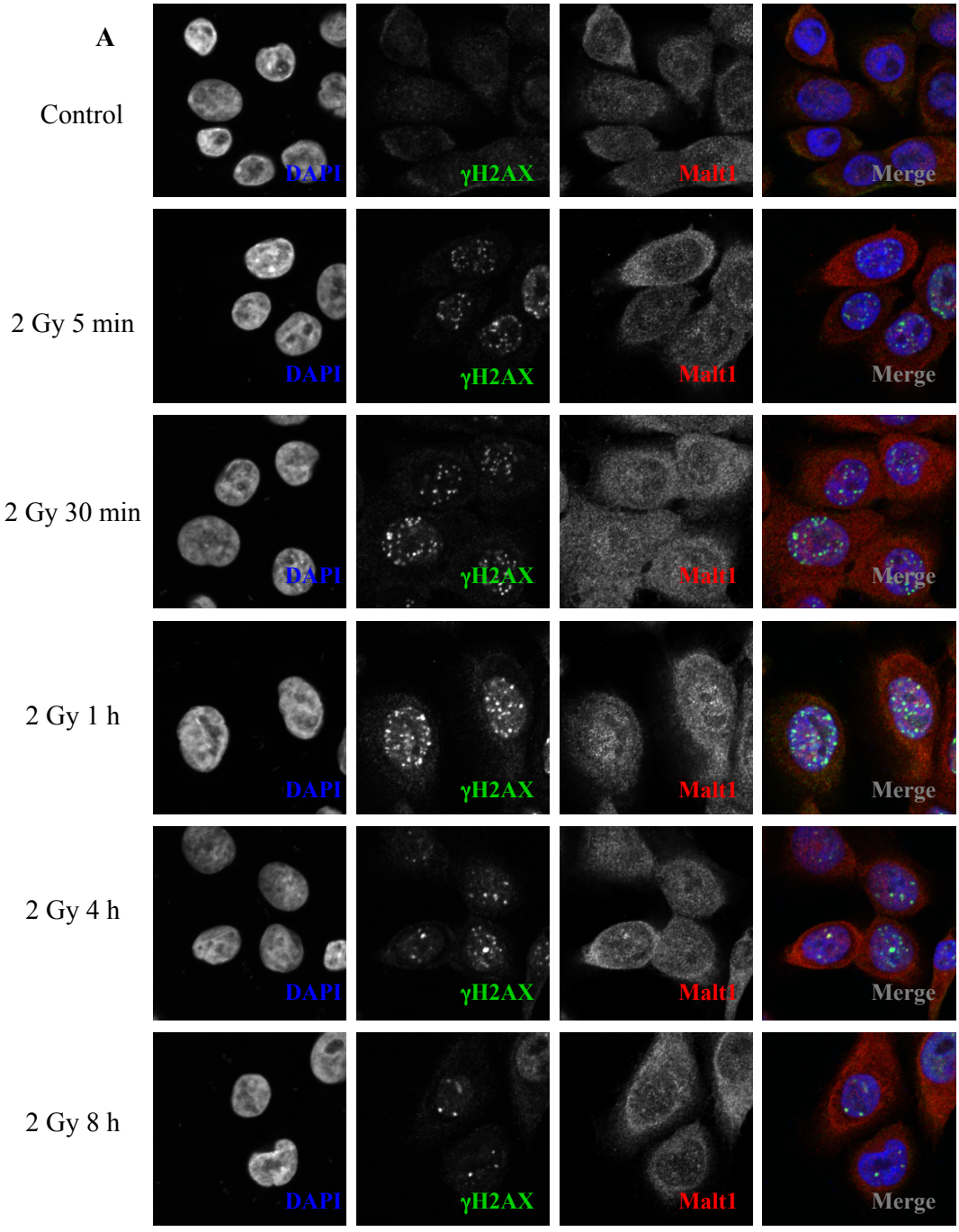

Supplementary Figure 2. MALT1 is not recruited to ionizing radiation-induced foci in hTERT-HME1. hTERT-HME1 cells were irradiated at 2 Gy (A) or 5 Gy (B) and fixed in 3.7% formaldehyde after 5 mins, 30 mins, 1 h, 4 h, and 8 h, unirradiated cells were fixed and stained as a control. (A) Fixed cells were stained with mouse anti-γH2AX (FITC, green), rabbit anti-MALT1 (Cy3, red), and counterstained with DAPI. Images are representative of at least two separate experiments.

B

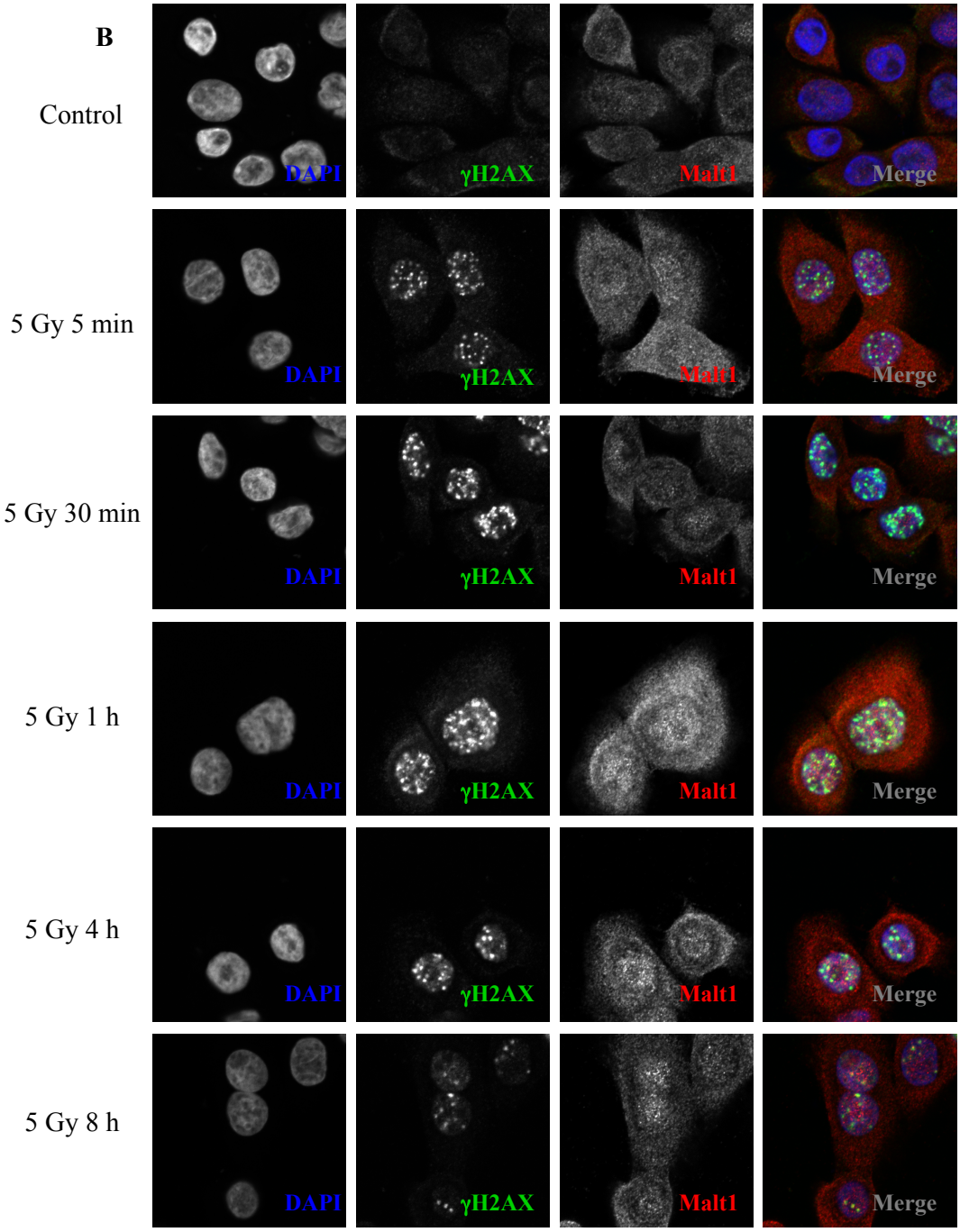
Control
DAPI
γH2AX
Malt1
Merge
5 Gy 5 min
DAPI
γH2AX
Malt1
Merge
5 Gy 30 min
DAPI
γH2AX
Malt1
Merge
5 Gy 1 h
DAPI
γH2AX
Malt1
Merge
5 Gy 4 h
DAPI
γH2AX
Malt1
Merge
5 Gy 8 h
DAPI
γH2AX
Malt1
Merge

6.2 Bcl10 is a potential target for P-ATM mediated phosphorylation

6.2.1 Materials and Methods

T47D cells were grown as described in materials and methods section 2.1. Cells were plated in 6-well cell culture dishes at a density of 20-25 x 10^4 cells/mL, and allowed to attach overnight. The next day cells were treated with 0.5 μM okadaic acid (100 μM stock), diluted in growth medium, for 30, 60, 90, and 120 min prior to protein isolation. Protein from untreated cells was isolated as a control. Cells were rinsed with 4-5 mL of cold PBS and then 160 μl of RIPA buffer (50 mM Tris-HCL pH 7.5 (Sigma, Oakville, ONT),150 mM NaCl (BDH Inc., Edmonton, AB) 1% NP-40 (Sigma), 0.5% sodium deoxycholate (Sigma), 0.1% SDS (Bio-rad, Mississauga, ON)) plus protease and phosphatase inhibitors (Roche, Mississauga, ON) was added to each well and the plates were incubated on ice for 5 mins. Following incubation, lysates were vigorously scraped from the dish with a clean cell scraper and transferred to an eppendorf tube. On ice lysates were repeatedly syringed through a 21G needle and then centrifuged at top speed for 10 mins at 4°C. Western blot analysis was then carried out as described in materials and methods section 2.7. With the exeption that samples were run on a 6% and 10% SDS-polyacrylamide gel.

6.2.2 Results

We monitored phosphorylation by western blot analysis. Okadaic acid selectively inhibits that phosphatase PP2A, allowing ATM to auto-phosphorylate itself producing kinase active monomers. These monomers are then able to

phosphorylate ATM target proteins. Therefore to determine if Bcl10 is a target for ATM phosphorylation we treated T47D cells with okadaic acid for various lengths of time. After 90 mins of treatment we begin to observe phosphorylated ATM, these levels are further amplified at 120 mins (supplementary figure 3). Similarly at 90 mins we begin to see an upward shift in the Bcl10 band (indicated by arrow), and by 120 mins we see smearing of this band indicative of change in molecular weight (supplementary figure 3). In this case this change in molecular weight is likely due to a phosphorylation event. The actin band serves as a loading control (supplementary figure 3).

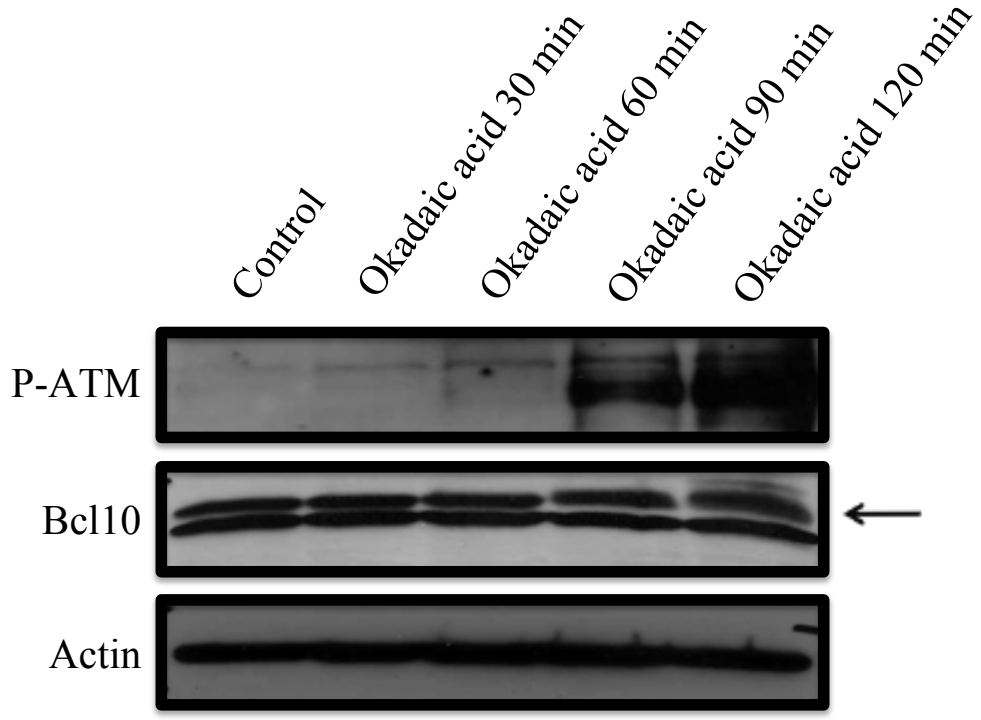

Supplementary Figure 3. Bcl10 is a target for phosphorylation. T47D cells were treated with 0.5 μM okadaic acid and protein was isolated after 30, 60, 90, and 120 mins. Protein from untreated cells was isolated as a control. Samples were electrophoresed in a 6% (top blot, P-ATM) or 10% (bottom two blots, Bcl10 and Actin) SDS-polyacrylamide gel. The samples were transferred to a nitrocellulose membrane and immunostained with mouse anti-P-ATM, mouse anti-actin, and rabbit anti-Bcl10. Primary antibodies were detected with goat anti-mouse IgG-peroxidase or goat anti-rabbit IgG-peroxidase and developed with Amersham ECL Western Blotting Detection Reagent. Arrow points to the specific Bcl10 protein band. This blot is representative of a single experiment.